THE IMPACT OF GENOMIC ABERRATIONS ON CANCER CELLS

from mitotic to replication failures

Von Frau **Kristina Keuper**, M. Sc., geb. in Hermeskeil

Rheinland-Pfälzische Technische Universität Kaiserslautern Landau

vom Fachbereich Biologie der Rheinland-Pfälzischen Technischen Universität Kaiserslautern-Landau zur Verleihung des akademischen Grades

Dr. rer. nat.

genehmigte Dissertation

Dekan:	Prof. Dr. Stefan Kins
1. Gutachterin:	Prof. Dr. Zuzana Storchová
2. Gutachter:	Prof. Dr. Jörg Fahrer
Vorsitzende:	Prof. Dr. Tanja Maritzen

Wissenschaftliche Aussprache: 17.01.2023

Kaiserslautern, 2023 – D 386

Declaration

Ich erkläre hiermit, dass die Dissertation von mir, Kristina Keuper, selbstständig unter Betreuung von Prof. Dr. Zuzana Storchová angefertigt wurde. Alle benutzten Hilfsmittel und Hilfestellungen in der Arbeit habe ich angegeben und die Ergebnisse beteiligter Mitarbeiter sowie anderer Autoren klar gekennzeichnet.

Die Dissertation dient der Erlangung des akademischen Grades „Doktor der Naturwissenschaften“ (Dr. rer. nat.) an der Rheinland-Pfälzischen Technischen Universität Kaiserslautern-Landau. Teile hiervon sind weder als Prüfungsarbeit für eine staatliche oder andere wissenschaftliche Prüfung eingereicht worden, noch wurde die gleiche oder eine andere Abhandlung der vorliegenden Arbeit bei einem anderen Fachbereich oder einer anderen Universität als Dissertation eingereicht.

Die Promotionsordnung des Fachbereichs Biologie der Rheinland-Pfälzischen Technischen Universität Kaiserslautern-Landau ist mir in ihrer derzeit gültigen Fassung bekannt.

Kaiserslautern, 30.01.2023

Kristina Keuper

_____

Kristina Keuper

For my loved ones ♡ For my passion for science

Table of Contents

Summary

Chromosomal aberrations are manifold changes in the configuration of the DNA. Each cell in a tumor may accumulate different karyotype changes, making it challenging to determine the causes and consequences of this instability. Therefore, model systems have been developed in the past to generate and study specific genome alterations. In this thesis, I present the results of my studies on three types of chromosomal aberrations, all of which may contribute to tumor development or progression.

Chromothripsis is a phenomenon that describes a one-off massive chromosomal disruption and reassembly, perhaps arising via DNA damage micronuclei (MN). MN are small DNA-packed nuclear envelopes. I tested potential causes of DNA damage in MN and found that the rupture of the MN envelope and the entry of cytosolic fractions increase DNA damage in MN. Furthermore, I addressed the question of what physiological consequences cell lines with an additional rearranged chromosome have compared to those with an intact extra chromosome. Strikingly, the cells with more rearrangements showed a functional advantage resulting in an improved fitness potential.

However, the engineering of polysomic cell lines with fully intact additional chromosomes increases various cellular stress responses and reduces the proliferation capacity. To investigate how cancer cells overcome the detrimental consequences of aneuploidy, I explored physiological adaptations of model cells with a defined additional chromosome that underwent *in vivo* and *in vitro* evolution. Interestingly, unfavorable phenotypes of aneuploid cells, such as the replication stress, were mitigated upon evolution. Furthermore, I examined the replication on single molecule resolution, showing alteration after evolution that might underlie the replication stress bypass or tolerance.

In contrast to these unbalanced forms of genomic aberrations, whole genome doubling (WGD) leads to a full doubled chromosome set, which was shown to evolve into aneuploid karyotypes by chromosomal instability (CIN), frequently by losing chromosomes. Cells that underwent WGD accumulate DNA damage in the S phase. I performed a single molecule analysis on the DNA during the first cell cycle after WGD to elucidate how the DNA damage arises and found that the number of active origins is not sufficient to replicate the doubled amount of DNA in the first S phase after WGD faithfully. This starts a genome-destabilizing cascade that eventually promotes tumorigenesis, metastasis, and poor patient outcome.

Taken together, these studies provide insights into the causes and consequences of three types of genomic aberrations: chromothripsis, polysomy, and WGD. However different these phenomena may be, they share one common feature – they contribute to tumor development and progression. Therefore, elucidating the aberrant cell functions caused by genomic aberrations contributes to a better understanding of a cancer cell's nature and will perhaps help to find new cancer therapy targets.

.

Zusammenfassung

Als Chromosomenaberration werden vielfältige Veränderungen in der DNA-Konfiguration bezeichnet. Dabei kann jede Zelle in einem Tumor einen anderen Karyotyps aufweisen, was es erschwert mögliche Ursachen und Folgen der Instabilität zu finden. Daher wurden in der Vergangenheit Modellsysteme entwickelt, um spezifische Genomveränderungen herbeizuführen. In dieser Arbeit werden die Studienergebnisse zu drei Arten von Chromosomenaberrationen vorgestellt, die alle zur Tumorentstehung oder -fortschreitung beitragen können.

Chromothripsis ist durch eine Restrukturierung gekennzeichnet, die auf DNA-Schäden beruht und hat vermutlich eine Ursache in sogenannten Mikronuklei (MN), kleine, mit DNA gepackte Kernhüllen. In dieser Arbeit wurden die Ursachen für DNA-Schäden in MN untersucht und herausgefunden, dass eine defekte Kernhülle und das Eindringen des Zytosols DNA-Schäden in MN erhöht. Darüber hinaus wurden Folgen von Zelllinien, mit restrukturiertem Chromosom untersucht und herausgefunden, dass sie einen funktionellen Vorteil gegenüber Zellen haben, die ein intaktes zusätzliches Chromosom haben.

Die Herstellung polysomischer Zelllinien mit intakten zusätzlichen Chromosomen führt jedoch zu einer Zunahme zellulärer Stressreaktionen und einer Verringerung der Vermehrungsfähigkeit. Um zu untersuchen, wie Krebszellen diese nachteiligen Folgen der Aneuploidie überwinden, wurden physiologischen Anpassungen von Modellzellen mit einem bestimmten zusätzlichen Chromosom, die *in vivo* und *in vitro* eine Evolution durchlaufen haben, analysiert. Interessanterweise wurden ungünstige Phänotypen aneuploider Zellen durch die Evolution abgemildert. Zudem wurde die Replikation auf Einzelmolekülebene untersucht und dabei Veränderungen nach der Evolution festgestellt, die der Umgehung oder Toleranz des Replikationsstresses zugrunde liegen könnten.

Die Genomverdopplung (GV) führt in der Folge chromosomaler Instabilität zu einem aneuploiden Karyotyp, meist durch den Verlust von Chromosomen. Zellen, die eine GV durchlaufen haben, akkumulieren in der ersten S-Phase DNA-Schäden. Mithilfe einer Einzelmolekülanalyse der DNA während des ersten Zellzyklus nach GV konnte gezeigt werden, dass die Zahl der aktiven Replikationsursprünge nicht ausreicht, um die doppelte Menge an DNA in der ersten S-Phase nach der GV zuverlässig zu replizieren. Dadurch wird eine Kaskade zur Destabilisierung des Genoms ausgelöst, die zur Tumorentstehung und Metastasierung führen kann.

Diese Studien bieten Einblicke in die Folgen dreier Arten genomischer Aberrationen: Chromothripsis, Polysomie und Genomverdopplung. So unterschiedlich diese Phänomene auch sein mögen, eines haben sie gemeinsam – sie tragen zur Tumorentwicklung und -fortschreitung bei. Die Aufklärung der abweichenden Zellfunktionen, die durch genomische Aberrationen verursacht werden, hilft daher bei einem besseren Verständnis von Krebszellen und wird vielleicht dazu beitragen, neue intrazelluläre Ziele für die Krebstherapie zu finden.

Publications

Research articles

Kneissig, M., **Keuper, K.**, de Pagter, M. S., van Roosmalen, M. J., Martin, J., Otto, H., Passerini, V., Campos Sparr, A., Renkens, I., Kropveld, F., Vasudevan, A., Sheltzer, J. M., Kloosterman, W. P., & Storchova, Z. (2019). Micronuclei-based model system reveals functional consequences of chromothripsis in human cells. eLife, 8, e50292. https://doi.org/10.7554/eLife.50292

Bernhard, S.V., Seget-Trzensiok, K., Kuffer, C. Krastev, D.B., Stautmeister, L.-M., Theis, M., **Keuper, K.,** Boekenkamp, J.-E., Kschischo, M., Buchholz, F. & Storchova, Z. (2022) Loss of USP28 and SPINT2 expression promotes cancer cell survival after whole genome doubling. Cell Oncol., 45, 103–119. https://doi.org/10.1007/s13402-021-00654-5

Prasad, K., Bloomfield, M., Levi, H., **Keuper, K.**, Bernhard, S. V., Baudoin, N. C., Leor, G., Eliezer, Y., Giam, M., Wong, C. K., Rancati, G., Storchová, Z., Cimini, D., & Ben-David, U. (2022). Whole-Genome Duplication Shapes the Aneuploidy Landscape of Human Cancers. Cancer research, 82(9), 1736–1752. https://doi.org/10.1158/0008-5472.CAN-21-2065

Gemble, S., **Keuper, K.**, Wardenaar, R., Srivastava, N., Nano, M., Macé, A. S., Tijhuis, A. E., Bernhard, S. V., Spierings, D., Simon, A., Goundiam, O., Hochegger, H., Piel, M., Foijer, F., Storchová, Z., & Basto, R. (2022). Genetic instability from a single S phase after whole-genome duplication. Nature, 604(7904), 146–151. https://doi.org/10.1038/s41586-022-04578-4

Reviews

Keuper, K., Wieland, A., Räschle, M., & Storchova, Z. (2021). Processes shaping cancer genomes - From mitotic defects to chromosomal rearrangements. DNA repair, 107, 103207. https://doi.org/10.1016/j.dnarep.2021.103207

Introduction

Cancer refers to diseases characterized by the uncontrolled growth of a cell population with the ability to invade different tissues in a body. App. 10 million people died from cancer in 2020. This corresponds to one in six deaths [1] and makes cancer a primary cause of death worldwide. Therefore, the relevance of cancer research remains high, even though the term "cancer" with its founder Hippocrates is over 2000 years old [2].

The origin of cancer

In the late 19th century, the German scientist Theodor Boveri described the centrosome as an organ of cell division in animal cells using an optical microscope. He found that centrosomes are essential for the formation of the mitotic spindle, a cellular scaffold required for chromosome segregation during mitosis [3,4]. After the discovery of this substantial concept in cell division, Theodor Boveri proposed the importance of a full chromosome set for cellular development [5], and established that the chromosomes are individual entities [6]. He hypothesized that carcinogenesis starts with a single cell, in which a defective cell division triggers uncontrolled proliferation, as it can result in unbalanced chromosome configurations [7]. Since then, enormous research drove the expansion of knowledge in molecular genetics and especially, in cancer genetics.

Nowadays, the concept of the hallmark of cancer is used to reduce the complexity of the multifaceted alterations in cancer and their connections [8–10]. Angiogenesis, immortality, the ability to metastasize, and to resist apoptosis are features of cancer cells that enable their survival in foreign and stressful environments (**Figure 1**). Hypoxia is one of many stressors the cancer cells need to adapt to during transformation. It triggers an increased blood vessel formation in tumor tissue mediated by hypoxia-inducible transcription factors [11,12]. These transcription factors are linked to the Warburg effect [13], which describes that tumor cells generate ATP by an abnormally high glucose uptake instead of an increased oxygen consumption [14–17]. Furthermore, natural telomere shortening is prevented in most cancer cells by upregulation of the telomerase. Consequently, the chromosome ends can be fully replicated, resulting in an extended lifetime of the cell [18]. Immune surveillance is based on the activation of both, the innate immune response and the adaptive one. Cancer cells become recognized, and the tumor antigen-specific lymphocytes, as well as the cytotoxic mechanisms, trigger cell death or adaptation [19]. This constant selection pressure is an essential step toward the immune evasion of cancer cells (**Figure 1**). The full escape from the immune system can be facilitated in three ways: First, the tumor-antigen sensitivity is disturbed. Second, the cells become resistant to activation of the cell death program, and third, immune tolerance is induced. The latter leads to the immune system

ignoring the cancer cells [13]. Noteworthy, cancer cells can enter quiescence that keeps them in a dormant mode for a long period of time [20].

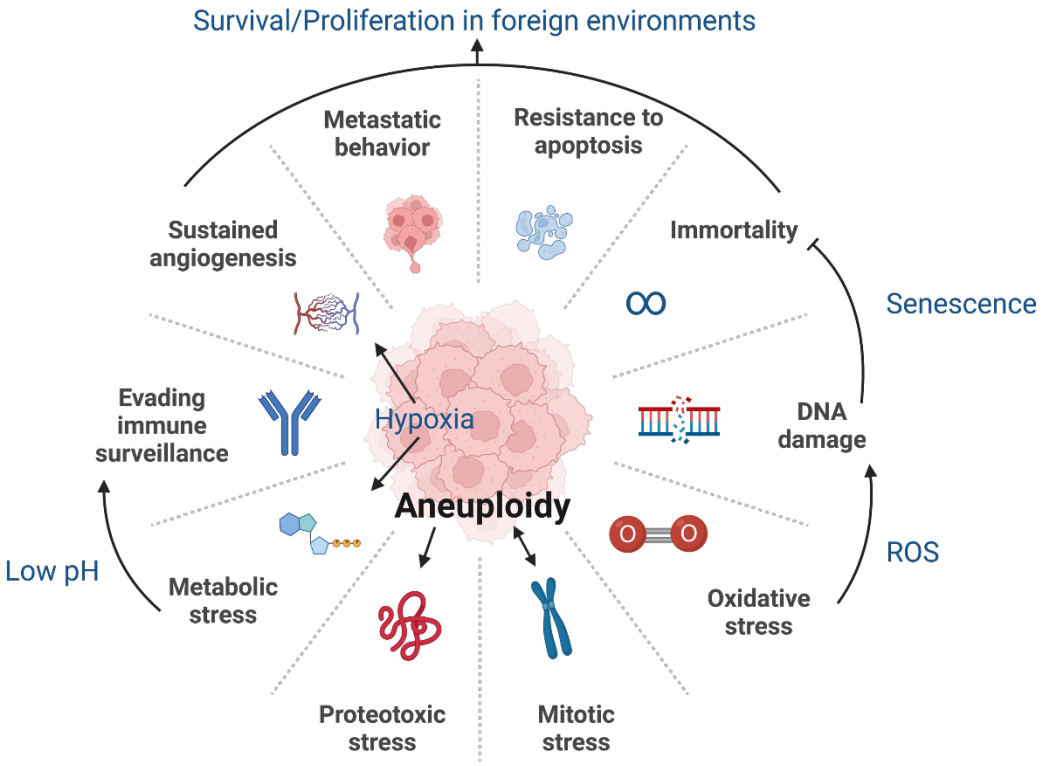

Figure 1: Hallmarks of cancer. Cancer cells differ from normal cells. They are immortal and able to evade apoptosis. They have metastatic behavior and sustained angiogenesis. The cells can evade the immune response and DNA damage is present, also, due to reactive oxygen species (ROS). Divers stress responses are active and mitotic errors cause aneuploidy (created with Biorender.com).

Free radicals are molecules with a high chemical reactivity due to unpaired electrons. Radical formation in cells occurs under normal conditions and is controlled by antioxidant processes, which are supported by certain vitamins (e.g. A, E, and C) and minerals (e.g. selenium, manganese, and zinc). However, acute inflammatory processes, environmental toxins, and UV light can contribute to the overload of cells with free radicals, resulting in so-called oxidative stress. The accumulation of the oxidation products together with subsequent increased cell death leads to premature aging. Another consequence of increased reactive oxygen species (ROS) production is DNA damage [21,22]. For example, ROS leads to oxidized bases, such as 8-hydroxydeoxyguanosine. These are highly enriched in lung cancers from smokers [23]. Oxidative stress is not the only intrinsic trigger of DNA damage and instability. Indeed, mitotic failures are linked to tumorigenesis as well. Cell division defects, such as lagging chromosomes, increase the probability of chromosomal instability (CIN) [24]. CIN is defined by continuous chromosomal aberration changes that cause aneuploidy [25,26]. Aneuploidy is the state of the cell with uneven gain or loss of chromosomes. If the unbalanced amount of DNA is transcribed and translated, it results in unbalanced protein amounts causing proteotoxic stress (**Figure 1**). Proteotoxic stress is characterized

by increased demand for protein folding, and overburdening the proteasome and autophagy, the cellular machinery to recycle unused or unwanted proteins and other cellular components [27]. A mechanism of the cell to maintain the crucial balance of proteins despite aneuploid karyotypes is dosage compensation at mRNA and protein level [28,29].

The general concept of tumorigenesis and tumor progression is that mutational processes alter the genome, and the most beneficial genome variation is selected. The adaptations on cell physiological level are driven by oncogene (OG) amplification and tumor suppressor gene (TSG) downregulation, both of which may contribute to the expansion of the hallmarks of cancer in the mutated cell [30]. Overall, the landscape of hallmarks of cancer is large and well-defined even if the details in this complex network are still widely unknown.

Genetic alterations drive tumorigenesis

The typical human set of chromosomes, the so-called karyotype, consists of 22 pairs of autosomes and two sex chromosomes. Deviations from the typical human karyotype can be either balanced or unbalanced.

Whole genome doubling (WGD) of the natural human karyotype results in a cell with 44 pairs of autosomes and four sex chromosomes. Thereby, WGD is a balanced genome alteration. 30-37% of cancers underwent WGD [31–33]. The karyotype after one WGD event in humans is called tetraploid, a sub-type of a polyploid karyotype, describing all multiples of a full set of chromosomes (**Figure 2** A). A WGD event can occur early during tumorigenesis [34,35]. Noteworthy, polyploid karyotypes exist naturally as well, for example in human hepatocytes [36].

In contrast to these balanced genome alterations, the state of aneuploidy is always unbalanced. Aneuploidy is defined as an alteration of the chromosome configuration and occurs in 90 % of solid tumors [37]. Formally, we distinguish between structural and numerical aneuploidy. While structural aneuploidy refers to aberrant subparts of chromosomes, numerical aneuploidy describes full chromosome abnormalities. There are several types of numerical changes: For example, monosomy refers to a loss of the respective chromosome, and a trisomy refers to the gain of one additional chromosome (**Figure 2** A). Structural aneuploidy manifests itself in sub-chromosomal deviations from the regular chromosome configuration. For example, DNA duplications within a chromosome can be tandem (directly following the other) or dispersed (insertion of the doubled part at a different position). Also, translocations and inversions are structural changes. Translocations are defined by a DNA exchange with the DNA of a different chromosome, whereas inversions describe the DNA exchange within one chromosome. Moreover, chromosome segments can be lost (deletion) or gained (insertion) (**Figure 2**B). Separately noted are arm-level changes as they compose large chromosomal structures but not full chromosomes. For example, a chromosome arm can be either lost or gained (**Figure 2**C). Additionally, complex rearrangements are known. Accumulation of multiple structural and numerical rearrangements can occur, but also catastrophic single events in a cell´s history, such as chromothripsis (**Figure 2**D). Chromothripsis is a massive chromosome-shattering and reassembly phenomenon discovered in the past decade [38].

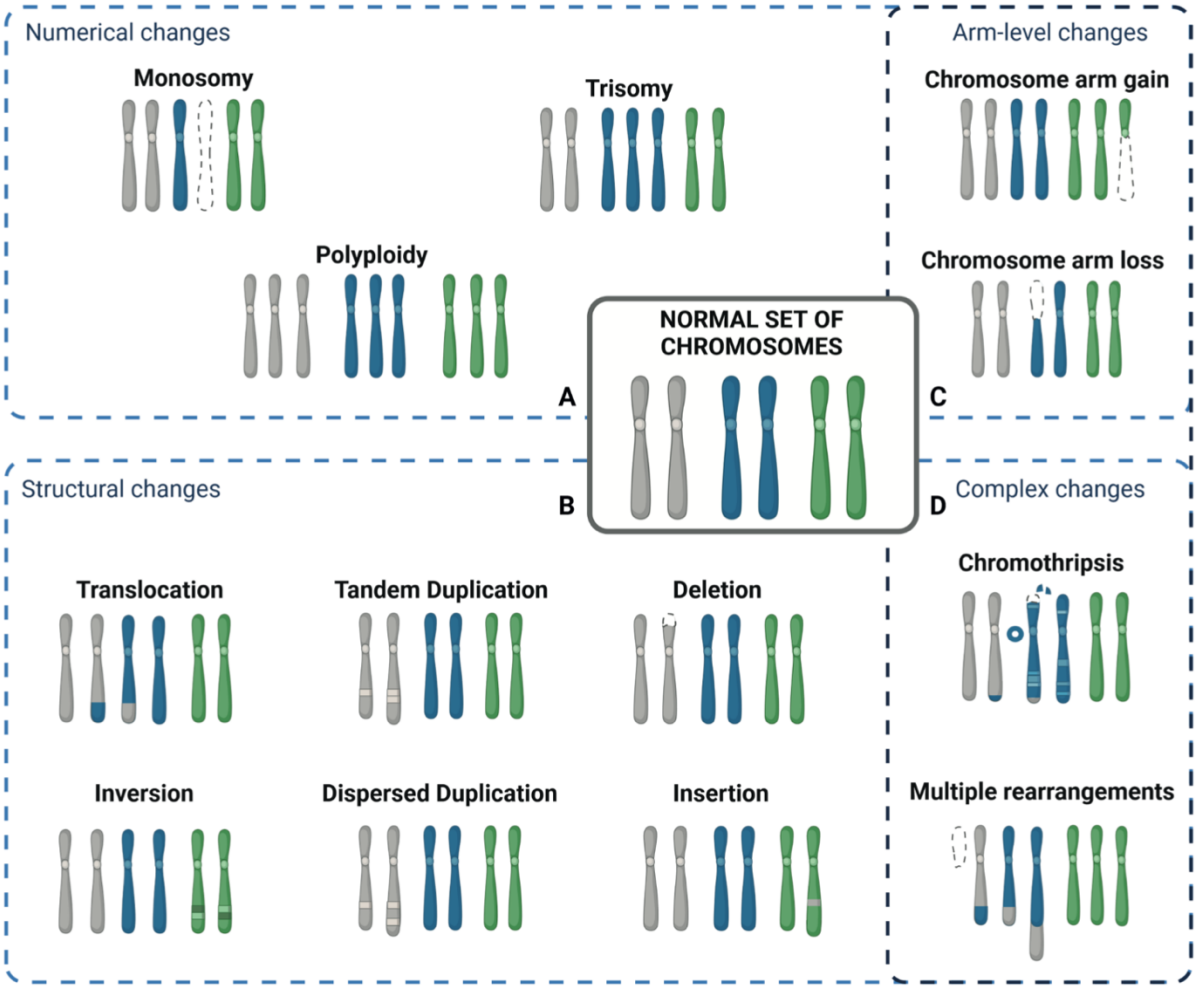

Figure 2: Genomic aberrations. A: Numerical changes: Chromosome loss (monosomy), chromosome gain (trisomy), a multiple of the karyotype (polyploidy). **B:** Structural changes: DNA exchanges (translocations: between chromosomes; inversions: within a chromosome), duplications (tandem: duplicated fragments is the direct neighbor of the original fragment, dispersed: a duplicated fragment is inserted at a different position), deletions (DNA loss), insertions (DNA gain). **C:** Arm-level changes: Loss and gain. **D:** Complex changes: Chromothripsis and multiple rearrangements (from Keuper et al, 2021 [39]).

Tumor cells within the same tumor harbor different karyotypes. This heterogeneity within a cell population is caused by ongoing karyotype changes with every cell division and are referred to as chromosomal instability (CIN)[9]. Constant mutative processes leading to sequence heterogeneity are known as genome instability (GIN). By changing the DNA sequence or the copy number (CN) of existing sequences, genes or their abundances are altered. This can lead to an aberrant mRNA sequence or transcription rate with potentially subsequent protein alterations or abundance alterations. As these genetic abnormalities can drive tumorigenesis or cancer progression[9], there is a high necessity to understand their causes and consequences.

The human somatic cell cycle

The cell is a fascinating timely accurate and precise self-reproduction system. The responsible mechanism for this is its cell cycle. Proteins involved are highly conserved in all eukaryotes. DNA replication in S phase and cell division via segregation of the chromosome content in mitosis (M phase) were the first discovered phases [40]. These two phases are separated in time by two gap phases (G1 and G2), in which the cells grow, doublecheck the content, and prepare for the next step. A checkpoint controls the state of the new-born daughter cells after mitosis and if a cell needs to enter G0, it does not take part in the following cell cycle (cell cycle arrest/exit) [41] (**Figure 3**).

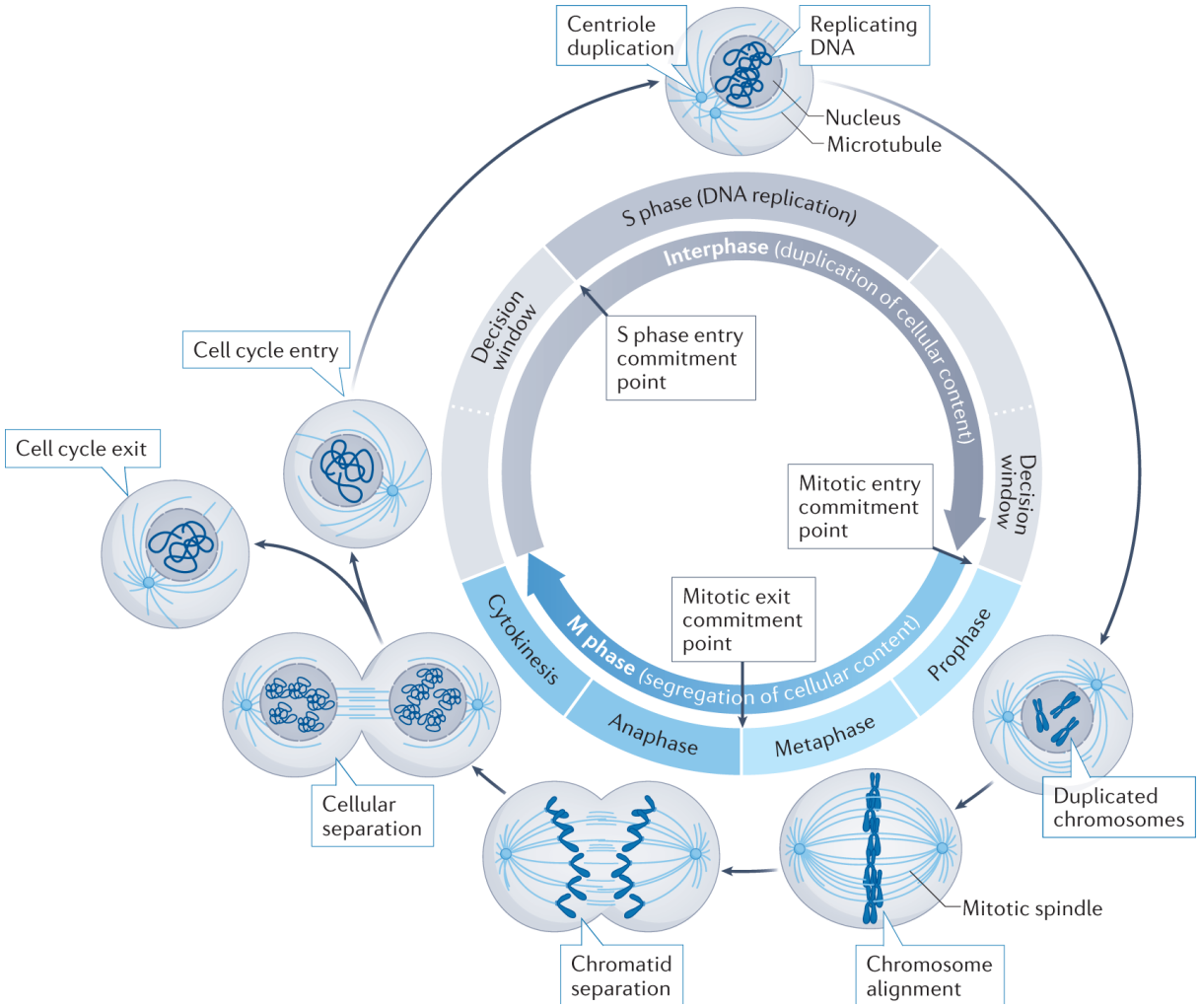

Figure 3: The eucaryotic somatic cell cycle. Proper cell division is based on a well-functioning signaling network in a time dependent manner. The phases are named S phase, in which the replication of the DNA takes place, M phase in which mitosis, the segregation of a cellular content is mediated and lastly, there are gap phases (light grey), in which a decision window for checkpoints (commitment points) is marked. The M phase, marked in blue, is subdivided in prophase, metaphase, anaphase, and cytokinesis. For all phases cell shapes with DNA and spindles demonstrate the stage. Cell cycle exit is equivalent to the gap phase 0 (G0) (from Matthews et al, 2022 [42]).

The interplay between cyclin dependent progression and checkpoint signaling

The cell cycle progression itself is mediated by a complex network involving cyclin proteins and their dependent kinases (CDK). Starting at the G1 phase, directly after mitosis, cyclin D and the kinases CDK6 and CDK4 are most abundant [43]. The G1 checkpoint controls nutrients and growth factors, but also DNA integrity. In G1 and G2 phases, DNA damage is recognized by p53 with its transcription target p21 that mediates cell cycle arrest [44,45]. The next stage is initiated by cyclin E and CDK2 [43]. DNA replication takes place in the S phase and cares for the precise doubling of the genetic material. The intra S phase checkpoint controls for DNA damage during replication and for properly duplicated DNA after replication. Damage signaling is either mediated by the "Ataxia telangiectasia and Rad3 related" (ATR) kinase in case of single-strand breaks (SSB) or in case of double-strand breaks (DSB) by "Ataxia Telangiectasia Mutated" (ATM) kinase [46]. Additionally, centriole duplication takes place during the S phase under the control of "polo-like kinase 4"(PLK4) (**Figure 3**) [47,48]. After the following G2 which is controlled by cyclin A and CDK1 [43], the G2/M checkpoint validates the cell growth and the DNA damage state. Errors result in an ATM-dependent signaling cascade [46]. The entry into mitosis is mediated by cyclin B and CDK1 [43], and leads to the chromatin condensing into visible chromosomes and to the spindle formation (prophase). The spindle formation and bipolar tension are controlled in a specific M phase checkpoint, also known as spindle assembly checkpoint (SAC) [49]. The chromosomes align in a metaphase plate (metaphase) and are subsequently pulled apart from each other (anaphase). The spindle formation machinery cares for the proper segregation into two daughter nuclei. Before re-entering the cell cycle, the separation of the DNA into the daughter nuclei is finalized (telophase), the nuclear membrane is formed and cytokinesis takes place [41] (**Figure 3**).

In conclusion, the timely cell cycle progression involves cyclins and their kinases while each step is tightly controlled by checkpoints that sense DNA damage via ATM and ATR pathways, leading to a p53 response. This allows to sort out cells or repair defects to progress further in the cell cycle, sometimes with a delay. All these accurate measures exist to prevent failures in the cycle that could eventually lead to genomic defects and subsequent related diseases. Thus, a stable and properly functioning cell cycle is highly relevant to prevent tumorigenesis and therefore, proteins involved in cell cycle regulation are potential therapy targets [50–54].

Mitotic failures

A regular healthy mitosis consists of the following five phases:

1. Prophase: Centrosomes duplicate and move to opposite poles of the cell to form microtubule organizing centers (MTOC) [41]. The spindle apparatus is assembled from here. In addition, replicated chromosomes condense and the transcription is silenced. The chromosomes are still connected at the centromeres via the sister chromatid cohesion complex [55]. Finally, the nuclear envelope disassembles in the cell. Thus, the preparations for the following phase are completed.
2. Prometaphase: The spindle fibers form in a star shape starting from the MTOC. Kinetochore microtubules attach to kinetochores on chromosomes and polar microtubules attach to an opposite polar microtubule, forming the spindle. The alignment of chromosomes can begin.
3. Metaphase: Chromosomes are aligned in the equatorial plane. The SAC is silenced by a complex signaling cascade [56], and the transition to the next phase is mediated by the disassembly of the sister chromatid cohesion no longer holding together the chromatids.
4. Anaphase: Chromatids of a chromosome are pulled apart towards the two spindle poles.
5. Telophase: Kinetochores depolymerize, and the nuclear membrane is reconstructed. Chromosomes decondense to transcribe DNA and facilitate cytokinesis.

In contrast to normal bipolar chromosome segregation (**Figure 4a**), the SAC is usually not silenced when the kinetochore-microtubule-centrosome connection is constructed incorrectly. This is the case if the tension of the spindle is too low [57,58]. The physical measure is translated into biochemical signals via the Aurora B kinase [59]. Tension loss of the spindles happens for example due to not existent attachment to the kinetochore (**Figure 4b**), only one-sided attachment to only one sister chromatid (monotelic, **Figure 4c**), or only one-sided attachment to both of the sister chromatids (syntelic, **Figure 4d**). In such cases the SAC signals repair mechanisms and the progress into anaphase pauses for the time the cell needs to repair the defect [60–62]. In addition, the syntelic attachment is very unstable [63]. Thus, it falls apart quickly and the SAC recognizes the empty sister chromatid. Noteworthy, without a properly functioning SAC all three mechanisms lead to chromosome segregation errors, resulting in aberrant karyotypes of the daughter cells. However, sometimes mitotic errors occur even with functioning SAC. The problem is hidden. For example, the SAC does not recognize if the attachment to one kinetochore comes from both sides of the spindle (merotelic, **Figure 4e**). Moreover, multipolar spindles are frequently unnoticed by the SAC (**Figure 4g**). The reason is the still high tension of the microtubules between centrosome and kinetochore is strong enough to ensure stability in both of the cases. The attachments may lead to incorrect separation in anaphase. Merotelic attachments,

frequently lag behind the main DNA mass potentially leading to aneuploidy [64]. Multipolar spindles are frequently observed in tetraploid cells as they also double the centromeres [65]. Importantly, multipolar spindle formation can lead to both, aneuploidy and polyploidy. Frequently, merotelic attachments occur during multipolar spindle assembly, and chromosomes are pulled toward all possible poles. Lastly, also the premature loss of sister chromatid cohesion triggers unfaithful segregation (**Figure 4f**). Together, not only SAC errors but also failures in the kinetochore-microtubule-centrosome connection that evade a SAC response might be causative for the mitotic failures. The described mitotic failures can result in aneuploidy or polyploidy and facilitate chromosomal instability (CIN) [64].

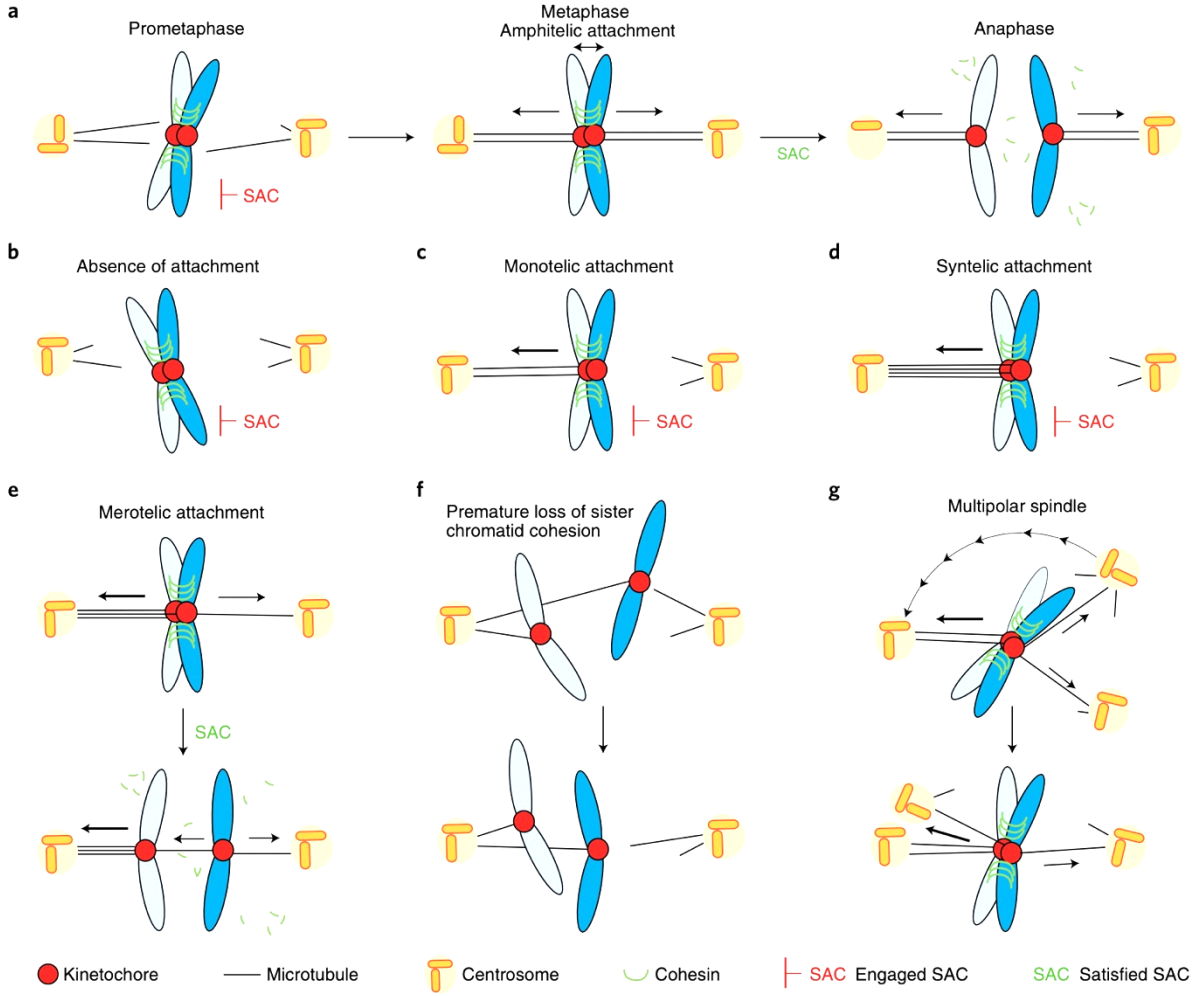

Figure 4: Chromosome mis-segregation events. a) Normal chromosome segregation. b) Absence of attachment. c) Monotelic attachment. d) Syntelic attachment. e) Merotelic attachment. f) Premature loss of sister chromatid cohesion. g) Multipolar spindle. The arrows show the chromosome path during anaphase (from Chunduri and Storchová, 2019 [66]).

Replication failures

DNA replication describes the process of the duplication of the DNA during one cell cycle. Replication needs to be complete and accurate. In addition, the DNA must be duplicated exactly one time per cell cycle to ensure the cell´s fidelity. Replication starts at multiple origins of replication (ORI), where the replication machinery assembles and separates the DNA in opposite directions. This process occurs temporally separated: First, ORIs are established (licensed) in the late M phase and G1 and become active in the late G1 / S phase. Subsequent firing in the S phase starts the actual duplication process [67]. Importantly, not all origins loaded onto the DNA start to replicate. Some remain in a flexible or dormant state and can serve as a backup. This is crucial in case a stressor prevents replication fork progression and the machinery slows down or stalls. If fork progression or restart is timewise not possible, a neighbouring flexible origin can take over the replication to prevent under-replicated DNA [68]. Endogenous and exogenous stressors are known that cause the replication machinery to slow or stop: For example, UV light, chemicals (e.g. aphidicolin that slows down the polymerase), ROS, and imbalances of the nucleotide pool [69,70]. Moreover, replication stress is also caused by transcription interfering with replication [71]. These findings highlight endogenous and exogenous threats of a proper replication. Studies have repeatedly documented that not only single-strand breaks (SSB), but also double-strand breaks (DSB) occur during replication, which, if not corrected or corrected erroneously, can lead to severe defects in the cell and to GIN [72,73]. A more detailed look at the replication should reveal essential proteins and complexes.

1. Origin licensing: All potentially activatable origins are loaded. This is done by the origin recognition complex (ORC). In addition, the proteins “cell division cycle 6” (CDC6) and “CDC10-dependent transcript” (CDT1) are recruited. This protein complex is essential to load the 6-subunit helicase “mini-chromosome maintenance” (MCM 2-7) (**Figure 5** A).
2. Pre-initiation complex (pre-IC) formation: Between G1 and S phase, DBF4-dependent kinase (DDK) and CDK proteins initiate the formation of pre-IC. They phosphorylate further proteins to facilitate their relocation onto the origins. Among these proteins are CDC45, GINS and DNA polymerase ε (Pol ε) (**Figure 5** B).
3. Origin firing: In S phase the pre-IC turns into a functional replisome: MCM 2-7 is phosphorylated at multiple sites to cause the double hexamer to split to two independent hexamers, unwinding the DNA in opposing directions. This activation of the helicase indicates the assembly of other replication factors, including proliferating cell nuclear antigen (PCNA) and replication protein A (RPA), that coats single-stranded DNA (ssDNA). The functional replisome is guided by the CDC45-MCM 2-7-GINS (CMG) complex (**Figure 5** C).

Importantly, the neighbouring flexible origins are blocked by checkpoint kinases as long as they are not needed. For example, ATR and ATM are involved in this process, but also the checkpoint kinase 1 (Chk1) and Chk2. The exact mechanisms of activation of flexible or dormant origins remain to be investigated [67]. Stalling or collapse of the replication machinery can lead to tremendous DNA damage and mutations that affect the cellular functions for example if TSGs or OGs are affected [74]. For example, the overexpression of the OG RAS affects the velocity of the replication machinery and in addition, it decreases the number of available nucleotides that are essential for the synthesis of new DNA [75]. Another example of a GIN-facilitating mechanism is the overexpression of cyclin E. This leads to premature replication start [76]. Overall, GIN can be triggered in replication for example, when the amount of nutrients is too low, replication factors are missing or defective, and when stressors give rise to changed replication dynamics. Replication dynamics describe the measurable parameters during replication, such as the velocity, the number of active origins, and the symmetry of opposing fork

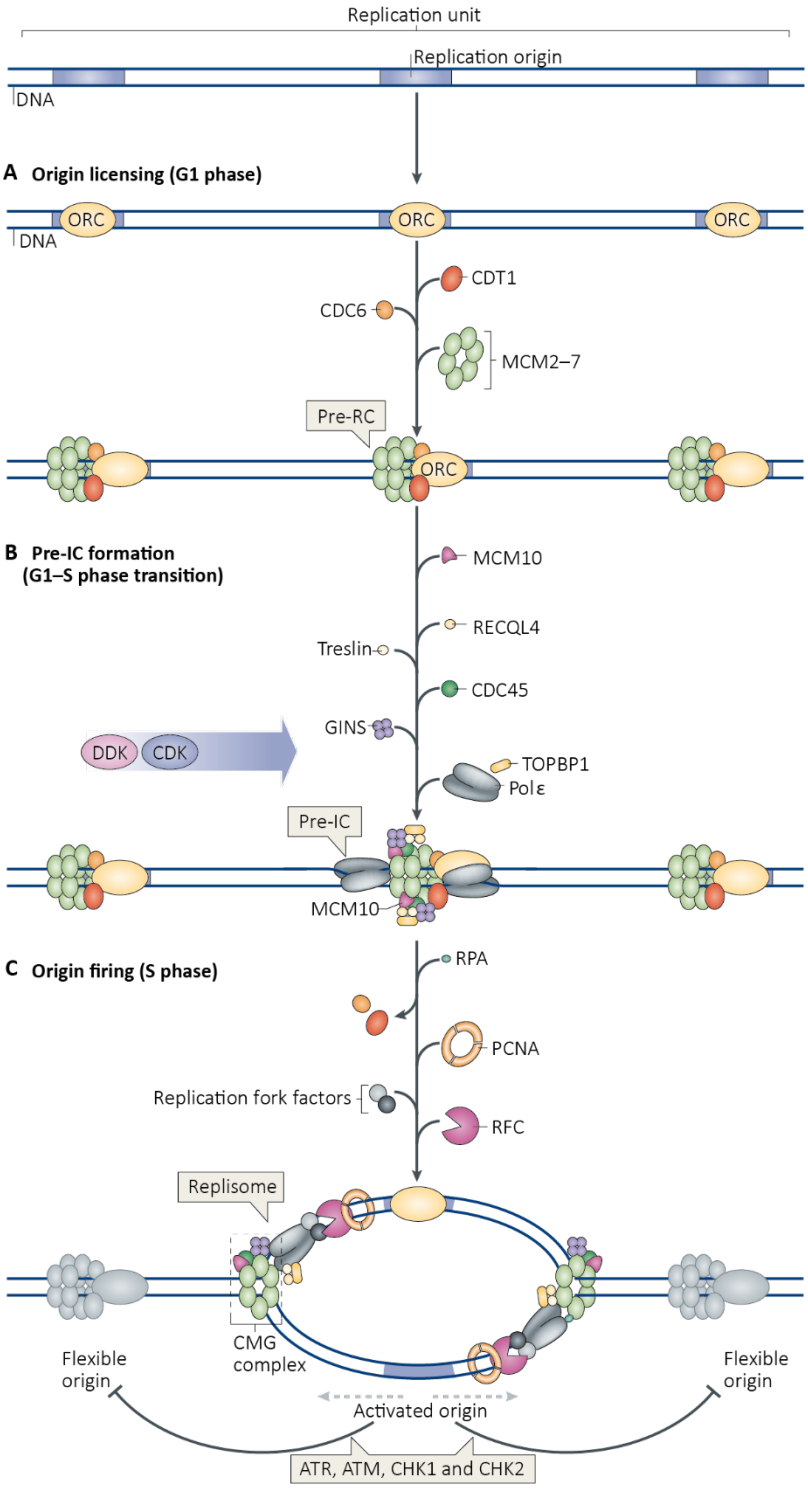

Figure 5: Replication machinery assembly. A: Origin licensing of all sites of replication by the origin recognition complex (ORC) leading to formation of the pre-recognition complex (pre-RC). B: Pre-Initiation (Pre-IC) complex formation on sites of active replication. C: Origin firing with formation of the replisome (adapted from Fragkos et al, 2015) [67].

progression. For example, by inhibition of ATR, all loaded origins fire. The activation of more origins leads to a slowdown of the replication velocity and vice versa [77–79].

To protect the DNA from damage and to repair it if necessary or to eliminate the cell, eucaryotes have developed an intricate mechanism known as DNA damage response (DDR). Replication stress usually leads to the increased formation of ssDNA. The accumulation of RPA with its three subunits RPA1-3 is essential for the stabilization of ssDNA during replication and repair as it coats ssDNA [80]. This protective mechanism ensures rapid sensing of ssDNA breaks via a phosphorylation cascade. Phosphorylation of RPA2 at position S33 occurs mainly in the late S and G2 phase by ATR and prevents the accumulation of ssDNA during replication stress [81]. ATR signaling activates Chk1, which directs the subsequent DDR[82]. The DNA-PK mediated hyperphosphorylation of RPA2 at S4 and S8 is part of the strand-end protection and repair mechanism upon DSBs during stalled replication. When it comes to DSBs and homologous recombination (HR) needs to be signaled, also ATM and ATR hyperphosphorylate RPA2 to signal the damage [83]. These phosphorylations prevent cell cycle progression and irregular HR at aborted replication forks [84–86]. ATM and DNA-PK have supportive functions during replication stress signaling. They mainly signal DSBs via Chk2 [87–91]. After the damage signal is transduced by the protein kinases ATM, ATR or DNA-PK to the corresponding mediators, Chk1 and Chk2, repair proteins are recruited to the broken sites. This task is performed by repair pathway-specific effectors, for example, RAD51 in HR. P53 is an essential regulator protein that contributes substantially to the cell fate decision. It regulates the transcription of p21, which is responsible for the inhibition of cell cycle progression by inhibiting Cdk2 and Cdk6. Upon phosphorylation and transport into the cytosol, p21 leads to the prevention of apoptosis [92]. Activation of p16 and p19 by p53 is linked to senescence [93]. This illustrates the complexity of the repair mechanisms. The proteins involved have frequently additional functions. Modifications of proteins signal the damage rapidly to ensure a faithful replication. The repair processes are dependent on the cell cycle and can slow it down and sort out cells from it. Especially during replication ATR and Chk1 are crucial because the proteins not only prevent excess firing of origins and halt the cell cycle but are essential for the DDR. If the obstacles hindering replication are removed or bypassed the replication can proceed.

Interestingly, under-replicated DNA can escape from monitoring and persist in mitosis even when ATR and Chk1 are present [94]. This might lead to the formation of anaphase bridges (ABs), DNA connections bridging the separating sister chromatids in the anaphase. If resolving the bridge is impossible, breakage would be a consequence eventually leading to extranuclear DNA encapsulated in a nuclear envelope, known as micronuclei (MN) [95–98]. MN are frequently observed in cancer and biomarkers of GIN [99]. Cancer cells generally downregulate repair mechanisms [100]. This includes cell cycle inhibitory proteins and those involved in both, repair and cell cycle checkpoint, e.g. Chk2 [101]. Defects in certain

DNA repair mechanisms are dependent on the type of cancer. For example, almost a third of all metastatic breast carcinomas exhibit mutations in the homologous recombination pathway [102].

Taken together, cell cycle checkpoints and DDR work together to prevent unstable genomes. It is likely that low replication stress has a higher impact on genome integrity, as mitotic checkpoints cannot sense or actively circumvent mild replication stress. In addition, too much stress during replication leads to cell death. Ultimately, not only DNA damage can accumulate and lead to GIN, but also structural and numerical chromosomal aberrations upon mitotic failures. GIN and CIN are closely connected to the hallmarks of cancer as they increase genomic flexibility and facilitate tumorigenesis [103–105].

Autophagy - recycling molecules

Macroautophagy (hereafter autophagy) is the process by which cells degrade and recycle unneeded or unwanted organelles or proteins in the cytoplasm. Typically, a double membrane vesicle, the autophagosome, forms surrounding the degradable structure. Subsequently, autophagosomes fuse with lysosomes, cellular organelles containing phosphatases, and hydrolytic enzymes. The fusion lowers the pH in the resulting autolysosome and starts the digestion of the engulfed cellular components. The resulting building blocks, such as amino acids and nucleotides, can then be reused by the cell (**Figure 6**) [106,107]. Autophagy is activated upon cellular stress, for example, due to increased ROS levels, nutrient limitation, or DNA damage [108]. The Unc-51 like autophagy activating kinase (ULK) complex initiates the vesicle formation for the construction of the autophagosome. This is regulated by the mTOR complex pathway as nutrient limitation or growth factor (e.g. insulin) downregulation leads to mTOR complex inhibition inducing autophagy. mTOR complex inhibitors are used to induce and study autophagy. After initiation of autophagosome formation, autophagy related (ATG) proteins take over multiple core functions of membrane assembly and elongation to surround and finally engulf the molecules of interest. The human homologs of ATG8 are the microtubule-associated proteins 1A/1B light chain 3B (MAP1LC3B, hereafter referred to as LC3). These are crucial components not only for elongation but also for complete closure and isolation of the vesicle. Therefore, LC3 is a standard biomarker of autophagy [109]. Moreover, LC3 interacts with the ubiquitin binding protein p62 to selectively target the molecules that should be incorporated into the autophagosome. The mature autolysosome is formed after fusion of the autophagosome with a lysosome. If this process is blocked, for example by bafilomycin A1, autophagosomes accumulate. A lysosomal membrane protein is LAMP1 and can be used to track the relative number of lysosomes and autolysosomes as it stays in the

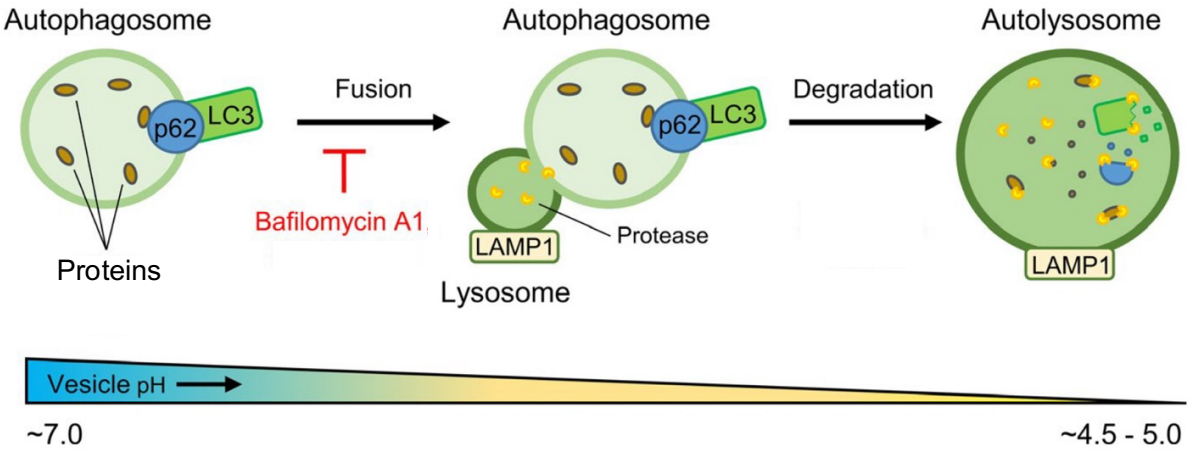

Figure 6: Markers of the macro-autophagy pathway. The chaperone p62 targets proteins marked for lysosomal degradation to autophagosomes. The autophagosomal membrane contains the marker protein LC3. Lysosomes carry LAMP1 in the membrane as marker. They have a low pH and contain proteases. By the fusion of autophagosomes to lysosomes the autolysosome is formed, where the low pH and the proteases degrade the encapsulated proteins, including p62 and LC3, but not LAMP1. An inhibitor of the fusion process is bafilomycin A1 (adapted from Coryell et al, 2020 [111]).

membrane after fusion, whereas the interaction of LC3 and p62 mediates their degradation by autophagy [110,111] (**Figure 6**).

Taken together, autophagy selectively degrades molecules to maintain cellular homeostasis by supplying the cell not only but especially in stress situations with macromolecular reusable building blocks. Autophagic flux estimation can be achieved by LC3 and p62 protein detection, as both are degraded in autolysosomes.

Massive chromosomal rearrangements in micronuclei (MN)

Micronuclei (MN) are extranuclear structures that form when a chromosome or a fragment of a chromosome is not integrated into one of the daughter nuclei. Unrepaired DNA damage, as well as dysfunctional spindle or defect kinetochore proteins, are examples of the origin of the MN formation [112]. MN are frequent in cancer and biomarkers of CIN. By this, they not only resemble a consequence of previous defects but also facilitate further aberrations. DNA encapsulated in MN is prone to DNA damage for a multitude of reasons some of which are further explained below. DNA damage coupled with repair mechanisms at a very distinct portion of the DNA make MN the most accepted hypothesis for the origin of chromothripsis to date.

Chromothripsis is a massive shattering and reassembly event

Tumor development is mostly explained by an accumulation of mutations over time. However, in 2011 Stephens et al discovered a phenomenon in lymphocytic leukemia [38] which is described as an extreme type of multiple mutations affecting only one, a few, or a subpart of a chromosome. Strikingly, this happens in a single catastrophic event during the cell´s history and is composed of double-strand breaks (DSB) and subsequent repair [113]. The phenomenon is known as chromothripsis (Greek: chromo from chromosome (= color) and thripsis (= shattering into pieces)) and it was initially proposed as a rare event happening in 2-3% of all human cancers [38]. Since then, the prevalence was found to be much higher than originally anticipated: A recent study found 49% of 316 tested cancer cases chromothripsis positive with the availability of WGS data from young adults and 28 different tumor types [114]. In another recent study, Cortés-Ciriano et al determined chromothripsis in more than 50% out of 2658 tumors from 38 cancer types using the TCGA database [115]. Remarkably, chromothripsis is observed not just in cancer, but also in congenital disorders, for example, leading to mental retardation [116,117]. An interesting aspect is the curative characteristic of chromothripsis. In the case of severe rare immunodeficiency, chromothripsis caused the deletion of the disease allele on chromosome 2 [118]. Nevertheless, most people suffer from chromothripsis due to fast tumor development, predominantly in young adults.

The classification of chromothripsis is not trivial and deep sequencing is necessary. At least two very similar phenomena need to be excluded. These two together with chromothripsis fall under the umbrella term chromoanagenesis:

1. Chromoplexy was first discovered in 2013 in prostate cancer. Since then, it was frequently found to be responsible for the PTEN disruption in these tumors, a TSG, leading to fitness advantage. In the case of chromoplexy DSBs occur on more than five chromosomes and lead to the reassembly of fragments from up to eight chromosomes. Mostly non-homologous end-joining (NHEJ) or alternative end-joining (alt-EJ) repair the breakages, which are usually

less than in a chromothripsis scenario. Mainly translocations and inversions are observed, but also deletions (**Figure 7** A) [119–121].

2. Chromoanasynthesis reflects the idea of synthesizing a new chromosome. In comparison to the two other types of chromoanagenesis, chromoanasynthesis is a replication error based phenomenon, in which microhomology-mediated break induced repair (MMBIR) and fork stalling and template switching (FoSTeS) are the processes that mediate the reassembly after breakage and lead to CN changes in specific regions (**Figure 7** B) [122,123].

In contrast to chromoplexy and chromoanasynthesis chromothripsis occurs very locally, distinct to only a very few chromosomes. Repair via NHEJ introduces inversions, duplications, deletions, and so-called double-minute chromosomes. These are small circular fused DNA fragments that might be composed of OGs and thereby, promote tumor progression (**Figure 7** C) [124,125]. For example, members of the MYC transcription family were detected in double-minute chromosomes in small-cell lung cancers [38]. In addition, double-minute chromosomes can lead to chemotherapeutic resistance [126].

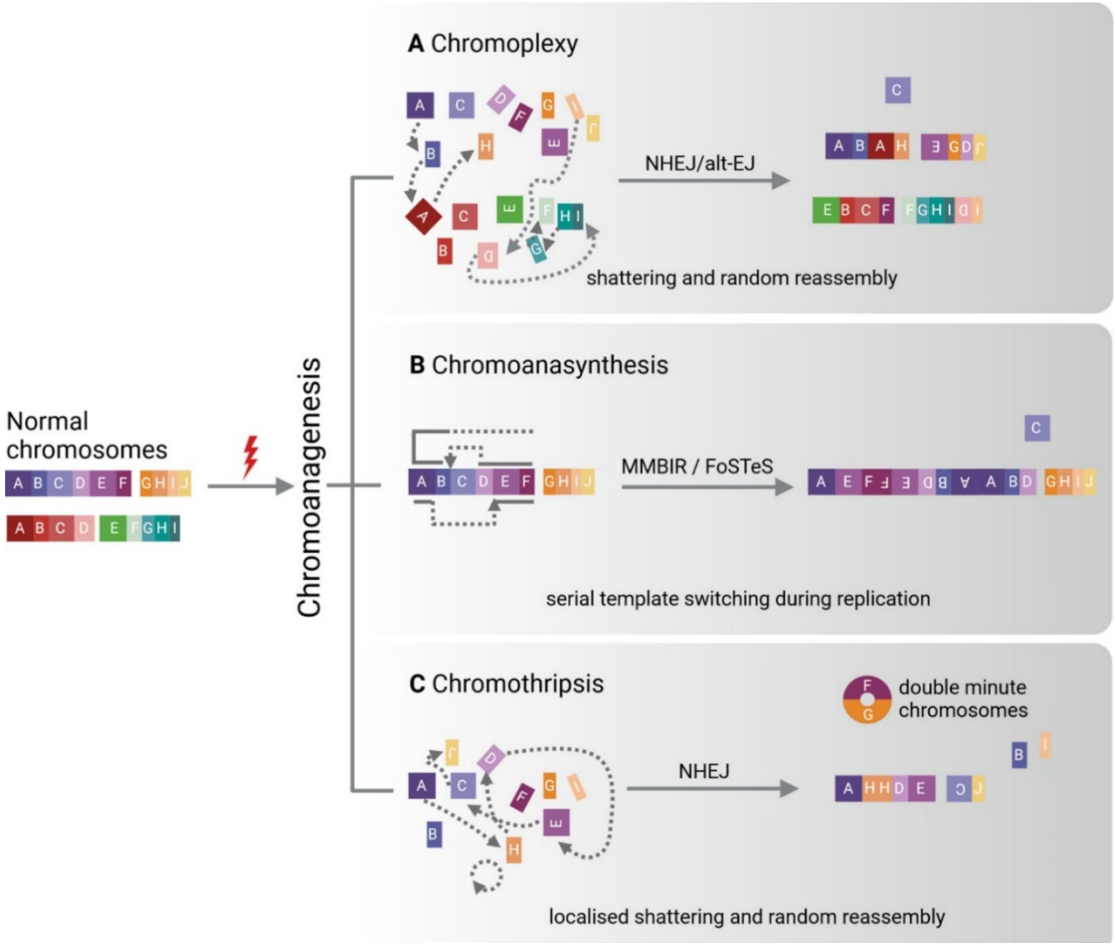

Figure 7: Chromoanagenesis. A: Chromoplexy**.** Repair via non-homologous end-joining (NHEJ) or alternative end-joining (alt-EJ)**. B:** Chromoanasynthesis. Repair via microhomology-mediated break-induced repair (MMBIR) or fork stalling and template switching (FoSTeS). **C:** Chromothripsis. Repair via NHEJ (from Keuper et al, 2021[39]).

Several characteristics have been established since the discovery of chromothripsis that help not only to identify the phenomenon but also to distinguish it from the other rearrangement types:

1. Oscillating CN states mostly between 2 or 3 states [38].
2. If fragments are not lost, then they join at a random position, and in random order and orientation [127].
3. A high number of complex rearrangements [128].
4. Those usually affect only one haplotype [127].
5. They arise from clustered DSBs (5–10 breaks in 50 kb followed by long tracts of intact chromosomal sequence) [38].

Taken together, chromothripsis is a recently discovered and already well-characterized catastrophic event in tumorigenesis and cancer progression. It remains fascinating that chromosome pulverization can be reassembled by cellular repair pathways. However, this occurs randomly and with many mistakes. The causes and consequences of this shattering of the DNA became a huge area of research.

Chromothripsis from micronuclei

The absolute understanding of the causes of such an intracellular catastrophe, such as chromothripsis, remains unknown. However, some theories explaining the mechanisms behind chromosome shattering emerged over the past couple of years. The basis of it is the fact that only a specific and small part of the DNA is affected: Less than five chromosomes, most frequently only one chromosome or a part of it. This suggests that the problem cannot occur in interphase because chromosome decondensation results in a DNA mass that is unlikely to break in such a defined way. Importantly, a reliable replication is the basis of an accurate mitosis. Incomplete replication or unrepaired damage in S phase can result in segregation errors in mitosis [95,98,105]. Upon chromosome segregation errors a MN envelope might form to protect otherwise free DNA. Therefore, any damage that occurs exclusively to this MN affects only the chromosomes encapsulated within it. Several processes, such as transcription and replication in MN are not functional or delayed [99,129,130]. DNA damage might be consequence for example due to stalled replication [128]. MN can be reincorporated into the main DNA mass in the next cell cycle. In this way, DNA damage and repair may occur very localized, potentially resembling chromothripsis.

In 2015, DNA entrapped in MN was studied using a combination of single-cell sequencing and life-cell imaging. The results of this study showed the shattering and reassembly of a single chromatid in the MN [113]. Potential sources for DNA damage in MN are based on membrane integrity failures. The nuclear membrane forms actually to surround and protect free DNA after telophase. But the membrane of the MN might be not fully intact. This can result in defective cytoplasmic/micronuclear transport and leads to compromised DNA replication in MN [113,131–133]. In fact, the DNA replication in the MN itself is delayed in comparison to the respective main nucleus. Coupled with the finding of TREX1, a cytosolic nuclease that can enter the MN and cause DNA damage [134], a fragmentation of the chromosomes within the MN eventually leads to the characteristic chromothripsis pattern [129]. Moreover, the condensation might be premature for DNA in MN leading to many DNA breaks localized to the chromosomes entrapped in MN, which is eventually repaired via NHEJ [126,130,135,136]. Taken together, the DNA damage in MN is a valid model for the origin of chromothripsis as MN are small structures with outrageous sources of error.

To understand how chromothripsis arises from MN we utilized a model system called micronuclei-mediated chromosome transfer (MMCT). It is a biochemical procedure used to engineer a cell line of interest with an additional and defined chromosome. Noteworthy, not only cells with fully intact additional chromosomes are an outcome of the MMCT, but also cells that underwent massive chromosomal rearrangements on the newly introduced chromosome [137]. The procedure is based on a mouse donor cell line with an additional human chromosome that carries an antibiotic resistance marker. Culturing the cells for 48 h with colchicine induces mitotic slippage. Consequently, the

chromosomes encapsulate into MN (see methods, **Figure 38**). After the isolation process of the MN, these are fused to an acceptor cell line of interest, such as the near diploid chromosomally stable human colorectal cancer cell line HCT116 or the human telomerase immortalized non-cancerous fibroblasts RPE1. After fusion and selection, whole genome sequencing (WGS) reveals the cell´s karyotype and gives insights into the intactness of the additional chromosome [137]. This allows us to use a model system engineered to produce trisomic and tetrasomic cell lines to study chromothripsis from MN in depth.

The aneuploidy paradox

Aneuploidy is found in app. 90% of solid tumors [37] with high intra-tumor heterogeneity. It is associated with metastasis and poor prognosis for cancer patients. Thus, cancer cells grow fast and aggressively. However, this contradicts years of research on aneuploid model cells, showing that the addition of a single chromosome leads to worse proliferation [29,138,139]. This discrepancy is termed the aneuploidy paradox.

Model systems to study aneuploidy in human cells

Aneuploidy is challenging to study for three main reasons. First, it affects multiple genes. This makes it hard to decipher which gene or which combination of regulatory chains is responsible for a specific effect. Second, aneuploidy is context-dependent. Therefore, the regulation of specific processes might be different in the model, in comparison to real tumors, making it hard to translate the knowledge gained by experimental models to real-world problems, such as drug targets. And third, aneuploidy is hard to model. There are not many working model systems available to produce defined aneuploidies. Even in the CRISPR-Cas9 era, it remains hard to remove a specific chromosome from a cell or to introduce one.

Despite these difficulties, some model systems are established. To generate karyotypically heterogeneous cells: First, induction of mitotic failures and second by mutation of genes involved in chromosome segregation (**Figure 8** A) [140–144]. In this way, the direct effects of the maldistribution can be studied. Because chromosome maldistribution is random in these approaches, the effects of defined chromosome aberrations cannot be studied in this

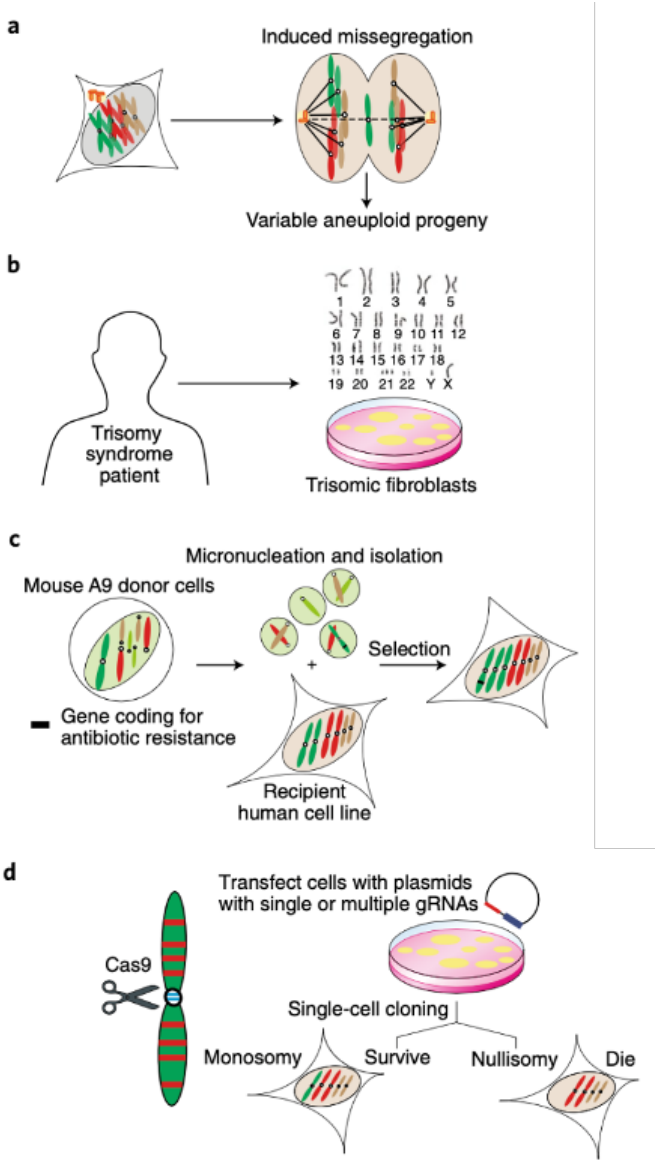

Figure 8: Model systems to study aneuploidy. A: Chromosome mis-segregation. **B: Patient-derived** cells. C: Micronuclei-mediated chromosome transfer. **D:** Whole chromosome depletion or deletion using CRISPR (clustered regularly interspaced short palindromic repeats) Cas9 (CRISPR-associated protein 9). gRNA = guide RNA (adapted from Chunduri and Storchová, 2019 [66].

setting. However, there are other systems available to study defined genomic aberrations: For example, cells can be collected from patients with trisomies for cell culture (**Figure 8** B). In addition, chromosomes can be specifically transferred to create defined trisomies or tetrasomies, for example using the MMCT (**Figure 8** C) [29,145,146]. Moreover, chromosomes can be selectively removed or silenced, e.g. using CRISPR-Cas9 (**Figure 8** D) [147–149]. Recently, an additional model system was shown to specifically target a chromosome of interest using guide RNAs for centromeric locations to induce defined mis-segregation [150].

Immediate consequences of chromosome gains

Cells that just gained additional chromosomes show independent of the cell or chromosome type common characteristics. MMCT-generated aneuploid cells with completely intact extra chromosomes have lower proliferative fitness in comparison to the wild type cells (**Figure 9**) [29]. A measure for this is the proliferation, which describes the cells' ability to grow and divide. It can be assessed using cell viability measurements based on intracellular ATP levels over a defined time course. Another measure is the ability of cancer cells to grow without anchorage. Soft agar assays allow the formation of colonies sitting within a layer of low-density agar. Forming colonies can be counted. The proliferation, as well as the growth on soft agar, are significantly reduced in cells with extra chromosomes. During the cell cycle, especially G1 and S phases are prolonged in newly engineered aneuploid cells [29,139]. This suggests a replication defect. Indeed, in 2016, Passerini et al. showed that the MCM 2-7 helicase is downregulated in aneuploid cells [138]. However, several studies showed that at least subunits of the helicase are upregulated in several human cancer tissues, for example in colon, breast, prostate, and renal cancers [151–154]. Aneuploid cells with additional chromosome experience elevated levels of replication stress associated protein phosphorylations, such as the phosphorylation of the replication protein A (RPA) at position S33 in the subunit 2 (pRPA2 S33). Moreover, the DDR, mitotic errors, and chromosomal rearrangements are of higher abundance in these cells as in the corresponding wild types [138]. Interestingly, autophagy and proteasomal activity are upregulated after chromosome addition, suggesting the cells suffer from proteotoxic stress based on the additional chromosome with transcribable and translatable genes [155] (**Figure 9**).

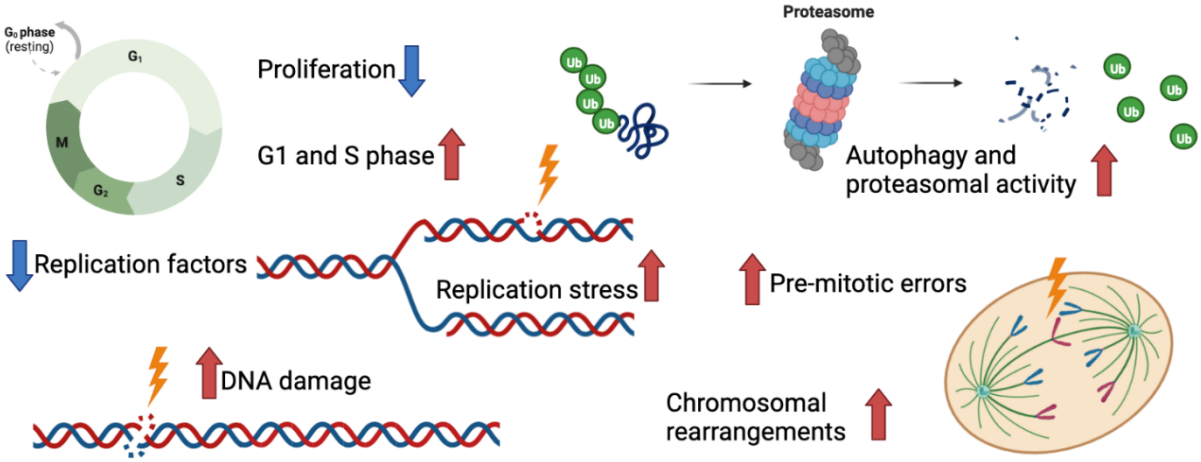

Figure 9: Immediate cellular consequences of aneuploidy. Characteristics of engineered aneuploid cells with full additional chromosome are a lower fitness, coupled with worse proliferation in comparison to the wild type and a prolonged G1 and S phase. Important replication factors, such as the MCM 2-7 helicase are downregulated, and replication stress is increased. More DNA damage is detected in cells with additional chromosomes leading to more mitotic errors, such as anaphase bridges and micronuclei. Further chromosomal rearrangements are observable in fresh engineered aneuploid cells and a higher autophagy and proteasomal activity (created with Biorender.com).

Consequences of whole genome doubling (WGD)

In metastatic cancers, the frequency of WGD reaches up to 56% [156]. Examples of WGD events are mitotic segregation errors, cytokinesis failures, and endoreplication (replication of all chromosomes without mitosis and cytokinesis) (**Figure 10**). A WGD event in humans causes most of the affected cells to arrest. Those which do not arrest do not necessarily maintain a tetraploid karyotype but frequently undergo karyotype changes over time, thus, WGD can start a CIN cascade. The resulting aneuploid karyotypes provide the cells with improved adaptability in stressful and new environments [31,156]. WGD is one of the most frequent genomic aberrations in cancer [156]. Thus, the instability-promoting consequences of WGD are essential to understand the implication of new biomarkers and potential therapeutic targets.

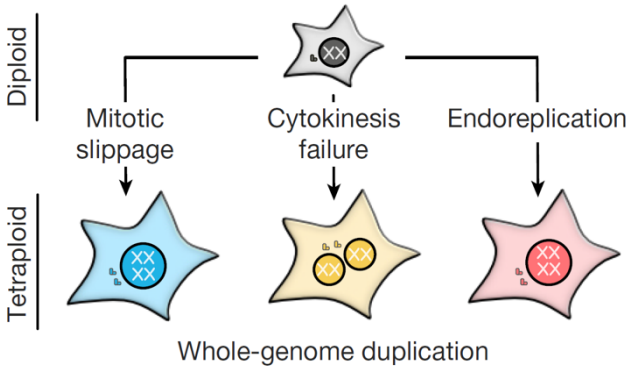

Figure 10: Induction of whole genome duplication (WGD) (adapted form Gemble et al, 2022 [197]).

WGD is linked to chromosomal instability (CIN)

WGD is known to happen early in human tumor evolution even without pre-existing genetic lesions. However, if a driver mutation is found, it is most frequently *TP53*, the TSG encoding for p53. In other cases, where there was not this TSG specifically mutated, a defective G1 arrest was detected, mediated by E2F [31]. The E2F transcription family is involved in cell cycle regulation, in which E2F 1-3 care for the G1/S transition [157–159]. A cell that underwent WGD tends to lose and less frequently also gains chromosomes over time, illustrating the instability of the chromosomes which is linked to cancer genome evolution [31,160–164]. CIN also connects WGD to metastasis, and drug resistance and thus limits a patient´s survival prognosis [31,156,165]. CIN facilitates a fast selection of OG upregulation and/or TSG downregulation as there is a high karyotypic heterogeneity within the cell populations and this enables the further expansion of the hallmarks of cancer.

WGD is not only linked to early-stage tumorigenesis but also to driving metastasis and worse prognosis [31,156]. Cells that undergo a WGD event have suddenly doubled the amount of DNA. This produces chaos as the DNA needs to be transcribed, translated, and eventually replicated. For this purpose, enough of the essential proteins and organelles must be present. This stressful situation causes many cells to undergo p53-mediated cell cycle arrest, senescence, or apoptosis. The p53 activity is mediated by the inhibition of murine double minute 2-protein (MDM2), an E3 ubiquitin-ligase that under normal circumstances acts in a negative feedback loop with p53 to signal its destruction [166–168]. But in hTERT RPE1 (hereafter RPE1) and in mouse embryonic fibroblasts, tetraploidy led to the initiation of the Hippo pathway activating large tumor suppressor kinase 1 and 2 (LATS1 and 2) that eventually inhibit MDM2

[169,170]. This way, p53 is stable and causes p21 upregulation, leading to G1 arrest [171,172]. Another p53 activating mechanism is the centrosome amplification and the formation of multipolar spindles (**Figure 4**). This activates p53 activity as well [173,174] but the exact mechanisms remain unknown. A study showed that additional centrosomes recruit the PIDDosome to induce MDM2 destruction via Caspase 2. This stabilizes p53 and leads to p21-mediated cell cycle arrest [175].

WGD is linked to genome instability (GIN)

An interesting observation during the replication of polyploid genomes is that there are specific under-replicated regions. This has been studied in drosophila salivary glands [176–178] and mammalian placental trophoblasts exhibiting huge polytene chromosomes [179]. Importantly, under-replicated regions contain genes [180–183], and can result in decreased gene expression [179,181]. GIN-driving occurrences are unique deletions with each endoreplication a cell might undergo [183] or localized specific gene amplifications, as seen in dipteran [184–187]. Taken together, these studies show that polyploidy, although it might balance the karyotype, can result in gene-specific CN changes. Thus, there is evidence that WGD causes sequence heterogeneity. To what extent this is reflected in human tumor development, though, remains to be investigated.

Aims of the study

Genomic aberrations are the basis for the adaptation of a cell to changing conditions. This applies not only to point mutations but also to CN changes from large genomic segments to entire karyotypes. We investigated the causes and consequences of these changes in three types of genomic aberrations with the following aims:

1. **To decipher the causes and consequences of massive chromosomal rearrangements in micronuclei**

MN are prone to DNA damage and are hypothesized to induce chromothripsis. We aimed to understand the molecular mechanism behind massive DNA damage in MN. Therefore, we investigated parameters of the MN envelope integrity, DNA damage, and replication using MN from the MMCT, a method to introduce a specific chromosome to a cell line of interest via MN. The transferred chromosomes often underwent chromosomal rearrangements during the MMCT, making it a decent model to study also the consequences of these massive rearrangements in defined chromosomes. To shed light on this aim, we investigated the anchorage-independent growth ability, and mitotic errors and correlated these functional parameters to the calculated extra DNA gained by each cell line.

2. **To shed light on how cancer cells overcome the detrimental consequences of aneuploidy**

In contrast to the cell lines with shattered additional chromosomes, the MMCT usually results in cell lines with a fully intact additional chromosome of interest. Interestingly, these aneuploid cell lines with whole chromosome gains showed worse proliferation with reduced levels of the MCM 2-7 helicase in comparison to their corresponding wild types. As this contrasts with fast-growing aneuploid cancer cells, we aimed to shed light on the question of how cancer cells overcome the detrimental consequences of aneuploidy. To approach this question, we cultured aneuploid cell lines for at least 160 generations. In parallel, we used previously generated post xenografts [139]. We aimed to identify altered biological pathways in the cells after evolution in comparison to before using multi-omics and aimed to validate the findings in the laboratory. Moreover, we asked whether the replication stress observed in aneuploid cells was alleviated upon evolution and performed a single-molecule analysis using DNA combing to assess the replication defect observed in aneuploid cells.

3. **To elucidate the consequences of WGD**

CIN as well as GIN are linked to WGD due to recurrent replication and mitotic failures raising several questions of the contribution of WGD to tumorigenesis. First, we aimed to investigate the molecular mechanisms that enable tetraploid cell survival. We asked why some cells survive WGD and others do not. To this end, we performed mass spectrometry data analysis of a coimmunoprecipitation of

candidate proteins identified in genetic screens. Second, we asked what happens immediately after a WGD event, as one tetraploidization event is sufficient to facilitate tumorigenesis [34]. We performed DNA combing to study potential replication defects directly after WGD. Third, cells that survive WGD become aneuploid with many chromosomal rearrangements. We aimed to decipher the patterns of aneuploidy in tumor cells that underwent WGD in comparison to those that did not. This might elucidate recurrence patterns that could craft them as biomarkers for further biomedical studies. To this end, we assessed the karyotypes of control and polysomic cells in comparison to post-tetraploid cells.

As different as these genomic aberrations may be, they have in common to alter the genome, and subsequently, to facilitate adaptations that could provide the cells with a fitness advantage. Understanding the detailed cellular consequences of genomic aberrations might therefore lead to a profound understanding of tumorigenesis and tumor progression.

Results

Massive chromosomal rearrangements in micronuclei (MN)

Micronuclei (MN) are prone to rupture which exposes the DNA content to fractions of the cytosol eventually leading to DNA damage [134]. To engineer aneuploid cells with defined additional chromosomes we perform the MMCT, a method in which the chromosomes are isolated and transferred to a cell line of choice using micronuclei. Upon genomic karyotype analysis, we found massive chromosomal rearrangements, including chromothripsis in 6 out of 51 aneuploid cell lines with the damage mostly on the additional chromosome itself [137]. This makes the MMCT a model to study the causes and consequences of massive genomic rearrangements in MN on defined chromosomes.

DNA in MN replicates asynchronously

A potential cause of DNA damage is delayed replication in MN in comparison to the respective primary nucleus (PN) and subsequent premature chromatin condensation of the DNA in MN [99,129,130]. To investigate if the DNA in MN replicates asynchronously, we treated RPE1 cells 20 h after an MN fusion with the thymidine analog 5-Ethynyl-2'-deoxyuridine (EdU) to visualize replicating DNA. Upon microscopy data analysis, we found only 1% of the captured MN replicating at the same time as the PN (**Figure 11**). While most of the asynchronous cell population was not replicating, 10% of the cells only showed EdU signal in the PN, whereas 4% showed the EdU signal only in MN. Taken together, among the replicating cells, most MN deviated in time from PN. This asynchronously replicating DNA

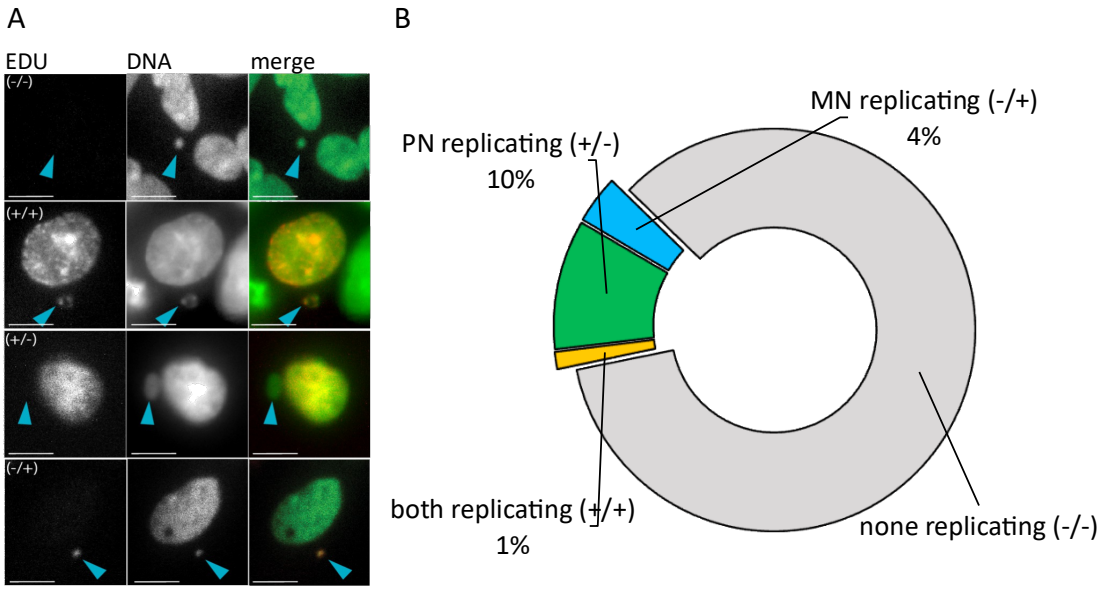

Figure 11: Asynchronous replication in MN after MMCT. The replication of RPE1 cells was captured with EDU 20 h after fusion with an additional chromosome. **A:** Representative captures. MN are marked with blue arrowheads. DNA was stained with SYTOX™ Green, and 78 cells were quantified. Scale bar: 10 µm. **B:** Quantification of replicating DNA according to the categories. A plus (+) stands for replicating DNA and a minus (-) for non-replicating DNA. The first sign in the bracket corresponds to the DNA in the primary nuclei (PN) and the second sign corresponds to the DNA in the MN (together with Aaron Gill; adapted from Kneissig et al, 2019 [137]).

in MN might be timewise behind the PN, eventually leading to premature condensation and DNA damage. Therefore, this asynchrony of the replication marks a first indication of the origin of DNA damage in MN after MMCT.

The membrane integrity of MN is compromised

The asynchronous replication suggests stress in the MN, which might be caused by the impairment of the nuclear envelope integrity. Previous studies showed that cytosolic fractions might enter the MN, eventually leading to DNA damage [134]. We asked whether this is the case for the MN in our experimental setup and co-transfected murine A9 cells with a plasmid encoding a cytoplasmic localization signal (CLS) and a plasmid encoding a nuclear localization signal (NLS). The CLS was the protein EB3, a microtubule-binding protein, tagged to the green fluorescent protein (GFP) (CLS-GFP). The NLS was tagged to the red fluorescent protein (RFP) (NLS-RFP) (**Figure 12 A**). Fluorescence microscopy revealed the CLS and the NLS colocalization after MN isolation, as we observed the signal mixture within 14% of the isolated MN. 2% of the MN showed only the NLS and 84% MN was visible only by the DAPI signal (**Figure 12 B, C**). This corresponded to an estimated transfection efficiency of 16%. Together, this suggested that MN are prone to rupture of the envelope and that cytosolic material can enter the MN after isolation.

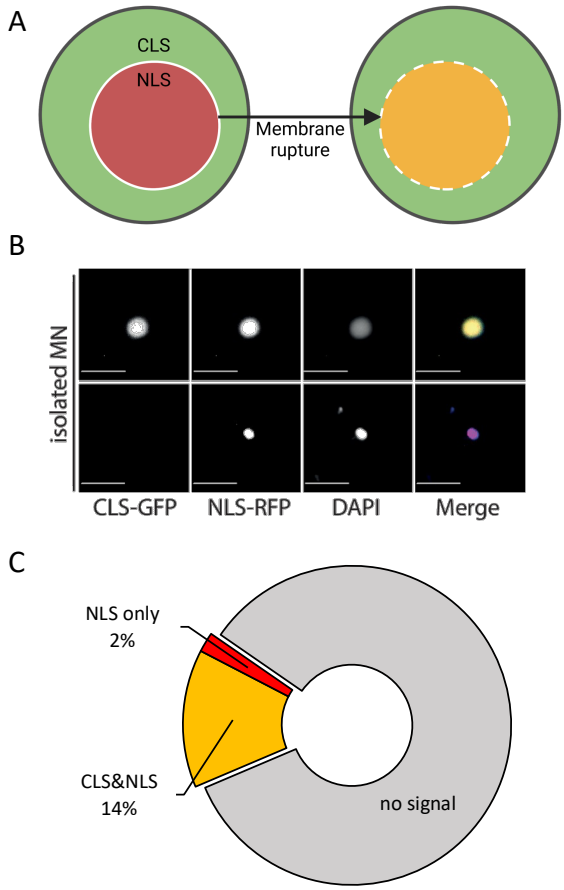

Figure 12: Membrane integrity loss after MN isolation during MMCT. A: Functional scheme of cytoplasmic localization signal (CLS-GFP) and nuclear localization signal (NLS-RFP). **B:** Example captures of isolated MN during MMCT. Top panel: MN with ruptured membrane. Bottom panel: MN with intact membrane. **C:** Percentage of isolated MN with and without colocalization of CLS and NLS. Scale bar: 10 µm (together with Jana Martin; adapted from Kneissig et al, 2019 [137]).

The isolation process of MN increases the potential for DNA damage

We asked whether mechanical stress during the MMCT influences the amount of DNA damage in MN as a long and intense centrifugation step was executed to isolate the MN. To test this, we performed γ-H2A.x immunostaining after four Cytochalasin B (DCB) incubation time points each, with and without centrifugation. γ-H2A.x is the phosphorylated histone 2A, a marker of DSBs. We found that the less time the MN spend in DCB, the less DNA damage occurs within them. Moreover, DCB incubation without centrifugation was less harmful to the DNA in MN compared to DCB incubation with centrifugation. Usually, the centrifugation during the chromosome transfer takes 30 min. After the prolonged timepoint of 45 min of DCB treatment, the percentage of MN with foci without centrifugation was almost as high as the percentage of MN with foci with centrifugation (**Figure 13**). Thus, the incubation in DCB and centrifugation contribute to the DNA damage phenotype after a chromosome transfer. We proposed that DCB which inhibits actin polymerization was at least partially responsible for the DNA damage in MN. To avoid bias based on isolated MN, we performed the subsequent research on the causes of DNA damage in MN in A9 cells after mitotic slippage, before isolation.

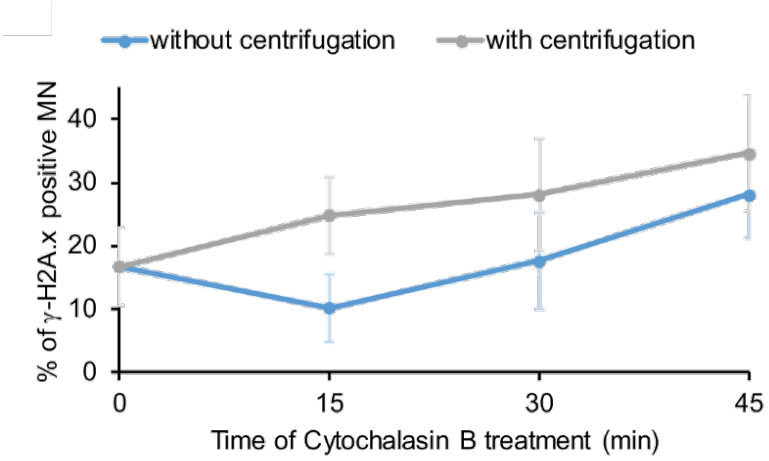

Figure 13: DNA damage in MN during Cytochalasin B treatment time. Immunostaining of γ-H2A.x to distinct timepoints after Cytochalasin B treatment with (grey) or without centrifugation (blue) (experiments were performed together with Jana Martin; adapted from Kneissig et al, 2019 [137]).

DNA damage occurs primarily in MN lacking lamin B1

MN are prone to lose important membrane-associated proteins, including stabilizing factors coating the inner of the nuclear envelope, such as lamin proteins [132]. The loss of these proteins impairs the integrity of the nuclear envelope and the DNA might be exposed to cytosolic components. This was shown to cause DNA damage [134]. Therefore, we asked whether the MN lacked functional lamin proteins and whether we could observe DNA damage immediately after mitotic slippage in the murine A9 donor cells. To this end, we transfected the cells with CLS-GFP prior to immunofluorescence to detect lamin B1 and γ-H2A.x. We determined the MN size, DNA damage, the lamin B1, as well as the CLS-GFP presence within one experimental setup (**Figure 14** A) and found several interesting aspects:

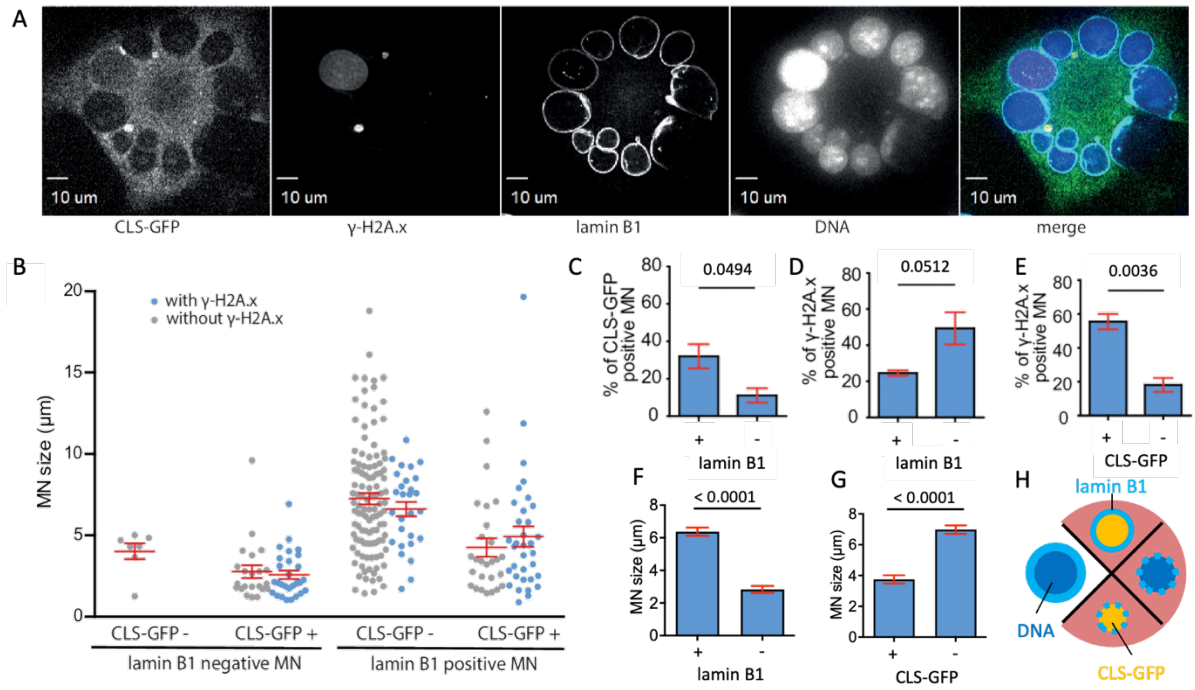

Figure 14: DNA damage in MN. A: Representative captures of CLS-GFP transfected micronucleated A9 cells. Immunostaining was performed to detect lamin B1 and γ-H2A.x. DNA was detected with DAPI. **B:** Quantification of MN size (diameter) that are lamin B1 positive and negative, CLS-GFP positive, and negative and have a γ-H2A.x signal (blue) or not (grey). **C:** Percentage of CLS-GFP positive MN comparing lamin B1 positive and negative MN. **D:** Percentage of γ-H2A.x positive MN comparing lamin B1 positive and negative MN. **E:** Percentage of γ-H2A.x positive MN comparing CLS-GFP positive and negative MN. **F:** MN size (diameter) of lamin B1 positive and negative MN. **G:** MN size (diameter) of CLS-GFP positive and negative MN. Two-sided unpaired student´s t-test p-values are shown. **H:** Schematic depiction summarizing studied MN parameters, where the red background shows the principally higher DNA damage potential (adapted from Kneissig et al, 2019 [137]).

First, among the MN that lacked lamin B1 only very few MN were detected without CLS-GFP. Most of them had the cytosolic signal, suggesting that membrane rupture caused CLS-GFP entry (**Figure 14** B, C). In line with that hypothesis, more γ-H2A.x positive MN were detected in lamin B1 negative MN and CLS-GFP positive MN (**Figure 14** D, E). Second, among the MN with intact lamin B1, still a high fraction of MN showed CLS-GFP entry and DNA damage (**Figure 14** B, C, D). This suggested that lamin B1 was not the only factor that upon its loss caused CLS-GFP entry. Third, lamin B1 negative MN were consistently smaller compared to lamin B1 positive MN. Moreover, CLS-GFP positive MN were smaller as well in comparison to MN without cytosolic fraction entry (**Figure 14** B, F, G). Together, this might imply that smaller MN are more error-prone in comparison to larger MN.

Overall, these findings underline the hypothesis, that lamin B1 stabilizes MN envelope integrity at least partially and that the entry of cytosolic fractions into the MN is at least to a certain extent causative for DSBs. Moreover, the size of the MN might be an important parameter for the MN envelope integrity (**Figure 14** H).

Therefore, we further addressed the observation of smaller MN undergoing more frequent DNA damage. As the MN size usually correlates with the DNA content, the finding raised the question whether the MN without lamin B1 also contained less DNA. To test this hypothesis, we counted the number of centromeres in MN using a centromeric antibody. We found a slight positive correlation between the MN diameter and the number of contained centromeres. Moreover, the size of the lamin B1 positive MN was consistently higher in comparison to the size of the lamin B1 negative MN (**Figure 15**). These results demonstrated that smaller micronuclei usually contained less DNA and more frequently lacked lamin B1. Interestingly, spontaneously arising MN in RPE1 cells had the same phenotype [137].

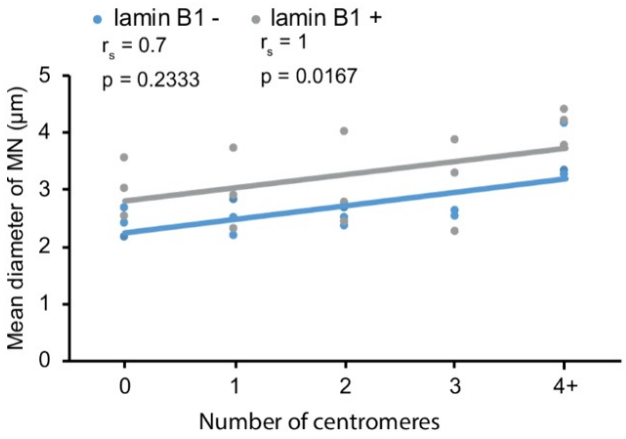

Figure 15: Size of MN and centromere counts in lamin B1 negative (-) and positive (+) MN. Number of counted centromeres vs. mean diameter of MN with (grey) and without (blue) lamin B1 after colchicine treatment. Three independent experiments with n=170 MN. r_s = spearman rank correlation coefficient (experiment was performed together with Jana Martin; adapted from Kneissig et al, 2019 [137]).

Altogether, there are multiple complications occurring in MN besides the asynchronous replication: First, the MN envelope integrity was compromised, leading to exposure of the DNA to the cytosol with subsequent DNA damage. Second, cytosol could enter the MN with and without lamin B1, suggesting an additional parameter leading to cytosol entry and DNA damage. And third, MN lacking lamin B1 were smaller. With the finding of asynchronous replication, the DNA in MN has the potential to result in massive chromosomal rearrangements, such as chromothripsis.

We identified massive chromosomal rearrangements in app. 11.8% of the studied cell lines [137]. In the following paragraph on the consequences of reshuffled chromosomes, I simplified the CN based category of cell lines with (nearly) intact additional chromosomes to "without rearrangements" and the category of cell lines with many rearrangements to "with rearrangements"(see methods **Figure 37**) (**Table 1**) [137].

Table 1: Cell line classification. Cell lines from CN analysis are classified by the presence or absence of rearrangements. If the additional chromosome had (nearly) no rearrangements, the cell line with its additional chromosome was considered as "without rearrangement". If the cell line harbored many changes on the extra chromosome, it was marked as "with rearrangements".

Without rearrangements	With rearrangements
Hte5_14	Hte5_01
Htr5_17	Htr5_16
Htr5_18	Htr5_19
Htr13_02	Htr13_03
Htr18_01	Htr18_02
Htr21_01	Htr21_03

Reshuffling of a chromosome leads to functional advantages for the cell

We determined the physiological consequences for the cells that were able to repair the shattering and compared them to cell lines that gained a full additional chromosome. First, we assessed the cancer cell´s ability to proliferate without anchorage in a soft agar assay. We found that the cell lines with more rearrangements (Htr5_16, Htr5_19, Htr13_03, Htr18_02) grew better in soft agar in comparison to their not rearranged controls (Htr5_17, Htr5_18, Htr13_02, Htr18_01) (**Figure 16** A). We asked whether more additional genomic material could hinder cells from anchorage-independent growth, as was shown by Sheltzer et al. in 2017 [139]. To this end, we calculated the amount of additional DNA based on the genomic CN data (**Figure 16** B). In almost all rearranged cell lines, the amount of additional DNA was lower, supporting previous findings that chromothripsis events resulted in loss of genomic material [113]. Strikingly, the ability to grow in an anchorage-independent manner negatively correlated with the amount of additional genomic DNA. Taken together, less additional DNA in cells with extreme rearrangements provided the cells with an improved fitness in comparison to the cell lines with fully intact additional chromosomes.

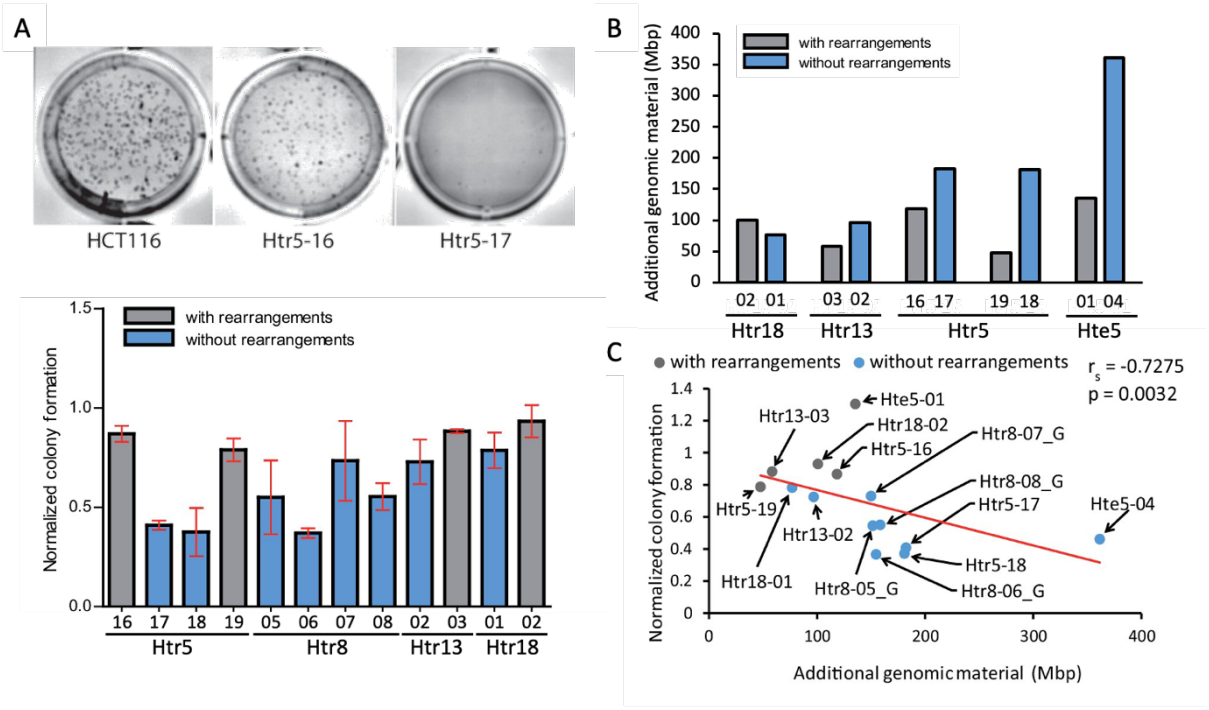

Figure 16: Anchorage-independent growth ability and additional DNA. A: Soft agar assay. Top panel: Example captures. Bottom panel: Quantification of colony formation ability of cell lines with (grey) or without rearrangements (blue). SEM of four biological replicates. **B**: Additional genomic DNA in cell lines with (grey) or without rearrangements (blue) calculated from sequencing data. **C:** Correlation of normalized colony formation ability and additional genomic DNA in cell lines with (grey) or without rearrangements (blue). Spearman rank correlation coefficient (r_s) and two-tailed t-test p values (p) are shown (together with Jana Martin and Maja Kneissig; adapted from Kneissig et al, 2019 [137]).

Finally, we asked whether the rearrangements influence the number of mitotic errors as functional parameters. To this end, we assessed the number of anaphase bridges (AB) as late consequences of replication stress and the number of MN as markers of GIN (**Figure 17** A). Quantification of AB revealed

that cell lines with rearrangements had either less or equal anaphases with bridges, but not more in comparison to the respective aneuploid model cells without chromosomal rearrangements (**Figure 17** B). The same pattern was observed for MN (**Figure 17** C). A correlation analysis revealed a negative relationship between the ability to grow anchorage-independently and the amount of AB (**Figure 17** D) or MN **(Figure 17** F). The strongest outlier in both cases was Hte5_01, a cell line that underwent

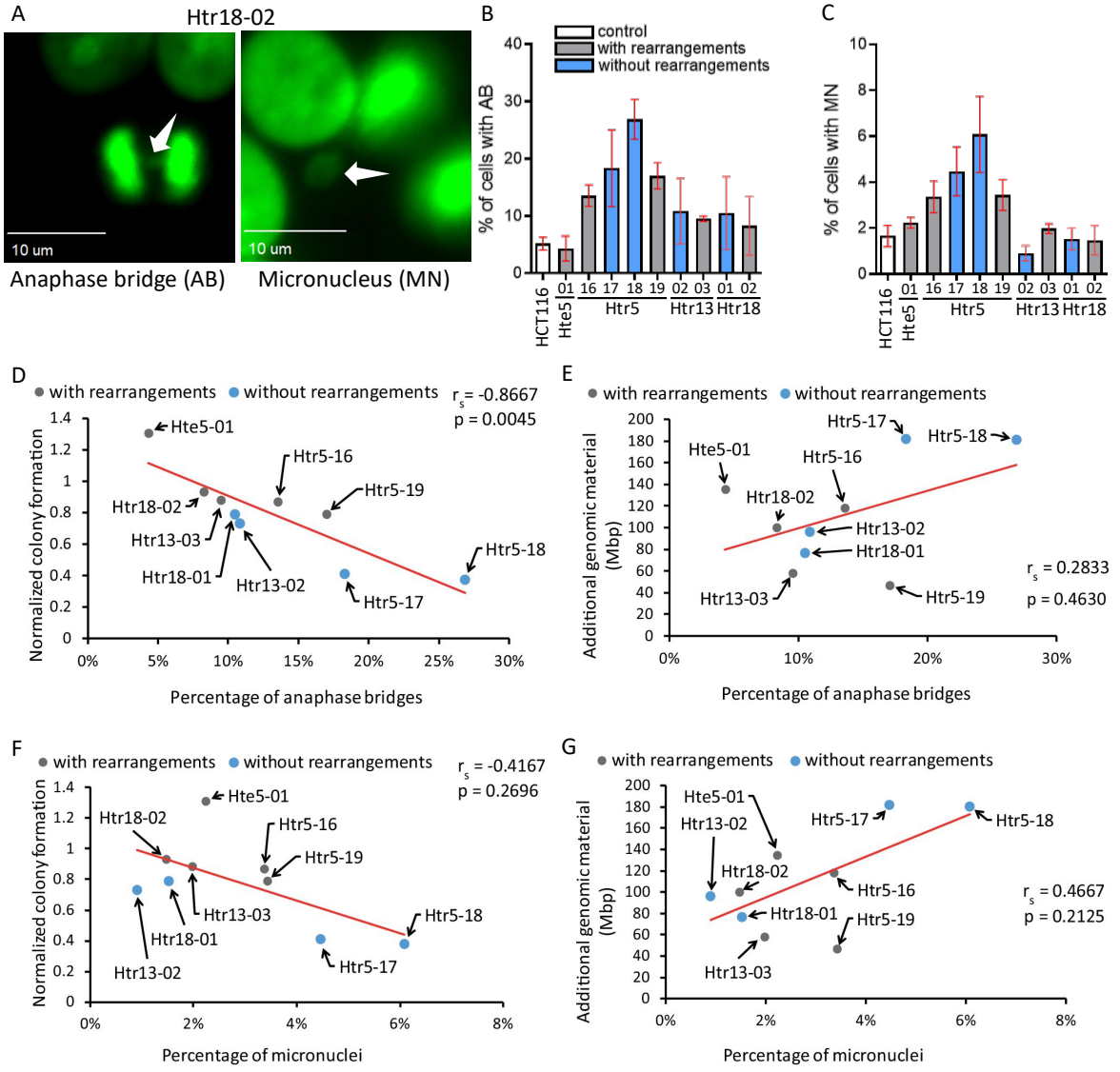

Figure 17: Functional advantage of cell lines with rearrangements. A: Exemplary capture of an anaphase bridge (AB) (left) and a micronucleus (MN) (right) from Htr18-02. The mitotic error is highlighted with the white arrow. DNA was stained with SYTOX™ Green. **B, C:** Quantification of AB (**B**) and MN (**C**) in cell lines with (grey) or without rearrangements (blue). SEM of 4 biological replicates **D:** Correlation of colony formation ability and AB. **E:** Correlation of additional genomic DNA and AB. **F:** Correlation of colony formation ability and MN **G:** Correlation of additional genomic DNA and MN. **D-G:** Cell lines with (grey) and without rearrangements (blue) are shown. Spearman rank correlation coefficient (r_s) and two-tailed p values (p) were calculated (together with Jana Martin and Maja Kneissig; adapted from Kneissig et al, 2019 [137]).

chromothripsis [137]. The cell line harbored only a very low number of mitotic errors and grew well in soft agar. Noteworthy, the correlation analysis between the amount of additional DNA and the AB (**Figure 17** E) or MN (**Figure 17** G) showed a positive trend in both cases. These results implied that cell lines with more intact DNA were more likely to undergo mitotic failures, such as AB and MN. In

contrast, the cell lines with less additional DNA, those that were more rearranged, were also less prone to mitotic errors. Consequently, the cells with many genomic aberrations showed not only a fitness improvement but also functional advantages.

To summarize, the replication in MN took place asynchronously and frequently the PN replicated while the MN did not. MN without functional lamin B1 and those with cytosol entry were smaller compared to those with intact lamina. Moreover, these smaller MN experienced more DNA damage. Interestingly, the rearrangements in the aneuploid cell lines led to a functional advantage of the cells in comparison to the cell lines with fully intact additional chromosomes. Cell lines with less DNA and more shuffled chromosomes improved the ability to grow anchorage-independently. These findings were suggestive of implementing the MMCT as a method to not only study defined aneuploidy but also defined chromosome shattering and reassembly. Since the cell lines with more rearrangements had consistently a fitness advantage, this might be linked to higher genomic flexibility provided by reshuffling events, such as chromothripsis, that increase the potential of tumorigenesis, metastasis and poor patient outcome [188–191].

The aneuploidy paradox

Engineering of model cells containing specific additional chromosomes resulted in poor outcomes of the cells ability to grow in an anchorage-independent manner and an increase in mitotic errors (**Figure 16**, **Figure 17**) [138,139]. The cells showed gene expression changes in several pathways, such as downregulation of the DNA replication, as well as an upregulation of lysosomes [29,138]. Moreover, the replication-associated MCM 2-7 helicase was downregulated in aneuploid cells [138]. This, and the proliferation decrease in aneuploid cells in comparison to the respective wild type [29,138] do not match the findings in aneuploid cancer cells, showing the ability to proliferate fast, sometimes by overexpressing the MCM 2-7 helicase [151–154]. To shed light on this so-called aneuploidy paradox, we used the previously MMCT-engineered cell lines with an intact additional chromosome and analyzed the physiological changes after the evolution of the cell lines in two approaches: First, we analyzed cell lines previously extracted from a xenograft model (post xenograft, px) [139] (**Figure 18**). These cell lines were evolved of the HCT116 derived trisomy 5 (Htr5) and tetrasomy 5 (Hte5). Second, we used an *in vitro* approach of prolonged cultivation (50 passages, p50) with the same cell lines, Htr5 and Hte5, and with RPE1 derived trisomy 21 (Rtr21) (generated previously by Sara Schunter, Martinsried, Germany). This evolution model was expanded by the prolonged cultivation of HCT116, HCT116 derived trisomy 3 (Htr3) and Hte5 for 80 passages in three independent biological replicates (e1-e3). All 20 passages, cells were collected (p0, p20, p40, p60, p80), and the CN of evolution clone 1 was analyzed after 50 passages (p50 e1). Using these evolution models, we performed proliferation assays and a global omics study to find deregulated pathways, which we aimed to validate. Furthermore, we addressed the replication machinery on single-molecule level and performed experiments to assess the replication stress and DNA damage signaling before and after evolution.

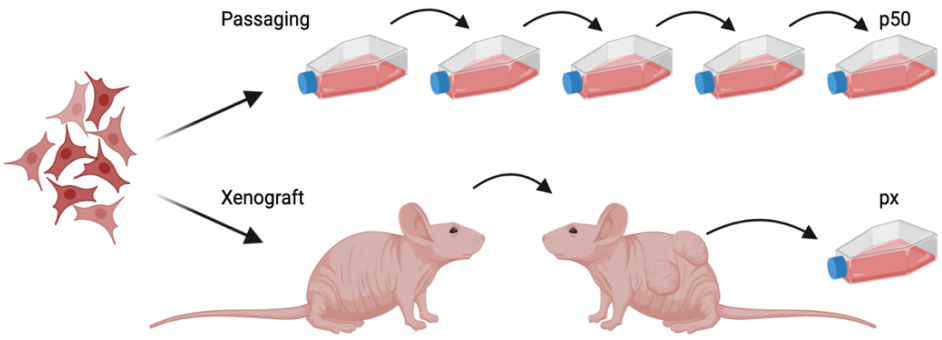

Figure 18: Evolution model systems. Upper panel: Passaging: *in vitro* cell culture-based approach to generate late passaged cell lines with at least 50 passages (p50). **Lower panel:** Mouse xenograft. *In vivo* evolution of cells in mouse xenografts and re-culturing of the post xenografts (px).

Aneuploid cells improve their proliferation over time

The proliferation is composed of cell division and cell growth and is therefore a parameter for the determination of cellular fitness. By this, it provides insights in how quickly the cells progress through the cell cycle. Aneuploidy was shown to reduce the proliferative fitness of cells [29]. Therefore, we tested whether prolonged culturing of the cells changes this phenotype, and if the cells adapt to the detrimental effect of aneuploidy. To this end, we performed CellTiter-Glo® Luminescent Cell Viability assays. Quantification of ATP in the cells allowed us to assess the relative cell number. To statistically evaluate the results, we determined the area under the curve (AUC) and calculated confidence intervals. Importantly, we observed a significant proliferation improvement of aneuploid cells after 50 passages. We did not see this change in wild type cells (**Figure 19** A, **Supplementary figure 7** A). To test interim steps during evolution, we performed another *in vitro* evolution by passaging HCT116, Htr3 and Hte5 for up to 80 passages, app. 260 generations. We collected cells from three independent replicates all 20 passages. Growth curves and AUC quantifications of these cells showed that the proliferation advantage in aneuploid cells happened mostly already within the first 20 passages, whereas aneuploid cells did not further improve the proliferation after 60 passages (**Supplementary figure 10**). Moreover, the proliferation of RPE1-derived trisomy 21 (Rtr21) slightly increased within 50 passages (**Supplementary figure 1** A). The proliferation of post xenografts was explored previously using focus formation assays. By this, Sheltzer et al. showed an improved capacity of anchorage-independent growth of the post xenografts in comparison to the aneuploid cells before evolution [139]. We asked whether the *in vitro* evolved cells improve the ability to grow without anchorage as well. To this end, we performed soft agar assays. In contrast to the post xenografts, the *in vitro* evolved cells

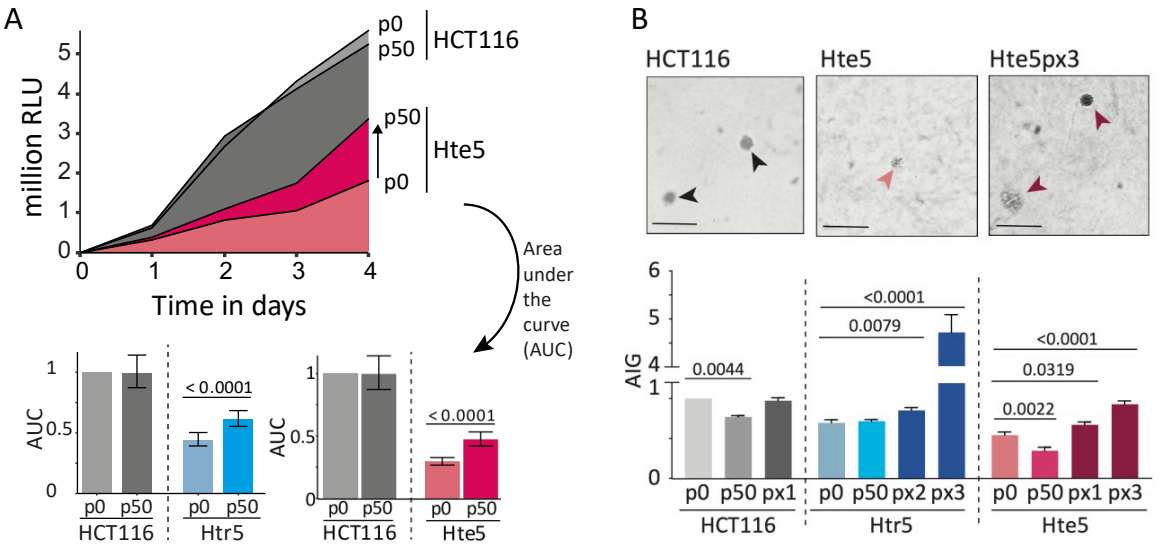

Figure 19: Cellular proliferation capabilities. A: Top panel: Exemplary growth curve of HCT116 and Hte5 before (p0) and after evolution (p50) in relative luminescence units (RLU). Bottom panel: quantification of area under the curve. 95% confidence intervals are shown (together with Sara Schunter and Jan Eric Bökenkamp). **B:** Top panel: Exemplary soft agar assay captures. Scale bar: 0.3 mm. Bottom panel: number of colonies per ml as measure for the anchorage-independent growth (AIG). Mann-Whitney test p values are shown (together with Stefan Redel).

did not improve this parameter of cellular fitness after 50 passages. Contrarily, in the wild type cells, as well as in Hte5 p50, we observed a decrease in the ability of anchorage-independent growth (**Figure 19** B). This suggested that the environment where the individual types of evolution experiments occurred shaped the cellular adaptations. Altogether, the cell culture-based model system revealed a significant proliferative advantage already after 50 passages, while these cells did not share the invasive phenotype of anchorage-independent growth that exists in the post xenografts.

Multi-Omics study reveals chromosome gains after evolution

Next, we performed a global top-down multi-omics approach by studying genomics, transcriptomics, and proteomics of the *in vitro* and *in vivo* evolved cell lines to determine aberrations at each level. The analysis was mainly performed by Jan-Eric Bökenkamp. Whole genome sequencing (WGS) revealed the CN of individual cell lines per chromosome. While Htr5 px2 indeed gained chromosome 3, all the post xenografts lost the engineered chromosome upon evolution as described previously [139] (**Figure 20**). However, the cell lines Hte5 and Htr5, as well as Rtr21 maintained the additional chromosome after 50 passages (**Figure 20**, **Supplementary figure 2**). Moreover, the cells accumulated other aberrations. Htr5 p50 lost parts of chromosome 12, which was additionally gained in Htr5 already before evolution. Strikingly, 50 passages in cells with additional chromosome 5 led to the amplification of chromosome 21, suggesting a connection between the gene expression on both chromosomes (**Figure 20**). The CN analysis during the prolonged evolution of HCT116-derived cells in evolution series/biological replicate1 (e1) revealed that Hte5 p50 e1 and Htr3 p50e1 lost the additional chromosome and Htr3e1 apparently did not have it at p0 (**Supplementary figure 11**). Together, the results allow the further investigation of the adaptation to aneuploidy in the *in vitro* evolved aneuploid cell lines Htr5, Hte5, and Rtr21 after 50 passages.

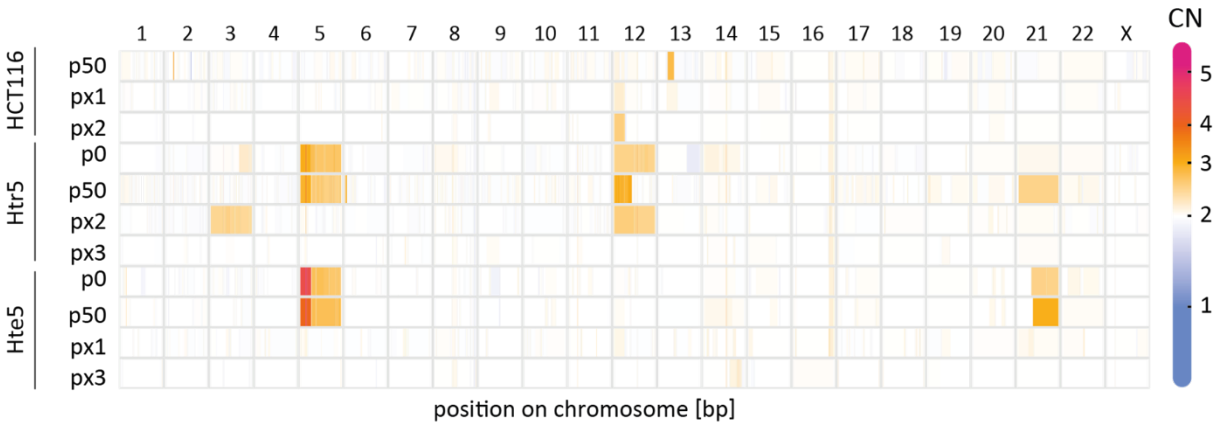

Figure 20: Karyotype analysis. Copy numbers (CN, see color scale) of individual chromosomes (columns) in analyzed cell lines (rows) per chromosome (columns) are shown. The copy number was normalized to HCT116 and is gradually color-coded (together with Jan Eric Bökenkamp).

Transcriptome and proteome analysis reveal deregulated pathways

Aneuploidy results in altered transcriptome and proteome levels that are partially dosage compensated [29]. Altered pathways were defined in the past. In comparison to the wild type, cell lines with chromosome gains have, among others, a lower amount of replication factors and a higher amount of lysosome-associated factors [29,138]. We recapitulated this phenotype with mRNA sequencing and tandem mass spectrometry (TMT) via annotation of the data with functional information from the Gene Ontology Cellular Compartments (GOCC) database. The data analysis was mainly performed by Jan-Eric Bökenkamp. We scored the transcriptome and proteome data according to a 2D annotation enrichment for visual comparison [192]. Changes after chromosome gain showed low abundances of replication associated pathways on mRNA and proteome level and, contrarily, upregulated lysosome associated pathways, both recapitulating the previous findings (**Figure 21** A). Strikingly, after 50 passages, the abundance of replication-associated pathways increased while the abundance of the lysosomal pathways decreased in comparison to Htr5 before *in vitro* evolution (**Figure 21** B). Thus, at least these two cellular machineries, replication, and lysosomes were regulated over the time course of app. 160 generations in adaptation to aneuploidy. This suggested that the initial proteotoxic burden of the cells with additional chromosomes, which likely activated the increased lysosomal activity was alleviated over time. In addition, the replication defect might be reduced as more replication proteins were available after evolution.

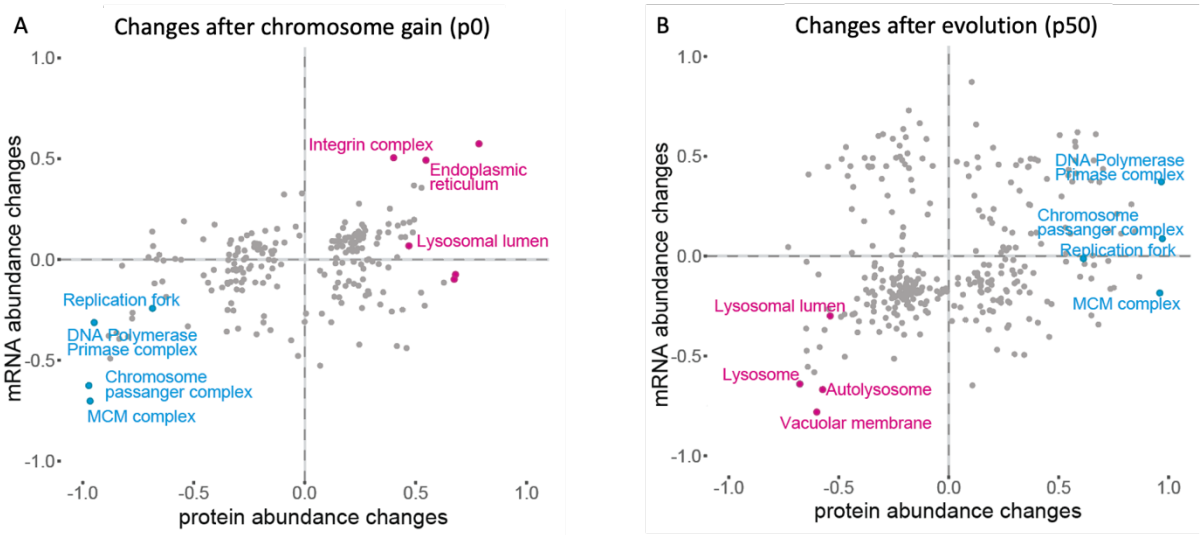

Figure 21: 2D annotation enrichment of transcriptome and proteome data before and after 50 passages of Htr5. **A:** Changes after addition of chromosome 5 to HCT116: Htr5 normalized to HCT116. **B:** Changes after serial passaging of Htr5: Htr5p50 normalized to Htr5. Score of proteins in specific pathways (Gene Ontology Cellular Compartments (GOCC)) was calculated (together with Angela Wieland, Markus Räschle and Jan Eric Bökenkamp).

The G1-S-transition is still delayed after evolution of aneuploid cells

In previous studies it was shown that aneuploid cells that have a lower amount of the MCM 2-7 helicase also encounter an impaired G1-S transition [29,138]. We asked whether a reversal of this defect by the increased replication protein abundances could be causative for the proliferation advantage. To test this, we performed FBS starvation to synchronize the cells in a G1 phase and subsequently collected seven timepoints after release. At all seven time points the cells were pulse labelled with the thymidine derivate 5-Ethynyl-2'-deoxyuridine (EdU) for 30 min to detect replicating DNA (**Figure 22** A**)**. With this setup, we were able to measure the approximate timepoint when most cells entered individual cell cycle phases. Replication entry was therefore defined as the timepoint measured to which the cells started incorporating EdU. We observed that wild type cells entered S phase after 8-12 hours both, before and after evolution. However, after evolution HCT116 had slightly more cells still in S phase after 24 h. In Hte5 p0 replication started later, with the previously described delay [29] after 12-16 h both, before and after evolution. Importantly, both, Hte5 p0 and p50, still had more cells in S phase in comparison to the HCT116 wild type after 24 h. Thus, the entry into S phase, as well as the progression through S phase were delayed with additional chromosomes. Thus, evolution of aneuploid cells did not change the cell cycle to a faster replication

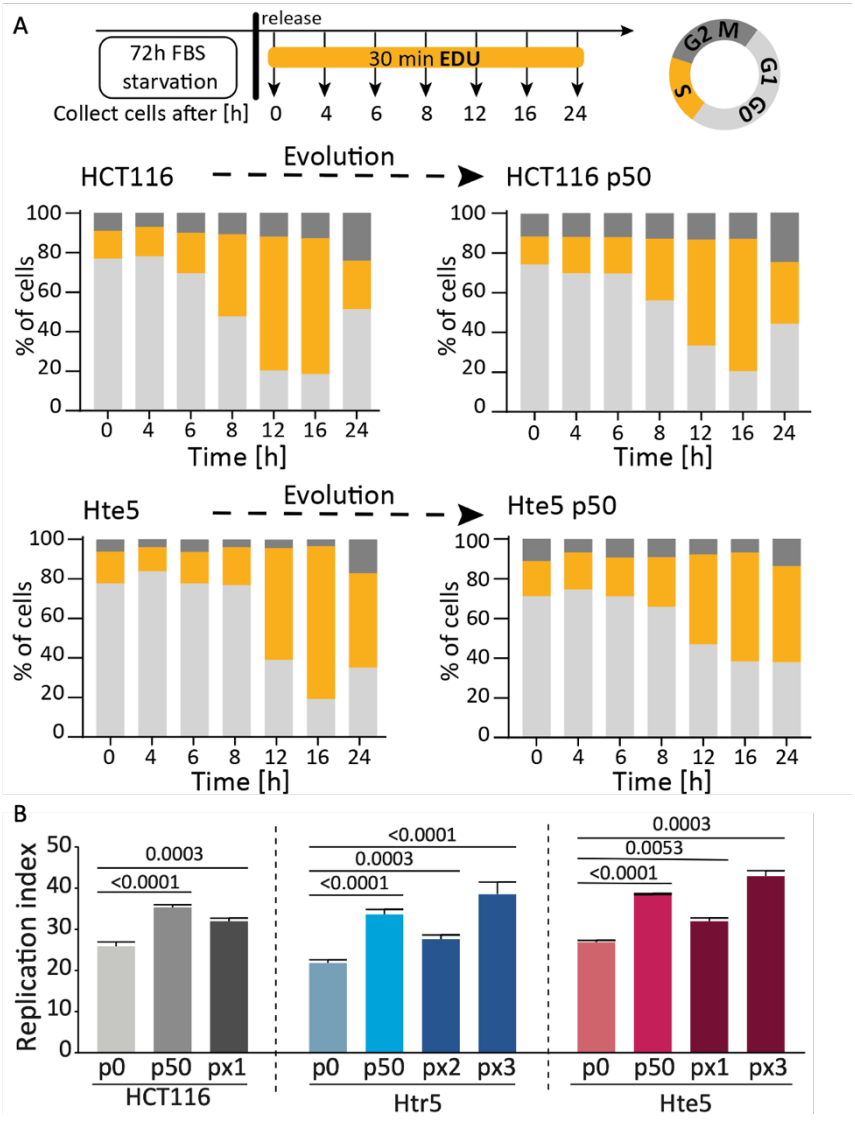

Figure 22: Cell cycle analysis. A: Synchronization experiment. Top panel: Model of synchronization with FBS starvation. Bottom panel: Percentage of cells in cell cycle stages according to color scale before evolution (left) and after evolution (right) in HCT116 wild type cells and Hte5. **B:** Percentage of cells in S phase calculated from unsynchronized cells (replication index). SEM and unpaired two-tailed student´s t test p values (together with Stefan Redel and Amelie Becker).

entry or progression as hypothesized. Indeed, Hte5 p50 had less cells in S phase between 12 and 24 h in comparison to the not evolved counterpart. More cells were in G1/G0 to this timepoint likely not overcoming the FBS starvation during the experimental time frame (**Figure 22** A**)**. Longer measurements might shed light on the question whether there are still replicating cells after 26-28 h in Hte5 p50. In line with these findings, the percentage of cells in S phase (replication index) in an asynchronous population was increased in all cell lines after evolution **(Figure 22** B**)**. This implied that the S phase progression took longer after prolonged culturing of the cells. The effect was higher in aneuploid cells after 50 passages in comparison to the respective wild type. Also post xenografts showed a slight increase of the replication index, whereas Htr5px3 and Hte5px3 had more cells in S phase then their other respective *in vivo* evolved counterparts **(Figure 22** B**)**. Moreover, RPE1 derived aneuploid cells with additional chromosome 21 did not show noteworthy differences in the percentage of cells per cell cycle phase, whereas both deviated from the RPE1 wild type that accumulated 25% less cells in early S phase (**Supplementary figure 1** B-D). Altogether, the observable delay in S phase after a chromosome gain was not rescued with evolution. In contrast, the progression through the S phase took even longer in HCT116 derived aneuploid cells after evolution. Despite this observation, the cells proliferated faster, which might be contradictory as replication timing is an essential part of the cell cycle.

Replication fork velocity is slowed after evolution

As an additional chromosome decreased replication protein abundances and delayed the S phase, we sought to investigate the replication before and after evolution on single molecule level. A possibility to explain the S phase slowdown, despite the faster proliferation after evolution might be a more faithful replication. DNA combing allowed to assess replication dynamics, such as the velocity of the replication fork and the number of active origins, as well as the fork symmetry (**Figure 23**). To investigate replication in the aneuploid cells, we treated the cell lines before and after evolution with two thymidine analogues: 30 min with 5-Chloro-2'-deoxyuridine (CldU) and subsequently, 30 min with 5-Iodo-2'-Deoxyuridine (IdU) to perform a single molecule analysis directly on the DNA fiber. After stretching the DNA via the so-called DNA combing, we used antibodies against CldU, IdU and against the ssDNA to visualize the full track length and analyzed different track patterns (**Figure 23**, see Methods for more details). Our data showed a tremendous slowdown of the replication machinery after evolution, which was not observed

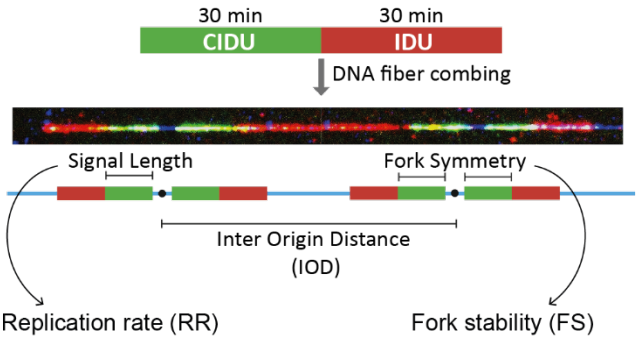

Figure 23: Schematic of DNA combing. Treatment with 5-Chloro-2'-deoxyuridine (CldU) and following 5-Iodo-2'-Deoxyuridine (IdU) allows for replicating DNA detection in form of stained tracks.

upon a gain of the extra chromosome. Moreover, the aphidicolin response led to the typical decrease of the fork velocity (**Figure 24** A, **Supplementary figure 4** B, **Supplementary figure 7** B). We observed this decrease of the replication rate in all cell lines that went through an evolution, no matter if there was an additional chromosome or not (**Figure 24** A). This suggests a general mechanism of HCT116 during adaptation to both, *in vivo* and *in vitro* evolution conditions. The slowdown of the replication speed was observed also in RPE1 derived trisomy 21 cells after evolution (Rtr21) (**Supplementary figure 4**). The inter origin distance (IOD) allowed for an estimation of the number of active origins. Mostly evolution caused a decrease of the inter origin distance, which translates into an increase in the number of activated origins (**Figure 24** B). Thereby, it compensates the replication machinery slowdown. We asked whether this balance of dormant origin firing as response to a decreased replication rate is related to an increased abundance of available replication proteins. To this end, we determined the abundance of the MCM 2-7 helicase by immunoblotting. In agreement with the proteomics results (**Figure 21**), the abundance of the MCM 2-7 helicase increased during the adaptation time of app. 160 generations (**Figure 24** C), the difference between Htr5p0 and Htr5p50 is visible but not significant, likely due to one strong outlier. The difference between Hte5 and Hte5p50 is significant. The MCM 2-7 helicase abundance of the evolved wild type increased only mildly, similar to the post xenograft cell lines that did not show a significant increase in the helicase levels. Of note,

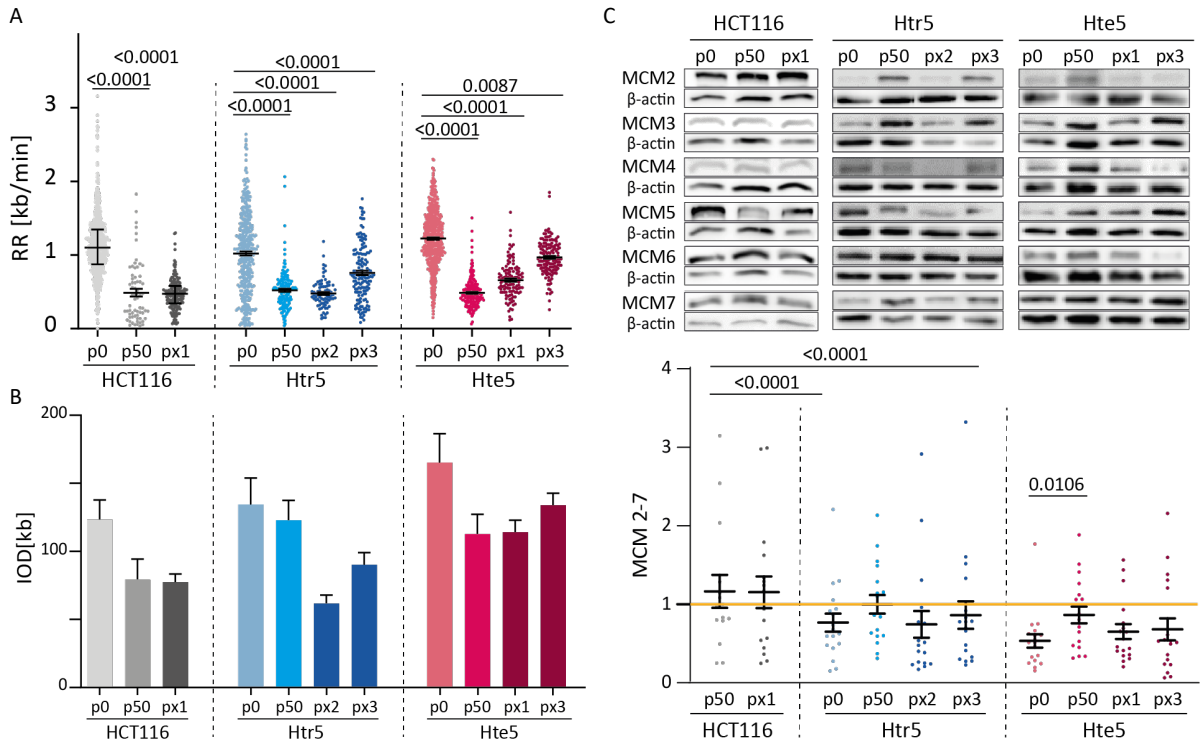

Figure 24: Replication dynamics and MCM 2-7 helicase abundance. A: Replication rate (RR). SEM and unpaired students t-test p-values are shown. At least 60 fork lengths were measured (together with Efrat Ozeri and Stefan Redel). **B:** Inter origin distance (IOD). At least 25 neighboring origins were scored. **C:** MCM 2-7 abundance. Upper panel: representative Western Blot. Lower panel: Quantification of three biological replicates with averaged MCM 2-7 protein abundances standardized to HCT116 wild type. Yellow line indicates HCT116 wild type. SEM and Mann-Whitney test p-values are shown (together with Carina Heinrich).

Rtr21 and Rtr21 p50 had downregulated MCM 2-7 levels, but did not show a difference between each other on transcriptome and proteome level (**Supplementary figure 3**). This supports that not more activated origins were measured upon evolution (**Supplementary figure 4** C).

Moreover, we observed a positive correlation between the number of active origins and the replication rate. Strikingly, the aneuploid cells after *in vitro* evolution tended towards a clustered subgroup with lower replication speed and higher IOD (**Figure 24** A). These cells might compensate the slower replication speed not only by increased origin firing. There is perhaps an additional mechanism how *in vitro* evolved cells maintain a faithful replication. Finally, correlation of the IOD and the abundance of the MCM 2-7 helicase showed that most of the analyzed cell lines correlated: If there is a high number of active origins, also a high amount of MCM 2-7 proteins was measured. *In vivo* evolved Htr5 cells did not share this observation. They contained a low amount of MCM 2-7 after evolution, but in contrast to all the other cell lines, they activated more origins. Taken together, all cell lines showed a decreased fork velocity upon evolution. This suggested a selection of cells that adapted to the replication stress by a slowdown of the replication machinery. The number of active origins correlated with the replication rate and the outlier fraction was composed of those evolved cell lines that maintained the additional chromosome. The MCM 2-7 helicase abundance correlated with the number of active origins. Cells that had a too small amount of MCM 2-7 also activated less origins highlighting the critical function of the MCM 2-7 helicase in the cell.

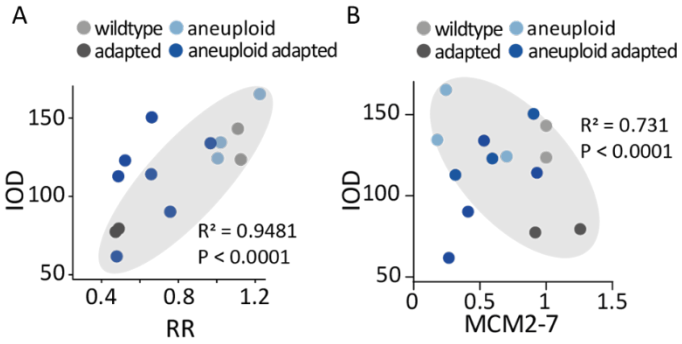

Figure 25: Replication correlations. A: Correlation between the inter origin distance (IOD) and the replication rate (RR). Outliers are the aneuploid *in vitro* evolved cell lines. **B:** Correlation between IOD and MCM 2-7 abundances from immunoblotting. Outliers are the *in vivo* evolved Htr5 cell lines. Spearman rank correlation coefficient and p-values are shown.

Replication fork asymmetry is reduced after evolution

We asked further whether a slowdown of the replication machinery observed after evolution in all cell lines corresponds to higher fork asymmetry which would indicate even higher replication stress after evolution. To explore this, we first investigated the symmetry of neighboring replication forks as an additional parameter of DNA combing (**Figure 23**). Assessment of outliers of these values allowed an estimation of the number of unstable forks. The outlier fraction resembles highly asymmetric forks (**Figure 26** A). Surprisingly, we observed that both, Htr5 and Hte5, had a lower percentage of highly unstable forks after evolution in comparison to newly generated aneuploid cells in both *in vitro* and *in vivo* evolution. We could not observe this in the wild type. HCT116px1 accumulated the highest fraction with 10% of unstable forks out of the measured ones. RPE1, Rtr21 and Rtr21 p50 did not show significant differences in the fork stability (**Supplementary figure 4** D). Furthermore, we correlated the fork stability (FS) outliers with the RR and IOD (**Figure 26** B, C). The evolved aneuploid cells clustered together at a state of low RR and low instability, whereas before evolution aneuploid cancer cells had high fork instability together with high replication rates.

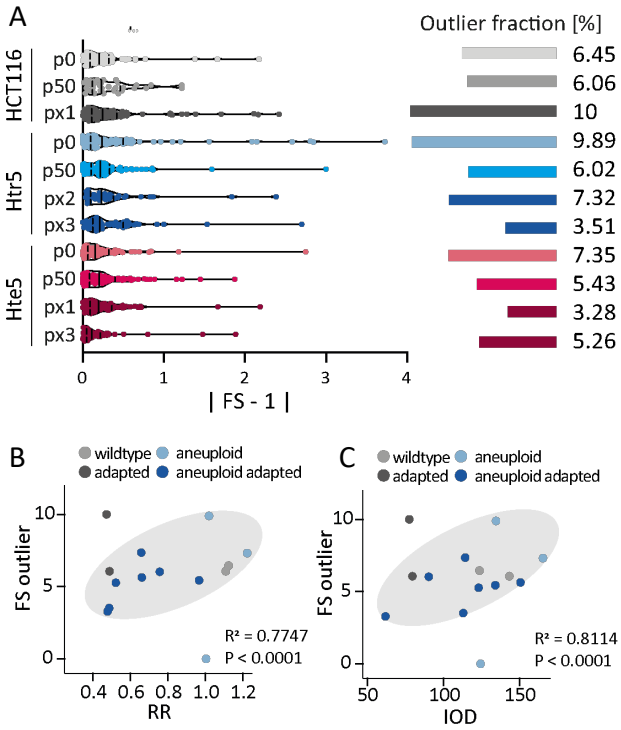

Figure 26: Replication dynamics – Fork stability. A: Replication fork symmetry (FS) as violin plots (left) and the 0.5 percentile of outliers as numbers and bar plot (right). **B:** Correlation between FS outlier fraction and RR and between **C:** FS outlier fraction and IOD. Spearman rank correlation and p values are shown.

Overall, the link between fork velocity and replication fork symmetry underlined that the replication machinery´s speed is not the only essential functionality during replication. It rather is the balance between compensatory mechanisms, that together lead to a faithful replication. Cells proliferated better even with slowed replication and cells with replication slowdown did not necessarily have increased replication stress measured by the asymmetry of the forks. Therefore, we hypothesized that evolution leads in aneuploid cells to a long-term adaptation to replication stress resulting in a more faithful replication providing the cells with a fitness advantage.

DNA damage signaling is altered after evolution

Sensing of DNA damage

If the replication was more faithful after evolution also the replication stress signaling should be reduced. To assess this, we investigated proteins and protein phosphorylation patterns among the DNA damage signaling cascade. First, we addressed the levels of the single-strand coating protein RPA, which becomes phosphorylated upon DNA damage. Its phosphorylation at position Serin 33 (pRPA2 S33) in the second subunit is mediated by ATR as an early response to single-strand breaks [81]. We performed flow cytometry after EdU treatment to quantify pRPA2 S33 in S phase (**Figure 27** A). In HCT116 only slightly more pRPA2 S33 was observed after evolution. In contrast, Htr5 had very high pRPA2 S33 levels. Interestingly, after the evolution of the aneuploid cell line, the pRPA2 S33 levels decreased to wild type levels. As these results might be caused by generally lower RPA2 protein abundance in the cells, we performed immunoblotting for both, pRPA2 S33 and RPA2 (**Figure 27** B). The wild type *in vitro* evolution deviated from the *in vivo* evolution in terms of single-strand break sensing: There was no ratio change after 50 passages of HCT116 as the cells harbored more RPA2, as well as pRPA2 S33 in comparison to the wild type. But the post xenograft showed higher pRPA2 S33 levels while maintaining the RPA2 levels. Unexpectedly, *in vitro* evolved aneuploid cells exhibited higher or equal pRPA2 S33 levels and increased RPA2 levels. In contrast, all *in vivo* evolved aneuploid cells had reduced phosphorylation levels upon immunoblotting, despite maintaining the RPA2 levels

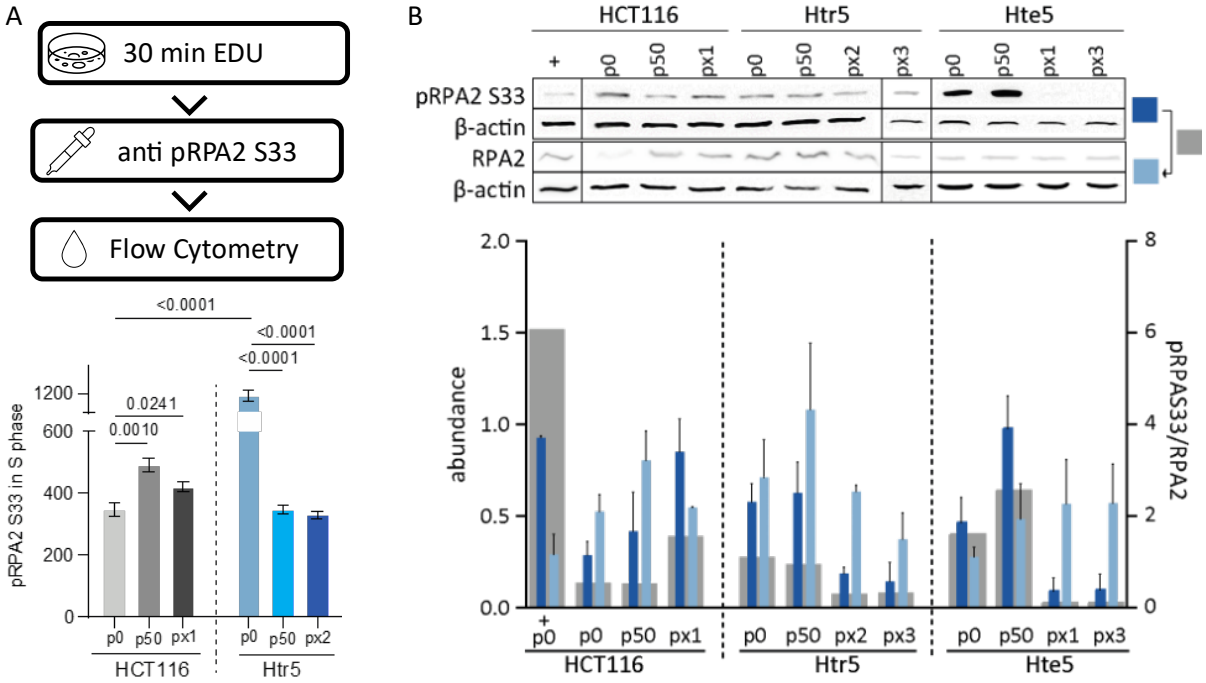

Figure 27: pRPA2 S33 quantification. A: Upper panel: Flow cytometry workflow: Cells were treated with EDU for 30 min, fixed and the anti pRPA2 S33 antibody was applied. Protein abundance per cell was assessed with flow cytometry (median pRPA2 S33 area of the pulse of EdU positive cells). Lower panel: Quantification of median S phase pRPA2 S33. SEM and unpaired two-tailed student´s t-test p values of >5000 cells per replicate are shown. Positive control (+) is HCT116 at p0 treated with 200 nM aphidicolin **B:** Upper panel: representative western blot. Lower panel: quantification of pRPA2 S33 / RPA2 ratio. Mean with SEM is shown. Positive control (+) is HCT116 at p0 treated with 1 µM doxorubicin (together with Stefan Redel and Amelie Becker).

(**Figure 27** B). This indicated, that losing the additional chromosome upon *in vivo* evolution, causes less replication stress sensing. We performed immunofluorescence staining of HCT116, Htr3 and Hte5, the cell lines of the prolonged evolution. Upon counting the number of foci per cell, we observed that cells with more than five foci were rarest in HCT116 p0, while it steadily increased until p40, after which a decline was visible until p80 (**Supplementary figure 13** A). Htr3 and Hte5 showed rather fluctuating behavior over time, whereas the highest ratio of cells with pRPA2 S33 foci was measured after 20 passages. Moreover, we performed immunoblotting and immunofluorescence staining of pRPA2 S33 for RPE1, Rtr21 and Rtr21 p50. The western blot data showed a trend towards more replication stress in Rtr21 p50 in comparison to all other tested cell lines, however, with a huge standard deviation in the abundance of pRPA2 S33 (**Supplementary figure 5** A, B). With a single cell investigation based on pRPA2 S33 foci, we found no essential difference between Rtr21 and Rtr21 p50 (**Supplementary figure 5** D). Overall, the investigations assessing directly the pRPA2 S33 in S phase showed a clear trend towards less replication stress signaling in aneuploid evolved Htr5.

RPA2 has many phosphorylation sites. RPA2 S4S8 hyperphosphorylation senses DSBs by DNA-dependent protein kinase complex (DNA-PK) mediated phosphorylation [84]. We asked whether the sensing of DSBs is affected by evolution of aneuploid cells. To this end, we performed immunoblotting of RPA2 and pRPA2 S4S8 (**Figure 28**). We observed Htr5 with a similar pRPA2 S4S8/pRPA2 ratio before and after *in vitro* evolution. In the post xenografts the DSB sensing was generally higher. In Htr5 px2 though, lower RPA2 abundances were measured, thereby increasing the ratio of pRPA S4S8/pRPA2, whereas the Htr5 px3 cells had a higher abundance, thereby increasing the ratio. Here, high standard errors were calculated. Interestingly, Hte5 had as high pRPA S4S8 levels as the positive control which decreased upon 50 passages. Hte5 px1 had slightly higher levels than Hte5 p50 but still lower levels than Hte5 before evolution. Hte5 px3 showed low RPA2 levels which increased the ratio to a higher level in comparison to Hte5 (**Figure 28**). In contrast, Rtr21 and Rtr21 p50 exhibited almost the same levels

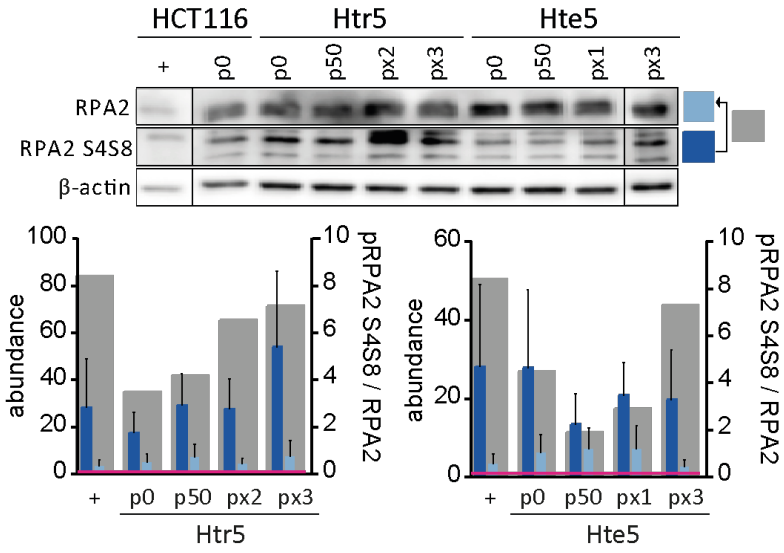

Figure 28: Western blot RPA2 and pRPA2 S4S8: Upper panel: representative western blot with color code. Lower panel: quantification of Htr5 derived evolved cell lines (left) and Hte5 derived evolved cell lines (right). HCT116 wild type levels are marked as violet line. Left y-axis shows total abundances normalized to β-actin of pRPA2 (light blue) and pRPA2 S4S8 (dark blue). Right y-axis shows ratio of pRPA2/pRPA2 S4S8 (grey) Positive control (+) is 1 µM doxorubicin. Three biological replicates were quantified (together with Carina Heinrich).

before and after evolution, whereas both showed reduced levels in comparison to the wild type (**Supplementary figure 5** A, C). These results show no significant alteration in the cell lines, suggesting no to very mild DNA damage recognition changes after evolution in comparison to before.

γ-H2A.x is a phosphorylated histone sensing DSBs mediated by the ATM kinase. The prolonged evolution of HCT116 showed an early decrease of cells with more than five foci. After 40, 60, and 80 passages this increases again slightly higher than HCT116 p0 levels (**Supplementary figure 13** B). Next, we correlated the percentage of cells with a high γ-H2A.x foci number with the percentage of cells with a high pRPA2 S33 foci number in Htr3 and Hte5 over a time course of 60 passages to assess the time-resolved changes in DNA damage sensing and replication stress sensing of the individual evolutionary replicates (**Supplementary figure 14**). Even though Htr3 never had the additional chromosome and Hte5 e1 lost it at some point during evolution, both shared common changes during the culture-based evolution. After 20 passages DNA damage signaling increased, and after 40 passages replication stress signaling decreased. Both, γ-H2A.x and pRPA2 S33 levels mostly increased after 60 passages. Together, this showed that DNA damage sensing via γ-H2A.x and replication stress sensing via pRPA2 S33 are regulated during evolution in divergent directions.

Mediation of DNA damage

The pRPA2 S33 phosphorylation mediated by ATR has Chk1 as its downstream target that mediates the DDR. We asked whether the partially divergent observations of pRPA2 S33 could be clarified by studying this checkpoint. Therefore, we performed immunoblotting of Chk1 and pChk1 (**Figure 29**). The engineered trisomic and tetrasomic cell lines showed higher pChk1/Chk1 ratios before evolution than after evolution, independent from the evolution type. This supported the hypothesis of a replication stress-dependent advantage in HCT116-derived aneuploid cells after evolution.

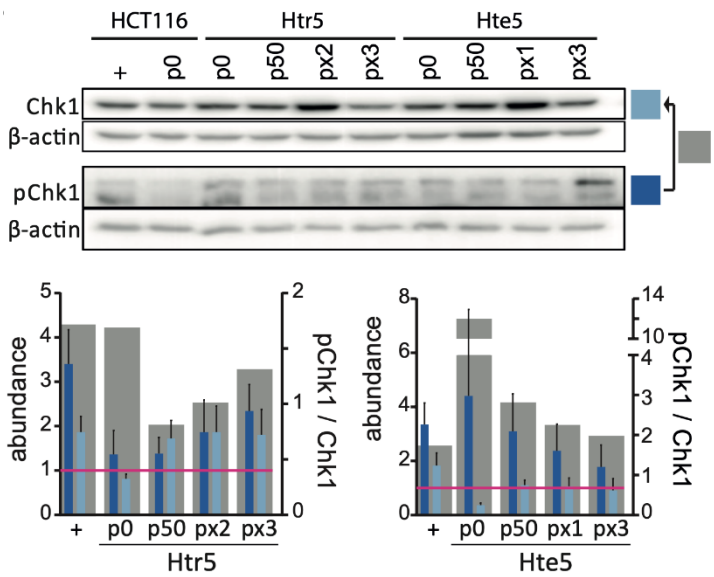

Figure 29: Chk1 and pChk1 S33 on Western Blot. Upper panel: representative western blot. Lower panel: quantification of Htr5 derived evolved cell lines (left) and Hte5 derived evolved cell lines (right). HCT116 wild type levels are marked as violet line. Left y-axis shows total abundances normalized to β-actin of Chk1 (light blue) and pChk1 (dark blue). Right y-axis shows ratio of pChk1 to Chk1 (grey). Positive control (+) is 1 µM doxorubicin. Three biological replicates were quantified (together with Carina Heinrich).

A mediator of DSBs is 53BP1, which allows the assessment of DSB signaling via the ATM pathway. We performed immunofluorescence imaging to quantify the number of 53BP1 foci in Cyclin A

negative cells. Cyclin A is specifically not active in G1 cells (**Figure 30**). By accounting for this, we were able to evaluate the DNA damage that remained unrepaired in prior cell cycle phases. Thereby, these damage sites have a high potential to persist and contribute to genome instability. We counted significantly more cells with more than ten 53BP1 foci in cyclin A negative cells in aneuploid cells in comparison to the wild type. This reflected previous findings [138]. Supporting the results of pRPA2 S4S8, also 53BP1 was not significantly altered after *in vitro* evolution. Similarly, high levels of 53BP1 in Hte5 and Htr5 after passaging were observed as before. Three out of four *in vivo* evolved aneuploid cell lines behaved the same, but Htr5 px2 exhibited even higher DNA damage signaling than the positive control. Together these results indicated that the DSB signaling pathway was not altered after evolution. In contrast, the replication-associated single strand break signaling cascade via ATR and Chk1 was alleviated upon evolution, at least to a certain extent.

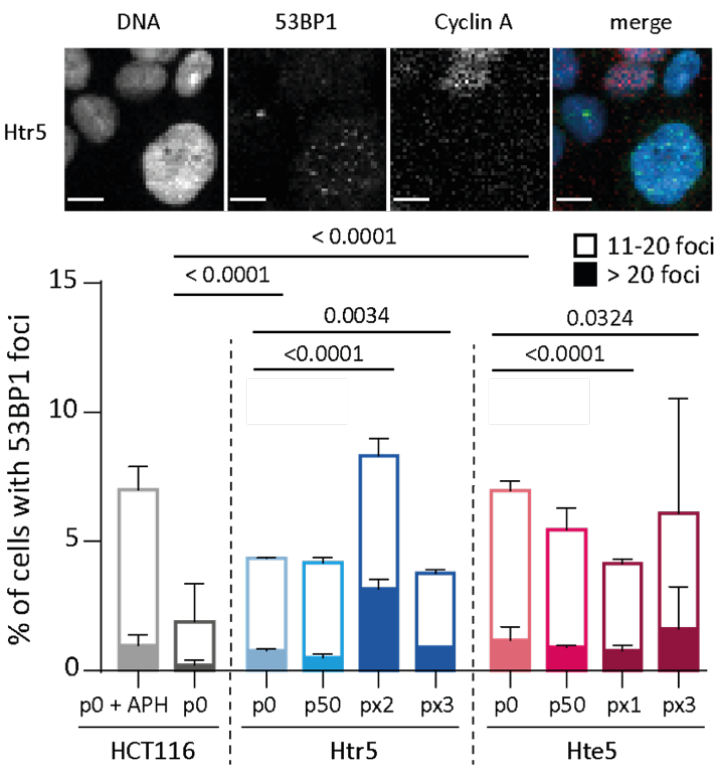

Figure 30: 53BP1 and cyclin A immunofluorescence staining. Upper panel: Exemplary captures. DNA stained with SYTOX™ Green. Scale bar: 10 µm. Lower panel: Quantification of the percentage of cells with foci >20 (filled) and with 11-20 foci (outlined). Nonparametric t-test p values are shown calculated out of at least 500 cyclin A negative cells per replicate in two independent experiments. Positive control is 200 nM aphidicolin (together with Carina Heinrich).

Mitotic errors

If DNA damage during replication remains unrepaired, anaphase bridges (ABs) can form in mitosis due to under-replicated DNA [193]. These can eventually result in chromosome breaks and cause chromosome missegregation. We asked whether fewer replication errors would result in fewer ABs after evolution. We assessed the percentage of ABs by DNA staining and found no significant difference between Htr5 and derived evolved cell lines (**Figure 31** A). Similarly, the post xenografts of Hte5 were only slightly reduced. But Hte5 showed significantly fewer ABs after passaging. Interestingly, also Rtr21 reduced the ratio of ABs per anaphase to wild type levels after evolution (**Supplementary figure 6** A). Micronuclei are markers of GIN as they are error-prone capsules surrounding free DNA after mitosis that can be re-incorporated back into the main nucleus DNA mass in the following cell cycle. We asked whether cells after evolution adapted this recurrent DNA damage biomarker after evolution. Upon

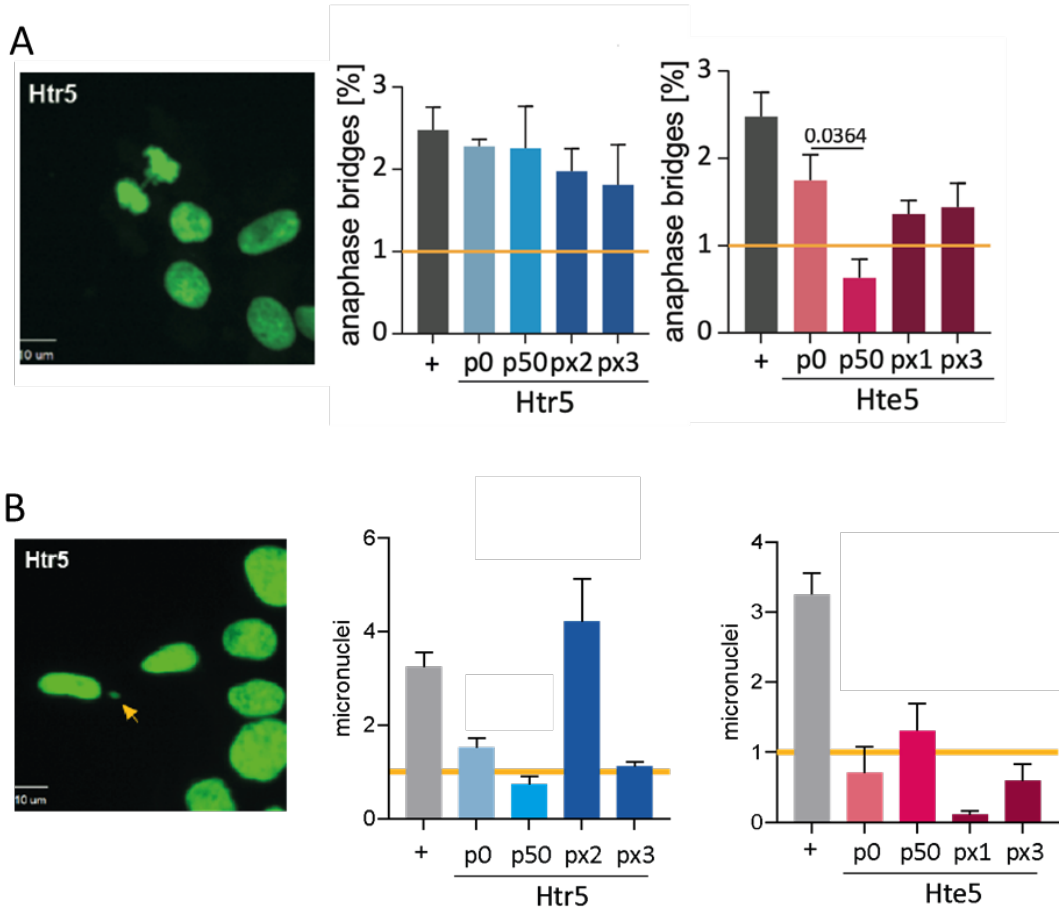

Figure 31: Anaphase bridges in aneuploid cells after evolution. A: Exemplary capture of an anaphase bridge (right). Percentage of anaphases with anaphase bridges in Htr5 (center) and Hte5 (right) derived cell lines. **B:** Exemplary capture of a micronucleus (right). Percentage of micronuclei in Htr5 (center) and Hte5 (right) derived cell lines. A and B: Yellow line represents HCT116 p0 and positive control (+) is HCT116 p0 treated for 24 h with 200 nM aphidicolin and 0.73 µM caffeine. SEM and two tailed unpaired students t-test p-values of at least three biological replicates are shown. Scale bar: 10 µm. At least 30 anaphases and 50 captures with nuclei per replicate were quantified (together with Aaron Gill, Carina Heinrich and René Göbel).

DNA staining, we quantified the number of MN per nuclei and found divergent results between Htr5 and Hte5 derived evolved cell lines (**Figure 31** B). Htr5 p50 had a lower percentage of MN than Htr5 whereas Hte5 p50 has higher levels than Hte5. However, the displayed differences were low and not significant. Htr5 px2 had the highest number of MN which corresponds to the high 53BP1 levels of specifically this cell line (**Figure 28**). All other in vivo evolved cell lines showed lower MN levels in comparison to the respective unevolved cell line. Rtr21 before and after evolution did not show a significant difference as well (**Supplementary figure 6** B).

Altogether, several replication stress associated parameters decreased upon *in vitro* evolution, in some experiments the results were inconsistent though. Throughout the tested proteins the DSB markers were unaltered active after *in vitro* evolution of aneuploid cells. The formation of mitotic errors was inconsistent between the cell lines.

Lysosomal markers are downregulated after evolution

According to our multi-omics study, not only replication-associated proteins were neutralized after evolution, but also lysosomal proteins (**Figure 21**). Lysosomes eventually fuse to autophagosomes for the degradation and recycling of unused or unwanted proteins. We first asked whether there is a lower number of lysosomes and made use of the low pH of the organelles. The LysoTracker™ is a red fluorescent dye that is highly selective for cellular compartments with a high number of protons. Upon immunofluorescence imaging, we quantified the percentage of cells with more than 10 foci (**Figure 32** A). Unexpectedly, Htr5 did not display less low pH regions after 50 passages than before. Only Htr5 px2 showed a lower percentage of foci in comparison to the unevolved counterpart. We noticed that HCT116 p50 had higher LysoTracker™ levels than HCT116 before evolution. We further performed immunofluorescence staining to detect a membrane marker protein of lysosomes, namely LAMP1. We found that Hte5 has a higher percentage of cells with more than five foci in comparison to all other tested conditions (**Figure 32** B). In other words, cells after *in vitro* and *in vivo* evolution showed a decreased percentage of cells with more than five foci. In addition, almost no cells with more than 20

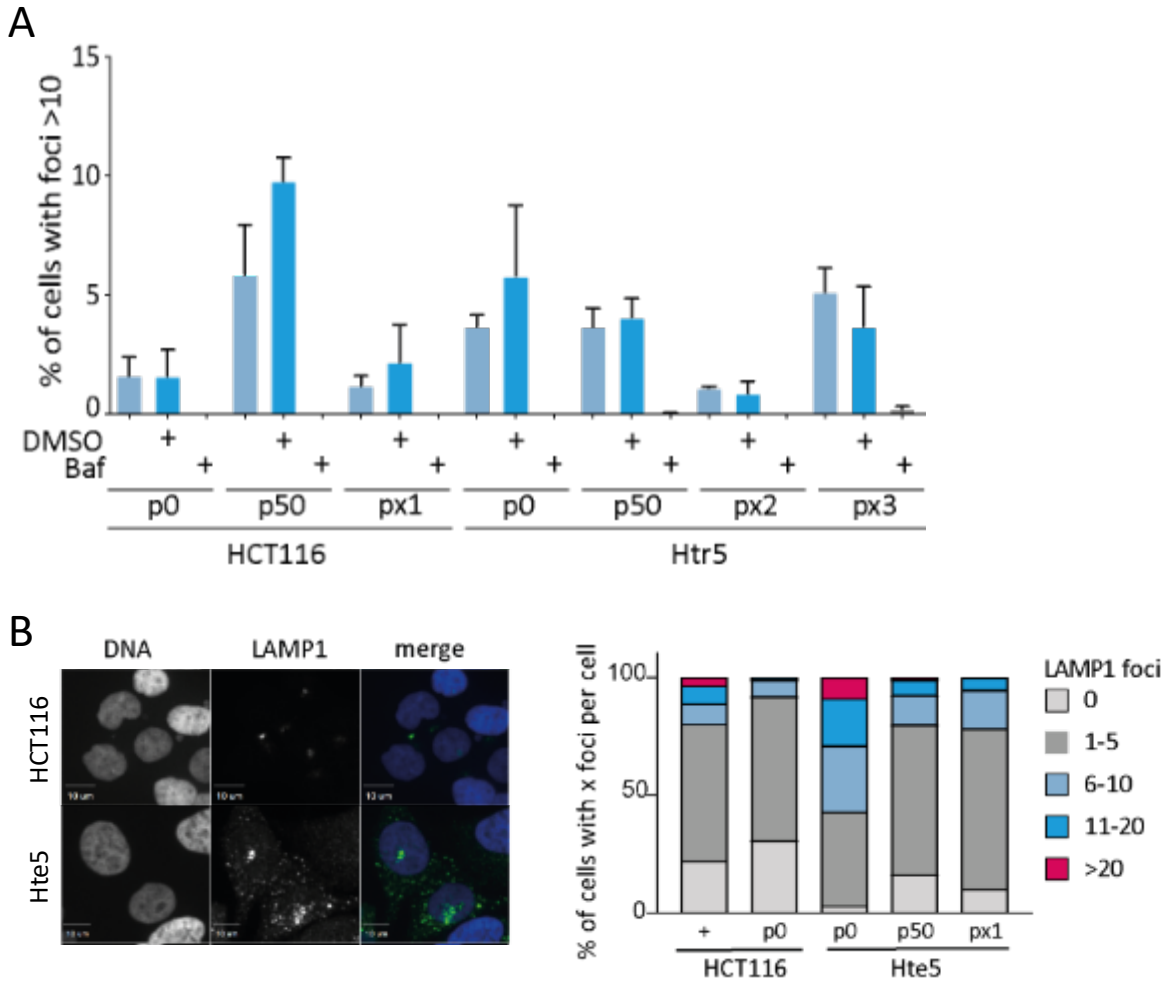

Figure 32: LysoTracker™ and LAMP1: A: LysoTracker™ quantification. Percentage of cells with >10 foci. SEM of three biological replicates (together with Amelie Becker). **B:** Immunofluorescence of LAMP1. Left panel: Exemplary captures. Scale bar: 10 µm. Right panel: percentage of cells with number of LAMP1 foci according to legend. Positive control (+) is 100nM bafilomycin A1 (Baf) (together with Assel Nurbekova).

foci were detected after evolution. Moreover, we asked whether more lysosomes fuse with autophagosomes to degrade encapsulated proteins. To this end, we studied the protein p62, which targets the molecule that should be degraded and guides it to the autophagosomes. The gene encoding for p62 is located on chromosome 5. Therefore, we hypothesized to see an amplification in cells with additional chromosome 5. Importantly, p62 becomes degraded in autolysosomes. By immunofluorescence staining and subsequent quantification, we saw no difference between Hte5 and Hte5 p50 (**Supplementary figure 9**). Even though Hte5 p50 lost one copy of the additional chromosomes during evolution (**Figure 20**), it was still able to maintain the p62 levels. Hte5 px3 had a lower percentage of cells with more than five foci compared to Hte5 before evolution, likely due to the loss of the additional chromosome 5. To assess another autophagosome marker that is not associated with chromosome 5 amplification, we studied LC3 using immunofluorescence staining (**Supplementary figure 8**). LC3 is degraded as well in the autolysosome and accumulates upon bafilomycin A1 treatment similar to p62. HCT116 did not show a change after evolution. In contrast, there were more cells with a high foci number in Htr5 than in Htr5 p50 and in Htr5 px2 visible, reflecting the proteomics analysis. Htr5 px3 had the highest percentage of cells with a high foci number.
Altogether, lysosomal and autophagosomal markers were not generally downregulated after *in vitro* evolution as hypothesized. Hte5 p50 had rescued LAMP1 but unchanged p62 levels. Htr5 p50 showed rescued LC3 levels but the LysoTracker™ did not reveal any difference after *in vitro* evolution.

To summarize, aneuploid cells with and without additional chromosome displayed a proliferation advantage after evolution, suggesting an adaptation to the detrimental consequences of the additional chromosomes. These phenotypic adaptations were not the same in all cell lines and all conditions, suggesting that multiple different pathway alterations may be involved in the evolutionary adaptation of aneuploid cells. As a result, replication stress parameters, such as the fork stability and the pChk1 signaling decreased and some lysosomal parameters, such as LAMP1, increased. We showed that the replication dynamics correlated with the abundance of MCM 2-7, highlighting the critical role of MCM 2-7 during S phase in aneuploid cells.

Consequences of WGD

WGD results in a doubled set of chromosomes. In humans, this refers to 92 pairs of chromosomes. In such a case, the amount of genomic material is balanced. This is contrary to aneuploid karyotypes, where the unbalanced amount of structural or numerical aberrations causes the cells to compensate for wrongly transcribed and eventually translated proteins. Interestingly, in cancer cells WGD gives rise to CIN, which is the continuous change of the karyotype with every cell division. Chromosomes or parts of those are gained and lost continuously over time. Therefore, the cells that underwent WGD frequently become chromosomally unstable and aneuploid. This provides the cells with an increased potential for fitness adaptations in stressful conditions. Expression changes of proteins, such as TSG downregulation and/or OG upregulation, might result in tumorigenesis or further expansion of the hallmarks of cancer. Finally, WGD and CIN lead to worse patient prognosis and elevated drug resistance. Here, we expanded the knowledge of the consequences of WGD.

USP28 and NUMA1 stabilize tetraploid cells for survival

A long-standing question was how tetraploid cells enable cell survival despite double the amount of DNA. We sought to investigate this with a high throughput RNAi screen for proliferation-limiting proteins in combination with the Fluorescent Ubiquitination-based Cell Cycle Indicator (FUCCI) system. Using this approach upon cytokinesis failure in HCT116 cells, we generated cell cycle profiles and calculated statistics based on the percentage of cells detected per cell cycle phase to evaluate the cell cycle progression per individual depleted protein [194]. Statistically significant hits were subsequently analyzed by pathway enrichment. Specific proteins of these pathways were selected and their effect on cellular proliferation was validated. Among those, the ubiquitin carboxyl-terminal hydrolase 28 (USP28) depletion reduced the cell proliferation after WGD, as the protein depletion led to increased

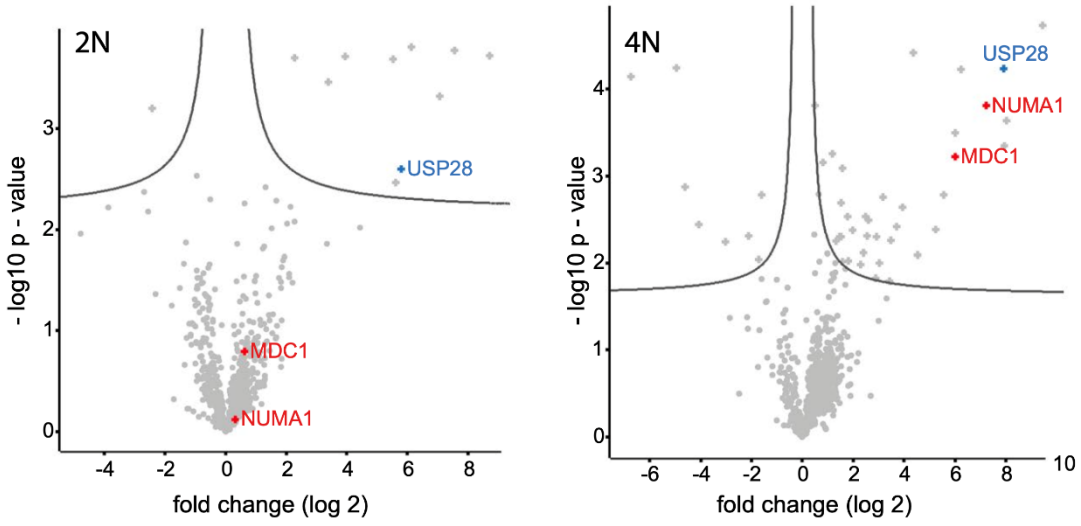

Figure 33: Interaction proteins of USP28. Volcano plots from mass spectrometry following co-immunoprecipitation of USP28 in diploid (2N, left) and tetraploid (4N, right) HCT116. Bait is marked in blue, highlighted in red are NUMA1 and MDC1 (together with Markus Räschle and Katarzyna Seget-Trzensiok, adapted from Bernhard et al, 2022 [194]).

number of replicating cells 24h and 48h after DCD treatment. Respective knockout and rescue experiments were successful as well [194]. We further evaluated USP28 by identifying putative interactors. To this end, we performed a co-immunoprecipitation of USP28 in diploid (2N) and tetraploid (4N) cells, analyzed them by tandem mass spectrometry (MS/MS) and evaluated the candidate interactors. The nuclear mitotic apparatus protein 1 (NUMA1) was a significantly enriched interactor of USP28 after WGD, but this was not the case in diploid cells (**Figure 33**). NUMA1 is involved in bipolar spindle formation [195]. The association of NUMA1 with USP28 has not been identified previously. Additionally, we identified the mediator of DNA damage checkpoint 1 (MDC1) enriched after WGD (**Figure 33**). The interactor of USP28 is involved in DNA damage signaling together with USP28 [196], suggesting elevated DNA damage in tetraploid cells soon after WGD.

Together, the co-immunoprecipitation of USP28 followed by tandem mass spectrometry (MS/MS) allowed the identification of at least two putative interactors of USP28: NUMA1 and MDC1. As an interactor of USP28, NUMA1 and MDC1 functions might be perturbed by the absence of USP28. Thus, USP28 is essential in early tetraploid cells for cell survival, likely by NUMA1 spindle formation and MDC1-related DNA damage signaling [194].

The first replication after WGD is causative for GIN

The findings shown in the previous chapter suggested that DNA damage occurs frequently soon after WGD. The main source of endogenous DNA damage is DNA replication. To determine the source of the DNA damage, we first induced WGD in several ways to produce tetraploid cells via endoreplication (EnR), mitotic slippage (MS), and cytokinesis failure (CS) (**Figure 10**). Next, we studied the first S phase after the WGD event with DNA combing on a single molecule level to identify potentially altered replication dynamics that could be indicative of the cause of the early DNA damage after WGD.

To this end, we determined the replication fork velocity, stability and inter origin distances. Surprisingly, during the first replication after WGD the replication fork speed was significantly increased in comparison to the diploid control cells (**Figure 34** A (left), B (left)). Additionally, the fork stability measurements showed more asymmetric forks after WGD (**Figure 34** A (right), B (center)). This might explain the accumulating DNA damage in the end of S phase. Next, we assessed the number of active origins on the fiber by measuring the inter-origin distance as the replication rate and the number of active origins usually correlate. We observed that the inter origin distance is higher after WGD. This refers to a lower number of active origins, which could explain the rapid fork progression, resulting in unstable forks. Taken together, cells that just underwent WGD show altered replication dynamics. The asymmetry of forks suggests replication stress and the lower number of activated origins might force the cells to accelerate replication, eventually leading to GIN. We showed in addition that the first replication after WGD is sufficient to introduce karyotypic changes in single cells [197].

Altogether, we identified the following key aspects of the causes of DNA damage after WGD: First, DNA damage accumulates in cells during the very first replication after WGD. Second, this damage arises due to altered replication dynamics with a low number of active origins, perhaps too low to compensate for double the amount of DNA that needs to be replicated. The consequence is an increase in the speed of replication, making the doubling of the DNA more error-prone, which results in unstable forks and eventually in DNA damage accumulation already in the very first cell cycle after WGD.

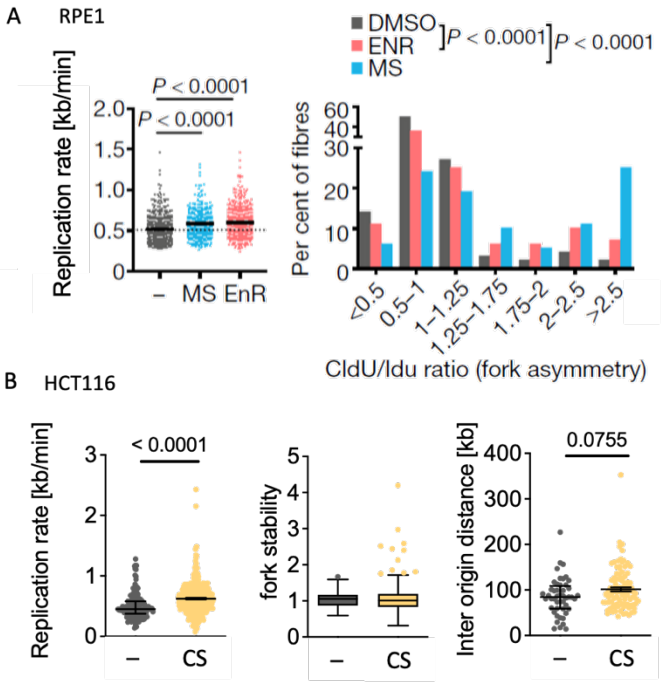

Figure 34: Replication dynamics of the first S phase after WGD. A: RPE1. Replication rate (kb/min) (left). Fork symmetry histogram based on CldU/Idu measures (right). ENR = Endoreplication, MS = mitotic slippage. SEM of > 330 forks. B: HCT116. Replication rate (kb/min) (left). Fork stability (center). Inter origin distance (right). CS = Cytokinesis failure. Mann-Whitney p-values and SEM of three biological replicates with > 120 forks (together with Simon Gemble and Sara Vanessa Bernhard, adapted from Gemble et al, 2022 [197]).

Aneuploid karyotypes are facilitated by WGD in human cancer evolution

The consequences of this early DNA damage after WGD might be severe and related to the previously described CIN phenotype of cells that underwent WGD [160]. An outstanding question is whether WGD creates specific recurrent patterns of aneuploidies depending on the cells' context and tumor type. This could cause aneuploidy to become a relevant biomarker to predict specific therapeutic targets.

An *in silico* study of TCGA suggested that cells that underwent WGD accumulated different damage than diploids [198]. We decided to test this finding *in vitro*. To this end, we used multicolor fluorescence *in situ* hybridization (mFISH) data of previously established HCT116 cell lines that underwent WGD by cytokinesis failure and were subsequently single-cell selected. These cell lines are indicated as HCT11-derived post-tetraploid cell lines (HPT) [165,199,200]. The cell line Hte5 was included as a comparative HCT116-derived cell line with defined tetrasomy 5 [29].

Upon counting the karyotypic aberrations using the mFISH data (**Figure 35** A), we detected a higher general aneuploidy in the HPT cells in comparison to the wild type cell line or the Hte5 (**Figure 35** B). We discovered more losses than gains in all analyzed cell lines (**Figure 35** C) supporting previous studies [31,160]. Interestingly, we found 100% of the HPT cells exhibiting whole chromosome aneuploidies (WCA), while the fraction of cells with WCA was much lower in the wild type and Hte5, with the mean reduced to app. 30%-40% (**Figure 35** D). In line with that, the percentage of WCA was the highest in HPTs in comparison to arm-level changes which make up app. 30% in HCT116 and Hte5 (**Figure 35** E). Noteworthy, WCA outweighed also structural chromosomal changes in aneuploid and post-tetraploid cells (**Figure 35** F). These findings support the results from the performed *in silico* investigation [198] and clearly show that WGD is one cause for CIN as the stable Hte5 does not harbor such strong chromosomal defects.

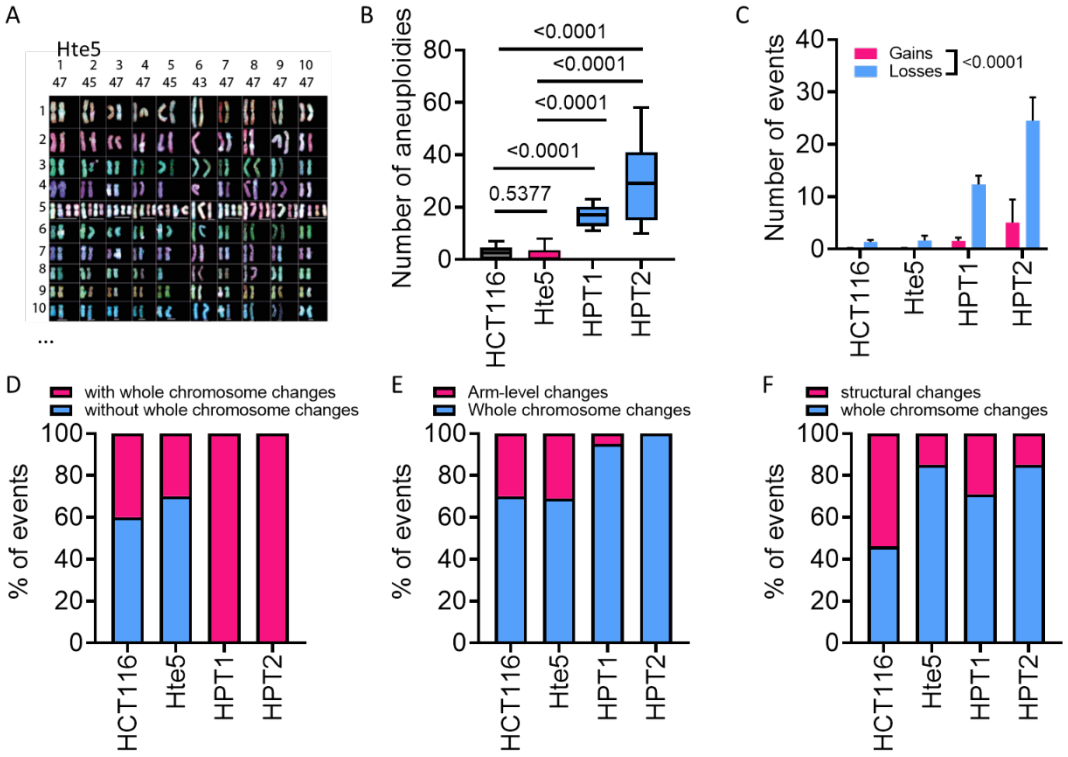

Figure 35: Karyotype analysis in aneuploid and tetraploid cells. Chromosome painting of ten exemplary cells showing chromosomes 1 – 10 in Hte5. **B:** Number of aneuploidies counted per cell line. Boxplot with whiskers method Tukey and two-sided students t-test p-values are shown. **C:** Number of whole chromosome gains vs chromosome losses. SEM and Two-way anova p value are shown. **D:** Percentage of cells with and without whole chromosome changes. **E:** Percentage of cells with arm-level changes and whole chromosome changes. **F:** Percentage of cells with structural and whole chromosome changes (together with Anastasia Kuznetsova and Sara Vanessa Bernhard).

To summarize, we found a more heterogenous karyotype in cells that underwent WGD with more frequent chromosome losses than gains. We described WCA being favored over arm-level changes, making WGD an important determining factor of aneuploidy.

Discussion

In this thesis, I presented the results of studies of the causes and consequences of chromosomal aberrations in human cells. I investigated how catastrophic genomic rearrangements, such as chromothripsis, might occur in MN and what impact these rearranged chromosomes have on cellular fitness. Furthermore, I explored the evolutionary trajectories of engineered aneuploid cells to understand how the detrimental effects of aneuploid cells are alleviated. Finally, I investigated cells after WGD to shed light on the consequences of this genome alteration. All these examined phenomena share tumor-promoting phenotypes. However, the physiological mechanisms in the cells that display causes and consequences differ between different types of genomic aberrations.

Massive chromosomal rearrangements in micronuclei

Chromothripsis is under extensive research since its first description in 2011 [38]. Massive chromosome breakage and reassembly were found in several cancer types and congenital disorders [38,116]. This highlights the importance of studying rearranged chromosomes, their origin, and their consequences. With the MMCT, we established a model system to engineer not only cells with a defined additional chromosome but also with a defined shattered and reassembled chromosome. Using WGS, we identified the cell lines that we used for the analysis of the physiological consequences of chromothripsis.

Sources of massive DNA damage in MN

Asynchronous replication leads to premature chromatin condensation

We showed that replication was often asynchronous during the MMCT and, even more frequently, the PN replicated while the MN did not (**Figure 11**). Others described that the MN experience a delayed replication with the consequence of premature DNA condensation leading to severe DNA damage [201]. Interestingly, lamin B1 loss is suspected to have a role in S phase prolongation and chromatin decondensation, suggesting a functional link between lamin B1 presence and faithful cell cycle progression [202–204]. We and others showed that most MN lack lamin B1 (**Figure 14** D) [132]. The MN with entrapped DNA content can reenter the main DNA mass after the mitosis [205]. Without lamin B1, the MN might exhibit inefficient chromatin condensation, which eventually leads to DNA damage and mitotic failures.

Compromised nuclear envelope integrity leads to exposure of DNA to the cytosol

MN are fragile constructs, in which the lamin B1 loss might lead to nuclear envelope collapse. By this, the majority of MN undergoes an irreversible loss of compartmentalization during interphase, which leads to DNA damage accumulation in MN [132]. The cause might be a defective transport between cytoplasm and MN exposing the DNA to the cytosol (**Figure 12**, **Figure 14**). In this case, the mechanism for DNA damage might be the entry of the cytosolic nuclease TREX1, known to partially degrade DNA [134,206]. Noteworthy, lack of lamin B1 was not the only factor causing cytosolic fractions to enter (**Figure**

14 C). Especially in intact MN, DNA replication and repair defects were causative for DNA damage accumulation [99,132]. An open question is whether this might be linked to the observation of cytosol entry despite lamin B1 presence or whether there are other proteins(s) in the MN envelope that could have a causative effect of the DNA damage. Taken together, compartmentalization is defective in MN during MMCT which has high potential to cause severe DNA damage.

Consequences of lamin B1 loss

Lamin B1 is usually part of a complex network composed of a multitude of proteins involved in maintaining the nuclear architecture. In addition, lamin B1 regulates gene expression, which directs proliferation and senescence in human cells via a ROS signaling cascade. High lamin B1 expression is linked to senescence, which gives the protein the ability to function as senescence biomarker [207,208]. Contrarily, loss of lamin B1 was observed to prolong the S phase [202]. Thus, preservation of lamin B1 levels is obligatory for a faithful DNA replication. Moreover, lamin B1 is associated with DNA repair, as it directly interacts with BRCA1 and RAD51 [209]. Therefore, the lack of lamin B1 might decrease repair capacities in the MN leading to an accumulation of DNA damage. In mouse development lamin B1 functionality is essential to avoid death early after birth and respective mouse embryonic fibroblasts revealed abnormal nuclear morphology upon loss of function of lamin B1 [210]. In pancreatic cancer, lamin B1 expression led to distant metastasis, and poor prognosis [211]. These findings show that lamin B1 has crucial functions that may lead to severe consequences upon lamin B1 loss, such as chromatin remodelling defects, DNA damage accumulation, DNA replication failures, lower senescence, and higher proliferation capacities.

A surprising result was that the lamin B1 loss was a phenotype more frequently observed in smaller MN with less DNA (**Figure 14** B, **Figure 15**). One potential explanation for the lamin B1 loss could be cytoplasmic blebbing and budding which frequently led to incorporation of double-minute chromosomes and lamin B1 loss after mitosis [203,212]. Double-minute chromosomes are extrachromosomal chromatin, comparably small and composed of acentric chromosomes that often locate to the nuclear periphery [213,214]. Therefore, the MN formed to surround double-minute chromosomes might be especially small and lack lamin B1. How lamin B1 loss is mechanistically linked to smaller MN remains to be investigated.

Technical acceleration of DNA damage in MN

There are other aspects that could lead to technical errors during the MMCT, which we addressed as far as possible. First, the generation of A9 cells with an additional human chromosome is also based on a chromosome transfer, harboring a similar potential for a defective chromosome. However, the human chromosome was intact in the donor cell, as shown in many engineered cell lines originating from the same donor cell line [137]. Second, the human chromosome in the A9 mouse donor does not originate from the same cell line we transfer it into. This might lead to cellular effects we would not

have a chance to determine. Moreover, an external trigger of DNA damage in MN after mitotic slippage might be the usage of colchicine to induce the MN formation. Colchicine is an alkaloid that binds to tubulin and inhibits microtubule polymerization[215]. By this, it causes inhibition of mitosis and leads to excessive MN formation. Colchicine treatment itself was shown to result in DNA damage [216]. Altogether, these sources of error during the MMCT might contribute to the DNA damage phenotype in MN.

Before colchicine treatment, the A9 cells display an asynchronous cell population. As the synchronization in mitosis takes place, some cells halt earlier than others within the 48 h timeframe of colchicine treatment, because they were at different cell cycle stages [137]. Some might finish first replication and gap phases until they finally form micronuclei due to the colchicine treatment. This could contribute to the existence of MN with lamin A/C but without lamin B1. Lamin A and C are translated during the full cell cycle whereas lamin B1 is synthesized mainly in S phase [217]. If there is not enough lamin B1 present during micronucleation and at the same time it cannot be translated either, then there might be no lamin B1 available to coat the inner of the nuclear envelope. This technical effect might be partially responsible for the lamin B1 loss in MN after mitotic slippage.

A model to engineer cell lines with defined shattered chromosomes

Hatch et al showed in 2013 that MN can disrupt due to mechanical stress during interphase. There is the possibility that MN isolation via centrifugation with DCB can in some cases lead to a similar effect. Based on our studies, the DNA damage in the acceptor cell can be facilitated for example by increasing the mechanical force through centrifugation, or prolonged DCB treatment (**Figure 12**). DCB binds to actin, thereby inhibiting the elongation and shortening of the filaments [218,219]. This results in several cellular consequences based on either actin polymerization inhibition or interference of DCB with the actin network. Among those are transport failures [220], blockage of cell division, migration [221], cytokinesis failure [222], and cell shape loss [223]. These strong effects of DCB clearly show the potential for instability that we introduced to ease the disruption of the cytoskeleton and cell membrane during centrifugation. We could use this knowledge to investigate diverse chromosome-specific massive rearrangements introduced with the MMCT in more detail, especially, since the introduced changes are stably proliferated in the acceptor cell line. For example, the DCB concentration can be increased and the centrifugation timing prolonged to increase the probability of the generation of cells with additional rearranged chromosomes. This way, it might be possible to introduce massive chromosomal rearrangements on every single chromosome to decipher shared and mutually exclusive phenotypes. Thereby, the consequences of chromothripsis on defined chromosomes can be explored. Taken together, we transformed a method to engineer cells with intact additional chromosomes to a model system used to study sub-chromosomal and massive rearrangements, including chromothripsis, in the context of a defined additional chromosome.

Cells with more rearrangements have functional advantages

The cell is a fascinating organized part of living. Even if it undergoes massive DNA damage, there is a chance, that it will survive the chromosome chaos by reassembling the DNA fragments. Our data showed that these cells do not only survive but proliferate better than their aneuploid counterparts that did not undergo massive DNA damage and reassembly during the MMCT (**Figure 16** A). The reason might be an increased genomic flexibility due to the reshuffled DNA [224]. Interestingly, only HCT116 cells were generated with chromothripsis or massive rearrangement patterns. This could be due to the fact that non-cancerous RPE1 cells do not tolerate DNA damage as well as the HCT116 cells since the checkpoints in RPE1 are fully functional.

Chromothripsis was shown to result in OG amplification, for example by the fusion of DNA fragments to double minute chromosomes[128,126,225]. Moreover, the repair mechanisms after shattering are likely end-joining based, which was shown to cause loss of TSGs[38,128]. OG upregulation and TSG downregulation may contribute to the proliferation advantage of cells with massive chromosomal rearrangements. However, the functional advantage might be not solely based on TSG and OG deregulation. Rearranged chromosomes in cells result in less additional DNA in comparison to a gained intact chromosome (**Figure 16** B, C). The loss of genomic material might be a general proliferation improving effect, as shown in various studies: For example, Sheltzer et al. showed in 2017 that the aneuploid cell lines that lost the additional intact chromosome during an *in vivo* evolution improved their proliferation[139]. The proliferation advantage of cells with chromothripsis was observed also in a tetraploid model [226]. Noteworthy, tetraploidy does not have such a detrimental effect for the cells as aneuploidy has it [34,165]. Thereby, chromothripsis does not only increase the probability of TSG downregulation and OG upregulation, but it might provide the cells with a general beneficial effect on proliferation based on the loss of genomic material. Here, we showed that a chromosome transfer into a near-diploid cancer cell line can lead to chromosome rearrangements, such as chromothripsis and that these cell lines gain a functional advantage by this.

Conclusion

The nuclear lamina structure is ruptured upon lamin B1 loss, which leads to cytosolic fraction entry and DNA damage accumulation. This might be caused by the entry of cytosolic endonucleases that damage the DNA [134]. Furthermore, transcription [227,228] and DNA replication [229] are impaired due to a lack of lamin B1. However, MN acquire DNA damage also with an intact lamina. Therefore, other causes of the DNA damage in MN were considered, for example, asynchronous DNA replication. Delayed replication would lead to premature chromosome condensation causing further instability of the genomic material throughout subsequent cell cycles. Altogether the chromothripsis-like rearrangements in MN likely occur due to multiple aberrant processes, some of which are due to the lamin B1 loss [38,123]. With the MMCT we expanded a model system for the engineering of cells with extra

intact chromosomes towards a new approach of creating cell lines with shattered chromosomes. In the future, this may allow us to investigate the consequences of chromosome shattering in more detail and chromosome-specific. Moreover, with emerging sequencing technologies and new computational tools, we are now able to decipher mutational signatures, which are distinct frequencies of mutations including their neighboring base pairs. Previously, a mutational signature was assigned to chromothripsis [230]. It would be interesting to further elaborate this finding by comparing the signature to chromosome-specific chromothripsis patterns Mutational signatures allow to reduce the complexity of the uncountable number of different mutation types observed after chromothripsis. Therefore, this may drive forward the understanding of tumorigenesis and cancer progression based on chromothripsis.

The aneuploidy paradox

In several studies it was shown that aneuploidy provides a fitness advantage in stressful conditions. For example, Hsp90 inhibition in yeast cells led to the amplification of chromosome XV [231] and chronic heat stress caused gain of chromosome IX. Extended adaptation time led subsequently to selection of cells without aneuploidy, though, suggesting that less unfavorable alterations, such as small mutations, were selected as adaptation to stress [232]. Another study on yeast strains that went through an evolution with initial CIN and divers starting aneuploidies showed that selection of cells with lower CIN was the first mechanism of survival the cells exhibited. Initial gains of chromosome X (*greek for 10 (yeast chromosome)*) in haploid yeast cells caused a growth advantage, but during evolution the chromosome gain disappeared again [233]. Further they and others showed that despite differences in initial aneuploidies, the cells selected for similar aneuploidy patterns during evolution providing the cells with the best fitness over an extended evolution time [233,234]. Remarkably, under stress conditions in the cell culture, aneuploid cancer cells were able to grow faster in comparison to the euploid control cells [235]. Moreover, loss of an additional chromosome in a xenograft model resulted in the fitness advantage the cells needed to survive within the mouse model [139].

Therefore, these studies provide evidence that aneuploidy might be an initial survival mechanism in stressful environments, giving the cells the opportunity to select from a large set of modifications caused by the chromosome alterations. This effect might be linked to the detrimental consequences of aneuploidy [29,138]. Despite being unfavorable for the cells, aneuploidy occurs in cancer at a high frequency, and with cancer type and environment specific patterns [37,198,236].

The environment shapes the evolution of aneuploid cells

We assessed the evolutionary adaptation of newly engineered aneuploid cells with additional defined chromosomes by studying post xenografts and late-passaged cells. The post xenografts lost the additional chromosomes during the *in vivo* evolution (**Figure 20**) [139]. Therefore, they might not provide the best evolutionary model to study the consequences of defined additional chromosomes. However, they served as a useful model allowing us to compare the changes after *in vivo* evolution in cell lines with additional chromosomes that survived the stringent mouse environment to the *in vitro* evolved ones with and without additional chromosomes. Several observed phenotypes were similarly changed in cells after *in vivo* and *in vitro* evolution, suggesting that even different paths of evolution with different conditions and environments can shape a phenotype that is overlapping to some extent.

However, post xenografts and cell culture evolved cell lines deviate in some phenotypes as well. A feature approximating the malignant potential of cells can be evaluated by the so-called soft agar assay [237]. We observed that post xenografts grew better in soft agar, whereas *in vitro* cultured HCT116-derived aneuploid cell lines did not (**Figure 19** B). Different environments during the evolution may caused different evolutionary trajectories. Cells in culture do not need to improve the same

parameters as post xenograft. For example, they do not need to become invasive or adapt to a high three-dimensional cell density to outcompete the other cells. There is enough space in the cell culture flask and the cell density is kept lower 80%. We also exchanged the nutrient-rich medium regularly, which would be difficult to address in the animal model. The differences between the available nutrients in tumors in comparison to cells in culture are at least to a certain extent responsible for metabolic differences between the cells in the two model systems [238–241]. This might also influence cellular adaptations to stress. For example, cancer drugs inhibiting cell growth were efficient in cell culture but not in the animal model [242,243]. Interestingly, proliferation-associated enzymes that are used for metabolism are differentially expressed in a tumor and in cell culture [244–246], suggesting environment-related adaptations in the model cells. Altogether, changing environmental conditions cause altered clonal selection leading to cell line diversification. Subsequently, this results not only in genomic and transcriptomic but also in phenotypic diversity [247].

We observed deviations also between the cell lines within one type of evolution. In most post xenografts, the mitotic errors were reduced (**Figure 31**). The outlier cell line was Htr5 px2 that perhaps experienced GIN, as evidenced by the high levels of MN and 53BP1 foci (**Figure 30**). Moreover, this cell line gained chromosome 3 during the *in vivo* evolution (**Figure 20**). In agreement with the other tested cell lines, Htr5 px2 harbored less replication stress (**Figure 27**, **Figure 29**) and downregulated the lysosomal autophagy (**Figure 32** A). This might contribute to higher proliferative fitness. Htr5 px2 is a cell line illustrating that not only losing the additional chromosomes but also gaining a chromosome can contribute to a fitness adaptation in tumor cells. Noteworthy, the *in vivo* evolution caused mainly selection for cells without additional chromosome in the post xenografts. Only *in vitro* evolved aneuploid cells were able to retain the extra chromosome in the evolution series of 50 passages. However, the follow-up evolution series up to 80 passages showed deviations from this as well: Hte5 p0 contained four copies of chromosome 5, which changed during 50 passages to a trisomy 5 (**Figure 20**). With the next evolution series, we observed that the Hte5 p0 was trisomic and experienced again a chromosome 5 loss after 50 passages in at least one of the evolution replicates. This was observed for the extra chromosome in Htr3 as well, resulting in cell lines karyotypically similar to the wild type (**Supplementary figure 11**). An explanation might be unavoidable passages of the “p0” cell lines. As these were established years ago and routinely thawed and expanded, the name “p0” does not reflect the actual passage. Therefore, it might be that the initial cell line adapted over time by losing the extra chromosome. Altogether, it remains challenging to model an evolution series that could shed light on the question of how cancer cells adapt to the consequences of aneuploidy. With our approach, we showed that all, the loss of aneuploidy, the gain of aneuploidy, and the retaining of aneuploidy can bring functional advantages to the cells.

Chromosome 21 gain may trigger a route to fitness advantage

Different tumor types prefer different non-random aneuploidies. For example, additional chromosome 7 and a monosomic chromosome 10 are present frequently in glioblastoma. Skin cancers tend to lose a chromosome 9 and 10, while also gaining chromosome 7. Colon cancers often lose the 5q arm [248]. This suggests that in specific tumor types a selection for cells with those aneuploidy patterns offer the cells a fitness advantage. Injecting embryonic stem cells (ESC) into mice showed that diploid ones caused benign tumor growth. However, these ESC sometimes became spontaneously aneuploid. Upon transplantation of those aneuploid ESC in mice the tumor growth was malignant [249]. Taken together, tumor types harbor distinct aneuploidies that promote cancer progression. Even in experimental systems, selection of a beneficial karyotype has a high impact on tumor growth and cellular fitness.

WGS revealed that *in vitro* evolution of Htr5 and Hte5 resulted in at least a partial chromosome 21 gain in both cell lines independent from each other (**Figure 20**). This result was surprising as it was not described before. Exclusively in RPE1 derived evolved cells with additional chromosome 21, no change in the inter origin distance, MCM 2-7 levels and fork stability was observed in comparison to Rtr21 (**Supplementary figure 3**, **Supplementary figure 4**). A future question to answer is therefore, whether chromosome 21 gain in aneuploid cells in combination with additional chromosome 5 would contribute to the proliferation advantage. To this end, newly engineered HCT116 or RPE1 with a trisomy 21 and trisomy 5 could be established and compared to the respective cell line with only chromosome 5 gain or chromosome 21 gain respectively. The cell line´s deregulated pathways or individual proteins could be identified by mass spectrometry to find those which are exclusively altered in the cell lines with both, chromosome 5 and 21. This might shed light on the question why a chromosome 5 gain over time results in an additional gain of chromosome 21. The combination of both chromosomes might result in a fitness improvement of the cells that compensates the negative effect given by only one of the two amplified chromosomes.

A faster cell proliferation with slower replication

We observed a reduced replication rate and more activated MCM 2-7 helicases, in all studied aneuploid cells, as well as in wild type HCT116 after evolution (**Figure 24**, **Supplementary figure 4** A). This was supported by cell cycle experiments showing a delay in S phase after evolution (**Figure 22**). However, replication is a substantial part of the cell´s overall proliferation, which was improved in aneuploid cells after evolution (**Figure 19**). To further validate this contradictory observation, a cell cycle study using the FUCCI system to circumvent potential stress, based on the synchronization, could be used [250]. However, if the observations will be confirmed, there are at least two options how a slowed replication rate might contribute to an improved overall fitness of the cells. First, the advantage of a generally slowed replication fork progression might be an improved tolerance to replication stress as shown in fission yeast. They showed that the slowdown of the replication machinery is a checkpoint-

independent effect [251]. In that case, the cell might still experience replication stress, but the signaling would be reduced as the cells found a way to disregard it. The second explanation would be that the slowdown of the replication machinery is a mechanism to prevent fork stalling events by a more faithful replication after evolution. The exact mechanism of how this might contribute to a faster proliferation remains to be investigated. Therefore, a question to answer remains if the replication speed reduction might be beneficial for the cells due to disregarding the potential replication stress or due to a more faithful replication.

A possible experimental setup to study the DDR in more detail with respect to a potentially quicker progression through the cell cycle would need a deeper knowledge of the DNA repair mechanisms in aneuploid cells before and after evolution. A question to answer would be how long the cells need before and after evolution to repair DNA damage in individual cell cycle phases. A more efficient DNA damage repair mechanism could also influence the progression through the cell cycle and may result in faster proliferation. An image-based screen of repair proteins, with several timepoints after DNA damage could shed light on this question. Another question to answer would be which proteins might be associated with slowed forks in comparison to those with normal fork speed. To shed light on this question, a pulldown of a specific replication-associated protein, such as a polymerase or the MCM 2-7 helicase in S phase synchronized cells before and after evolution could be performed followed by mass spectrometry to specifically identify proteins that are associated with slowed forks. Two controls could be first, aphidicolin-treated cells that reduce the fork speed, and second, ATR-inhibited cells that activate all dormant origins. A third open question is whether the slowed replication sites are at specific loci in the genome. This could be addressed using either EdU seq [252] or FISH probes combined with DNA combing [253]. Taken together, there are multiple ways to address the mechanistic link between DNA repair and replication dynamics that might help to answer the question of why the cells can improve proliferation after evolution despite the reduction of the replication rate.

The reduction of the replication speed was a general observation upon evolution, unlike the proliferation advantage. Another hypothesis for this difference between aneuploid cell lines and near diploid chromosomal stable cell lines might be that the proliferation capacity of diploid cells is the highest possible in the defined setup. The additional chromosome leads to detrimental effects, including the proliferation decrease[29,138]. Therefore, the aneuploid cells started the evolution with a disadvantage. While the wild type did not have much scope for improvement, the aneuploid cell had at least the potential to reach wild type levels.

To sum up, if the replication turns out to be causative for the proliferation advantage, the cell cycle of aneuploid cells must benefit from the observed changes in the time course of evolution more than wild type cells benefit from the slowed replication. Mechanistic links between a potential disregard of replication stress or a more faithful replication due to the replication rate reduction remain to be

investigated. Moreover, it might be that the ability to improve is faster saturated in wild type cancer cells in comparison to aneuploid cells, which exhibit proliferation disadvantage due to the additional chromosome.

Interplay between replication and autophagy

We showed that lysosomal pathways are downregulated after evolution (**Figure 21**), which led us to try the validation of these observations. The lysosomal marker protein LAMP1 supports the finding of the TMT data, whereas the LysoTracker™ investigation showed a decrease only upon in *vivo evolution* (**Figure 32**). Autophagy in cancer is currently not well understood. Depending on the stress conditions and the tumor stage autophagy can have both, tumor suppressive and oncogenic roles [254]. On the one hand, autophagy was shown to alleviate metabolic stress and DNA damage [255] and on the other hand, oncogenic outcomes due to autophagy were found, for example, reduction of chemotherapeutic effects and promotion of early-stage cancerous lesions [256,257].

The DDR during replication is deregulated based on a set of activated OGs or downregulated TSGs in cancer cells. For example, the oncogene *RAS* induces replication stress [75] and autophagy upon its upregulation [258]. Moreover, autophagy has the potential to induce senescence [259], eventually limiting the proliferation of abnormal cells. Yet, autophagy induced by RAS could also reduce metabolic stress and thereby facilitate tumor growth [260,261]. Htr5, Htr5p50, and Htr5px2 have the p-arm of chromosome 12 in three copies (**Figure 20**). Noteworthy, the *KRAS* gene is located there, providing a potential explanation for the differences between Htr5 and Hte5 derived evolved cell lines in terms of their lysosomal autophagy markers. In line with this hypothesis, Htr5 px3 does not share the partial trisomy 12 and shows consistently high lysosome content (**Figure 32**)(**Supplementary figure 8**). Mostly, replication stress signaling, and lysosomal autophagy measures were decreased upon the evolution of aneuploid cells. A question remains about whether there is a direct link between these two observations of slowed replication and increased autophagy after evolution in aneuploid cells.

The proteotoxic stress caused by the additional chromosome is triggered by mis-and unfolded proteins [262–264], which could activate a higher lysosomal degradation and thereby saturate the protein recycling machinery, explaining the high abundance of lysosomal proteins after chromosome addition [264,265]. To test this, one could isolate autophagosomes and perform mass spectrometry to see whether specifically, replication-associated proteins are present in these vesicles in aneuploid cells before evolution. Comparison to the effects after evolution may shed light on explaining the replication defect in aneuploid cells. Moreover, cells require autophagy to stabilize the dNTP pools by recycling molecules after replication [260]. If more DNA needs to be replicated, also more dNTPs need to be present. This is crucial for a faithful replication, and otherwise, shortage of nucleotides causes replication stress. Furthermore, cellular stress that is related to the newly engineered aneuploid cell lines might have a destructive impact on DNA replication and repair, causing the cells to accumulate DNA in the cytosol.

Consequently, the cGAS-STING-pathway becomes activated, which in turn leads to lysosomal gene expression [265]. The adaptation to the presence of free DNA in the cytosol over time would alleviate the consequences of it and could explain the downregulation of the lysosomal pathway after evolution (**Figure 21**). To test this, the abundance of cGAS-STING pathway-associated proteins could be tested in cells before and after evolution, for example, IRF3. Malfunctioning autophagy also destabilizes DNA repair, thereby linking autophagy to genome stability. Autophagy depletion, for example, causes homologous recombination defects [266,267]. As evolution at least partially restored autophagy levels, it might be causative for improved homologous recombination during replication, ensuring a robust DNA replication. However, the mechanisms, as well as the impact on aneuploid cells in this study remains to be investigated.

Future perspectives

To further investigate early-onset changes as seen during the prolonged evolution series (**Supplementary figure 10**, **Supplementary figure 13**, **Supplementary figure 14**), it would be useful to karyotype more evolved clones especially early on, for example at p20, to understand at which timepoint Hte5 e1 lost the additional chromosome. Furthermore, to circumvent phenotypic differences based on a heterogenous cell population, that exists after passaging, it might be worth comparing the obtained results to another type of evolution that is composed of a homogenous cell population. A more homogenous evolution model would be the selection of single-cell clones from chromosomally stable cell lines. This type of *in vitro* evolution would allow us to specifically select small and large colonies for direct comparison between fast and slow proliferating cells. A naive calculation revealed that the cells in large colonies might need 11 generations and in small colonies 13 generations before one could pick and re-culture the individual colonies in separated small dishes (**Table 2**). Despite this time frame, this would be the most homogenous population from a near diploid chromosomally stable cell line allowing phenotypic assessment without using single cell techniques. It would be interesting to compare the results to the aberrations in cells after *in vitro* evolution, especially, since adaptive changes in aneuploid cells appear already after 20 passages (**Supplementary figure 14**).

Table 2: Simulative calculation. Exponential growth estimation of the cell number, doubling time in hours (h) and generations for an exemplary small (ø 2mm) and large (ø 4mm) colony size after 14 days of culture starting with one cell per colony. RPE1 cell size was used [268].

parameters					
days in culture to reach assigned colony size	14				
start cell number	1				
RPE1 average cell size (um)	33.5				
area of the cell (sqmm)	0.0009				
		simulated results after 14 days growing to the respective colony size, assuming exponential growth			
diameter of colony to be picked (mm)		**colony area (sqmm)**	**cell number**	**doubling time (h)**	**generations**
big	4	12.57	14257.07	24.35	13.80
small	2	3.14	3564.27	28.48	11.80

Another future perspective could be to trace back the evolved cell lines to their origin for example from a karyotype's point of view to understand the evolutionary trajectories of aneuploid cells. To this end, single-cell sequencing or transcriptomics could shed light on population heterogeneity and would be a great tool, to identify specific genomic alterations during evolution. Selmecki et al. showed in 2015 that specific chromosomal aberrations are linked to variable cellular fitness in yeast [269]. Another study revealed that adaptations to CIN happen dependent on the ploidy of the cells and result in distinct chromosomal changes [233]. Therefore, the study of the *in vitro* evolution-dependent changes might shed light on recurrent genetic abnormalities, and their physiological consequences that eventually result in a fitness advantage of the cancer cells.

Consequences of whole genome doubling

Although it is a common and natural phenomenon in some species and distinct cell types [36,270,271], WGD drives tumorigenesis, facilitates metastasis, drug resistance and poor patient survival [188–191]. Tetraploidy can quickly evolve into chromosomal instability (CIN), continuous chromosomal aberrations that change the baseline for adaptations and this with every single cell cycle [31]. Therefore, WGD provides the cells that survive a WGD doubling event with a higher genomic flexibility. Here, we explored potential drivers of the proliferation after WGD and the very first S phase in single-molecule resolution immediately after a WGD event that leads to DNA damage accumulation. Finally, we assessed the karyotypic consequences of WGD.

Cellular WGD response patterns in surviving cells

A large fraction of the cells arrests after a WGD event. Double the amount of DNA leads to the inhibition of MDM2, p53 stability and p21 mediated cell cycle arrest [169,170].

USP28 negatively regulates the cell cycle

USP28 is a deubiquitinase [272] that is required to stabilize Chk2 and TP53BP1 in response to DNA damage [273]. We identified USP28 within 140 candidate genes from an RNAi screen that clearly showed improvement in cell cycle progression upon their depletion in tetraploid cells [194]. Thus, USP28 negatively regulates the cell cycle in tetraploid HCT116. USP28 is required for MYC stability in tumor cells, as it antagonizes the ubiquitin-dependent degradation of MYC. Thus, USP28 has a role in cancer progression [272,274] and the inhibition of its enzymatic activity may be a potential target for cancer therapy [274]. This shows that USP28 has already some known target specific functions in the cell, as in the DDR. However, a function of USP28 in centrosome clustering upon cytokinesis failure was new. Upon USP28 deletion centrosome clustering is increased eventually leading to more pseudo-bipolar and less multipolar mitosis [194].

The association of NUMA1 with USP28

NUMA1 functions as connector between microtubules and dynein/dynactin. This generates tractive forces to control the exact localization of the spindle poles [275]. Thereby, NUMA1 functions in clustering multiple centrosomes [276], allowing a bipolar spindle formation [195]. A reduced amount of NUMA1 in tumor cells leads to higher centrosome clustering, whereas an increased abundance of NUMA1 causes more multipolar mitoses [276]. The abundance of NUMA1 stays unaffected upon USP28 loss [194] suggesting another yet undiscovered regulation involving NUMA1 and USP28. The novel putative interaction of NUMA1 and USP28 allows an explanation of why some tetraploid cells might survive after a WGD event. If USP28 interacts with NUMA1, the normal function of NUMA1 in bipolar spindle formation might be compromised in tetraploid HCT116. By counting aberrant mitosis it was found that absence of USP28 increases the efficiency of spindle pole clustering towards pseudo-bipolar spindles [194]. These spindles are formed in cells with multiple centrosomes which clustered together to

form bipolar spindles. This so-called pseudo-bipolarity allows faithful chromosome segregation even in cells with multiple centrosomes. Thus, pseudo-bipolar spindles are less lethal for cells in comparison to multipolar spindles [173]. Besides the function in centrosome clustering, NUMA1 might have a role in the DDR [277]. Together, the association of NUMA1 with USP28 allows to annotate an additional deregulating function of USP28, namely in the clustering of spindle poles. Upon the absence of USP28 the cell more frequently divides pseudo-bipolarly, perhaps with the help of NUMA1, leading to a higher potential to survive WGD.

The association of MDC1 and USP28

The second identified interactor of USP28 that is enriched specifically in tetraploid cells is MDC1, which has been previously implied to function in DNA damage signaling together with USP28 [196]. DNA damage is elevated in tetraploid cells, for example seen by imaging of the 53BP1 and γ-H2A.x foci [194,278]. DNA damage accumulation was shown in binucleated human cancer cells, but also in Drosophila after WGD upon asynchronous replication [279,280]. Already in the very first cell cycle after WGD DNA damage accumulates in S phase [197]. Moreover, the DNA damage repair was delayed in tetraploid HCT116, and immunoblotting of proteins involved in the DNA damage signaling cascade revealed a general upregulation of the replication checkpoint signaling cascade in tetraploid cells. Importantly, the checkpoint activation was weakened by depleting USP28 [194]. Survivor cells after WGD might undergo mitotic failures from which the daughter cells gain aneuploid karyotypes, further increasing the likelihood for DNA damage and replication stress [138]. However, the mechanism of replication stress as direct response to WGD remained unknown so far.

A low number of active origins immediately after WGD accelerates fork speed and induces replication stress

DNA damage accumulates in the first replication after WGD [197]. We performed DNA combing to shed light on the replication dynamics and found a compromised fork stability and a lower number of active origins. Surprisingly, DNA combing revealed an increase in replication speed after WGD through all approaches: CF, MS, and EnR (**Figure 34** A (left), B (left)). Inter origin distance and replication speed are highly interdependent, and although the exact mechanisms behind are not yet understood, it is known that dependent on the conditions an increase in replication fork velocity can be either cause or consequence of less activated origins [281–283]. In this scenario of DNA damage accumulation in the S phase early after WGD, the increase in replication fork velocity was likely a consequence of too less activated forks as important replication factors were not scaled up [197]. Moreover, the altered fork symmetry after WGD implies fork collapse as a general slowdown was not observed. In line with that RAD51 as well as FANCD2 foci were of elevated number in cells after WGD [197]. These two proteins are markers for replication restart [284,285]. G1 phase prolongation was able to restore replication-associated protein levels and decrease replication-associated DNA damage [197]. Placing this finding in the context

of another recent study it is feasible that the DNA damage after WGD is based on low preRC formation [286]. Not yet sufficient MCM proteins were assembled to bind to the DNA, causing a faster error-prone replication. But also replisome factors, such as Treslin and PCNA, failed to scale up appropriately after WGD [197]. Indeed, Treslin downregulation elevated the replication machinery velocity [287]. Overall likely both, low replisome and low preRC formation levels contribute via increased fork speed and higher fork stalling to the DNA damage accumulation in the S phase early after WGD. But G1 extension gives the cells more time for transcription and translation, thus, more replication proteins can be assembled, which eventually lowers the DNA damage phenotype. Importantly, there is a crucial balance between replication proteins and replication dynamics, both contributing to a tight scheduled faithful and full duplication of the DNA in the S phase. This homeostasis is compromised by WGD in the very first S phase. The study shows that GIN in WGD has its origin in the first interphase after WGD. Long-term effects of WGD are in contrast a balanced protein level according to the amount of DNA [288,289], implicating an evolutionary adaptation towards protein levels that replicate the DNA more faithful.

A timely and accurate replication is critical also for the proliferation of whole genome doubled cells. It will need further investigations to understand the exact mechanisms that drive the adaptation towards a karyotype that supports physiological proliferation benefits in tetraploid cancer cells.

Karyotypic WGD response patterns in surviving cells

WGD drives karyotype heterogeneity

The dependence on the context makes aneuploidy a fascinating to study subject [236]. But in all the diverse contexts, for example different immune systems of cancer patients and different tumor stages, genetic alterations do overlap. WGD+ and WGD- tumors were systematically compared. Importantly, WGD+ tumors have a higher level of aneuploidy and experience more chromosome losses than gains [31–33,164,198]. This is reflected by the karyotype study in human cancer cell lines. Moreover, whole chromosome aneuploidies were more frequent than arm-level changes (**Figure 35**). A possible explanation is that cells after WGD undergo more frequently chromosome mis-segregation [34,160,162,165,288]. Alternatively, a cause could be that the cells tolerate whole chromosome imbalances more than arm-level aberrations. Nevertheless, chromosome-arm aberrations in WGD+ tumors were identified recurrently, for example, the genetic interaction of chromosome 8p being lost and chromosome 8q being gained together in app. 20% of colon cancers. In the same tumor type, the complete chromosome 8 is rather gained than lost [198]. It remains speculative to conclude the chromosome arm 8q gain as being a cancer driver.

Our findings demonstrate that WGD-associated aneuploidies differ from those aneuploid patterns that arose without WGD in human cancers. Also, in yeast differences between aneuploidy patterns dependent on the ploidy of the cells were observed [233]. Interestingly, cells with a leaner distribution of the CN were characterized as energetically more likely to undergo WGD [290]. This thermodynamic adaptation reflects the findings of different genetic reoccurrences and mutual exclusive observations in WGD+ and WGD- tumors [198].

In 2020 Corsello et al showed that aneuploidy can serve as a biomarker to infer cancer therapeutics: Screening of >100 cancer cell lines with 5000 FDA-approved common drugs (most of them having no link to cancer) revealed that a drug named disulfiram is a candidate for cancer therapy. Disulfiram is used to treat chronic alcoholism but in presence of metals, it becomes a proteasome inhibitor, thus killing cancer cells. Surprisingly, loss of the long arm of chromosome 16 in this cancer cell cohort was strongly associated with sensitivity to disulfiram. Scientists previously found metallothionein-encoding genes on this lost part of chromosome 16 [291]. Upon knockout of those specific genes, the s could confirm that the cancer cell lines become more sensitive to disulfiram [292]. Thus, a realistic goal at this point is to specifically target aneuploid patterns in cancer cells and try to selectively kill them.

Conclusion

These investigations on the consequences of WGD provided insights into the question how tetraploid cells survive after WGD and showed that the DNA damage that accumulates in the S phase during the first cell cycle after WGD is based on a not appropriate upscaled number of active origins. Under replicated DNA facilitates GIN. The DNA damage due to GIN may alter TSGs and OGs but also genes

involved in genome maintenance which could eventually lead to CIN and aneuploidy, thereby promoting tumorigenesis or tumor progression [25].

The fine balance of replication dynamics

In two of the here discussed studies replication dynamics were assessed as a parameter describing distinct features of the cellular replication based on a single molecule analysis. In both studies the results were surprising. First, we showed that aneuploid cells that suffer from replication stress do not show a decrease of replication speed as observed with aphidicolin treatment. And second, replication speed in early tetraploid cells was even amplified, despite DNA damage accumulation in S phase. Moreover, the fork stability was compromised in both studies: Early after engineering, aneuploid, as well as tetraploid cells have more unstable forks in comparison to the wild type. A low number of active origins can be causative for the rapid fork progression as both are balancing each other. But if that is not sufficient to replicate the DNA faithfully, it results in unstable forks, signs of replication stress. The cell has a surplus of MCM 2-7 proteins [286]. However, the amount of replication proteins is not unlimited and might be not sufficient to replicate the doubled amount of DNA. In the scenario of DNA damage accumulation in the S phase early after WGD, the increase in replication fork velocity is likely a consequence of too less activated forks as important replication factors are not scaled up [197]. Nucleotide imbalance was shown to slow S phase progression and induce checkpoint activation [293,294]. However, in the first interphase after WGD it was not observed that the medium supplemented with nucleosides rescued the DNA damage phenotype [197]. This observation might be caused by a sufficient amount of nucleosides available in the cells, unlike other tested replication factors, such as MCM2, CDT1, PCNA, and E2F1 [197]. These not-upscaled replication-associated proteins cover the eventual effect of nucleoside supplement. As broken machines, this would cause the replication machinery not to be able to utilize the additional nutrients and result in unstable forks, DNA damage, and GIN. Thus, the replication dynamics resemble a causative cascade in the S phase that needs to stay in homeostasis to perform a faithful replication (**Figure 36**).

The MCM 2-7 helicase is downregulated in aneuploid cells as well [138], suggesting that a similar mechanism involving too few active origins causes the fork asymmetry. In HCT116-derived aneuploid cells, there is a slight decrease in the number of active origins

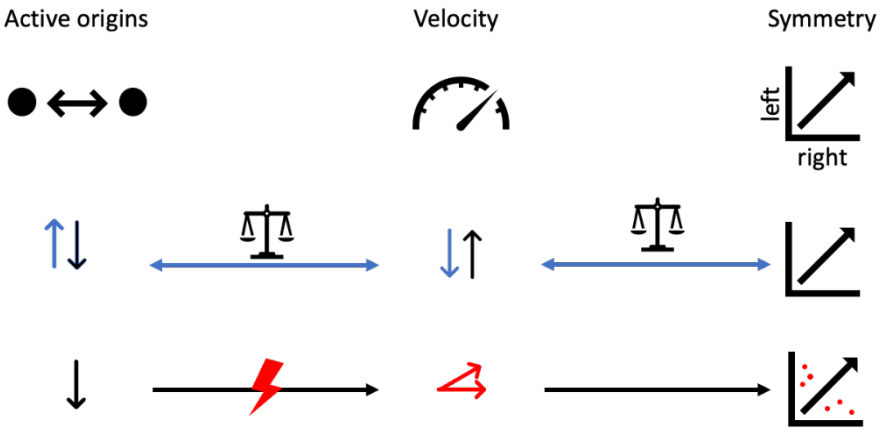

Figure 36: Simplified scheme of fine balancing replication dynamics. The number of active origins and the replication fork velocity are in a balance to ensure a faithful replication. A decrease of replication speed elevates the number of active origins (blue) to care for no fork stalling events measurable by fork symmetry assessment. An increase of replication speed might be caused by fewer activated origins. If this deficit is too high to be compensated, the fine balance is in trouble (red), which eventually leads to asymmetric forks as marker of replication stress.

visible. However, observations of the ability to replicate with low MCM 2-7 abundance showed in *Caenorhabditis elegans* [283], *Drosophila melanogaster* [295], and human cells [296,297] that a decrease up to 90% would not influence the S phase progression much and that a surplus of MCM 2-7 proteins usually ensures a faithful replication [286]. The mechanistic understanding of the replication dynamics of aneuploid cells is missing so far. Future studies will shed light on understanding of the replication dynamics observations and perhaps answer the question of why cells do not reduce the replication rate as hypothesized after a chromosome addition.

Taken together, the replication dynamics are a powerful tool to study replication at a single molecule level. However, we need to understand the regulation of the fine balance between replication speed, activated origins and fork symmetry to further elucidate mechanistic associations of the causes and consequences of the replication dynamics changes.

Material and Methods

Material

Equipment

Table 3: Equipment.

Equipment	Company
ASI MS-2000 stage	Applied Scientific Instrumentation, Eugene, USA
AttuneTM NxT Flow Cytometer	Life Technologies, Carlsbad, USA
Azure c300 system	Azure Biosystems, Dublin, USA
Bullets	Custom made at core facility
c500	Azure biosystems, Dublin, USA
Cell culture dish (all sizes)	Sarstedt AG & CO, Nürmbrecht, Germany
Combicoverslip clip holder	Genomic Vision, Paris, France
CoolSNAP HQ2	Teledyne Photometrics, Tucson, USA
Countess II	Thermo Fischer Scientific, Waltham, USA
CSU-X1 Confocal Scanner	Yokogawa GmbH, Herrsching, Germany
Disposable Reservoirs	Genomic Vision, Paris, France
Engraved CombiCoverslips	Genomic Vision, Paris, France
Eppendorf centrifuge 5415R	Eppendorf SE, Hamburg, Germany
Epson perfection V370 Photo	Epson, Suwa, Japan
FiberComb® (Molecular Combing System)	Genomic Vision, Paris, France
Glass-bottomed black well 96-well plate	Greiner Bio-One, Kremsmünster, Österreich
Heat Block	Störk Tronic, Stuttgart, Germany
HERA cell incubator	Fisher Scientific, Waltham, USA
HERA safe clean bench	Heraeus Instruments, Hanau, Germany
Integra Vacusafe	Integra Bioscience GmbH, Biebertal, Germany
Inverse-Microscope AE 2000-Trino	MOTIC, Wetzlar, Germany
JA25-50 Sorvall centrifuge rotor	Thermo Fischer Scientific, Waltham, USA
LaserStack (473 nm, 561 nm, 640 nm)	Intelligent Imaging Innovations, Denver, USA
LLG Tube uniRoller 10	Lab Logistics Group, Meckenheim, Germany
Mini-PROTEAN® Glass plates (1mm)	Bio-Rad Laboratories, Hercules, USA
Mini-PROTEAN® Short plates	Bio-Rad Laboratories, Hercules, USA
MS-2000 stage	ASI, Eugene, USA
Nalgene polycarbonate centrifuge tubes	Thermo Fischer Scientific, Waltham, USA
Nitrocellulose Blotting Membrane	GE Healthcare, Chicago, USA
Objectives 20x air, 40x air, 60x oil	Zeiss, Oberkochen, Germany
Photometrics CoolSNAP HQ2 and Cool SNAP EZ 22	Teledyne Photometrics, Tucson, USA
PowerPacTM HCHigh-Current Power Supply	Bio-Rad, Hercules, USA
Precision Scale PCB	KERN & SOHN, Balingen, Germany
Promega GloMax EXPLORER	Promega, Walldorf, Germany
Rotina 420R	Hettich, Beverly, USA

Sterile Cloning Discs	Sigma-Aldrich, St.Louis, USA
Swinnex filter holder and gaskets	Merck, Millipore, Darmstadt, Germany
Trans-Blot Turbo	Bio-Rad, Hercules, USA
Vortex Genie 2	Scientific Industries, Bohemia, USA
Water bath Typ1008	GFL, Burgwedel, Germany
Whatman Cyclopore/Nuclepore filters: 8µm, 5µm, 3µm	VWR, Radnor, USA
Zeiss Axio Observer Z1	Carl Zeiss AG, Oberkochen, Germany

Antibodies

Table 4: Antibodies.

Antibody	Reference	Dilution
DNA combing		
Rabbit anti ssDNA	IBL International 18731	1:5
Rat anti CldU	Abcam Ab6326	1:10
Mouse anti IdU	BD Bio- sciences 555627	1:10
Anti mouse Alexa Fluor 647 donkey	Biozol JIM-715-605-151	1:25
Anti rat Alexa Fluor 594 donkey	Biozol JIM-712-585-153	1:25
Anti rabbit Brilliant Violet 480 donkey	Jackson Immuno Research 711-685-152	1:25
Immunofluorescence and Flow cytometry		
Rabbit anti lamin B1	Abcam ab16048	1:500
Mouse anti gamma H2A.x	Abcam ab26350	1:10000
Human anti centromere	ImmunoVision HCT0100	1:500
Anti rabbit Alexa Fluor 647	Jackson ImmunoResearch 711-605-152	1:1000
Anti rabbit Dylight 405	Jackson ImmunoResearch 711-475-152	1:1000
Anti mouse Alexa Fluor 594	Jackson ImmunoResearch 715-858-150	1:10000
Anti-human antibody Alexa Fluor 647	Jackson ImmunoResearch 715-858-150	1:1000
Rabbit anti γ-H2A.x	Abcam, Ab2893	1:1000
Rabbit anti 53BP1	Millipore MAB3802	1:500
Mouse anti cyclin A	Abcam Ab181591	1:500
Anti rabbit Alexa Fluor 594 Donkey	Jackson Immunoresearch 715-858-152	1:500
Anti mouse Alexa Fluor 647 Donkey	Jackson Immunoresearch 715-605-151	1:500
Mouse anti p62	Santa Cruz sc-28359	1:500
Rabbit anti LAMP1	Abcam, ab24170	1:200
Mouse anti LC3	Cell signaling, 4108	1:100
Rabbit anti pRPA2 S33	Abcam, ab2175	1:500
Western Blot		

Rabbit anti MCM2	Abcam ab4461	1:500
Rabbit anti MCM3	Cell Signaling 4012	1:500
Rabbit anti MCM4	Cell Signaling 12973	1:500
Rabbit anti MCM5	Biorbyt orb128349	1:500
Rabbit anti MCM6	Biorbyt orb48461	1:500
Rabbit anti MCM7	Cell Signaling 3735	1:500
Goat anti MCM2	Santa Cruz sc-183	1:1000
Mouse anti MCM5	Santa Cruz Sc-165994	1:1000
Mouse anti RPA32/RPA2	Abcam ab2175	1:1000
Rabbit anti pRPA21 S33	Bethyl A300-246A	1:1000
Rabbit anti pRPA32 S4S8	Bethyl ICH-00422	1:1000
Mouse anti β-actin	Sigma-Aldrich A5441	1:1000
Anti rabbit HRP Goat	R&D Systems HAF008	1:2000
Anti mouse HRP Goat	R&D Systems HAF007	1:2000
Anti goat HRP	R&D Systems HAF009	1:2000
Rabbit anti Chk1	Abcam, Ab32531	1:1000
Rabbit anti pChk1	Cell Signaling, 2341	1:1000
Goat anti histone 3	Abcam, Ab12079	1:1000

Chemicals

Table 5: Chemicals.

Chemicals	**Company**
Acetic acid	Sigma-Aldrich, St.Louis, USA
Acrylamide/Bis Solution 37.5:1, 30% w/v	SERVA Electrophoresis, Heidelberg, Germany
Agarose	Carl Roth GmbH, Karlsruhe, Germany
Albumin Bovine Serum (BSA)	BWR Life Sciences, Leuven, Belgium
Antifade Mounting Medium with DAPI, VECTASHIELD	Biozol, Bellingham, USA
Aphidicolin	Sigma-Aldrich, St.Louis, USA
APS	Thermo Fisher Scientific, Waltham,USA
BlockAid	Thermo Fisher Scientific, Waltham,USA
Blocking aid DNA combing	Thermo Fisher Scientific, Waltham,USA
Bromophenol blue	Sigma-Aldrich, St.Louis, USA
ClarityTM Western ECL Substrate	Sigma-Aldrich, St.Louis, USA
ClDU	Sigma-Aldrich, St.Louis, USA
Colchicine	Sigma-Aldrich, St.Louis, USA
Cytochalasin B	Sigma-Aldrich, St.Louis, USA
Cytochalasin D	Sigma-Aldrich, St.Louis, USA
DAPI	Carl Roth GmbH, Karlsruhe, Germany
Dimethylsulfoxid (DMSO)	Roth, Karlsruhe, Germany
DMEM + GlutaMAXTM-I	Thermo Fisher Scientific, Waltham,USA
Doxorubicin	Sigma-Aldrich, St.Louis, USA
EdU	Sigma-Aldrich, St.Louis, USA
Ethanol	Sigma-Aldrich, St.Louis, USA

FBS	Thermo Fisher Scientific, Waltham,USA
Hydroxyurea	Sigma-Aldrich, St.Louis, USA
IDU	Sigma-Aldrich, St.Louis, USA
Lipofectamine	Fisher Scientific, Loughborough, UK
Lumigen ECL Ultra Solution	Lumigen, Southfield, USA
LysoTracker™ Red DND-99	Thermo Fisher Scientific, Waltham,USA
Methanol	Fisher Scientific, Loughborough, UK
Opti-MEM	Thermo Fisher Scientific, Waltham,USA
PEG	Sigma-Aldrich, St.Louis, USA
Pen-Strep	Thermo Fisher Scientific, Waltham,USA
PHA-P	Sigma-Aldrich, St.Louis, USA
PhosSTOP EASYpack	Roche Diagnostics, Mannheim, Germany
Ponceau	Sigma-Aldrich, St.Louis, USA
Precision Plus ProteinTM All Blue Standards	Bio Rad Laboratories, Hercules, USA
Propan-2-ol (Isopropanol)	Fisher Scientific, Loughborough, UK
Protein Assay Dye Reagent Concentrate	Bio Rad Laboratories, Hercules, USA
RNaseZap™	Thermo Fisher Scientific, Waltham,USA
Skim Milk powder	Serva, Electrophoresis GmbH, Heidelberg, Germany
Sodium Azide 1mM NaN3	Sigma-Aldrich, St.Louis, USA
Sodium chloride (NaCl)	Sigma-Aldrich, St.Louis, USA
SYTOX™ Green	Thermo Fisher Scientific, Waltham,USA
TEMED	AppliChem, Darmstadt, Germany
Tris-HCl	Carl Roth GmbH, Karlsruhe, Germany
Tris(hydroxymethyl)aminomethane	AppliChem, Darmstadt, Germany
Triton X-100	Carl Roth GmbH, Karlsruhe, Germany
Trypsin-EDTA	Thermo Fisher Scientific, Waltham,USA
Tween-20	Sigma-Aldrich, St.Louis, USA
β-Mercaptoethanol	AppliChem, Darmstadt, Germany

Kits

Table 6: Kits.

Kit	**company**
24XCyte Human Multicolor FISH Probe Kit	MetaSystems Probes GmbH, Altlußheim, Germany
CellTiter-Glo® Luminescent Cell Viability Assay	Promega, Fitchburg, USA
Click-iT™ EdU Imaging Kit	Thermo Fisher Scientific, Waltham,USA
DNA easy® Blood and Tissue	Quiagen, Venlo, Netherlands
FiberPrep® (DNA Extraction Kit)	Genomic Vision, Paris, France
Rneasy®Mini kit	Quiagen, Venlo, Netherlands
Subcellular Protein Fractionation Kit	Thermo Fisher Scientific, Waltham,USA
TMTduplex™ Isobaric Mass Tagging Kit	Thermo Fisher Scientific, Waltham,USA

Buffers and solutions

Table 7: Buffers and solutions.

Buffer or solution	Composition
Bjerrum Schafer-Nielsen Buffer	48 mM Tris, 29mM glycine, 20% (w/v) methanol (absolute).
Blocking solution for immunoblotting	5 % (w/v) skim milk in TBS-T
Blocking solution for immunofluorescence staining	3% BSA in PBS-T
Bradford solution	20 % Bradford reagent; in H2O
Denaturation solution	0.5 M NaOH; 1.5 M NaCl in nuclease-free H2O
EdU Click-iT reaction mix	Eterneon-Red 645 10 mM; Tris 1.5 M (pH 8.8); CuSO4 500 mM; Ascorbic acid 500 mM in PBS
Fixation solution with formaldehyde	37% formaldehyde diluted 1:10 in PBS
Fixation solution with methanol	25% Acetic acid in methanol
Freezing solution	10% DMSO in FBS
Lämmli buffer	62.5 mM Tris/HCl pH 6.8, 2% (w/v) glycerol, 0.002% (w/v) bromphenol blue, 2.5% β-mercaptoethanol.
Lower SDS-buffer (pH 8.8)	1.5 M Tris-HCl, 0.4% (w/v) SDS
PBS 1x (pH 7)	140mM NaCl, 2.7mM KCl, 6.5mM Na2HPO4, 1.5mM KH2PO4
PBS-T	0.05% Tween-20 in PBS
Ponceau solution	0.2 % Ponceau, 1 % acetic acid
Radioimmunoprecipitation assay (RIPA) buffer (pH 7.5)	10 % NP-40, 10 % sodium deoxycholate, 5 M NaCl, 0.5 M EDTA, 1 M Tris, protease inhibitor cocktail (cOmplete Mini, EDTA-free) and phosSTOP following manufacturer's instructions.
Resolving gels	12,5% polyacrylamide gels
SDS-PAGE running buffer	25 mM Tris-HCl, 200 mM glycine, 0.1% (w/v) SDS
Stacking gels	5% polyacrylamide gels
TBS-T (pH 7.5)	50 mM Tris, 150 mM NaCl
Upper SDS-buffer (pH 6.8)	0.5 M Tris-HCl, 0.4% (w/v) SDS
Wet Transfer buffer	25 mM Tris; 192 mM glycine; 20 % (v/v) methanol; in H2O

Cell lines

Table 8: Cell lines.

Cell line	Parental cell line	Induced polysomy	comment
HCT116	-	-	near diploid chromosomally stable colorectal cancer cell line
Hte5_14	HCT116	chr. 5	
Htr5_17	HCT116	chr. 5	
Htr5_18	HCT116	chr. 5	
Htr13_02	HCT116	chr. 13	
Htr18_01	HCT116	chr. 18	
Htr21_01	HCT116	chr. 21	
Hte5_01	HCT116	chr. 5	With rearrangements
Htr5_16	HCT116	chr. 5	With rearrangements
Htr5_19	HCT116	chr. 5	With rearrangements
Htr13_03	HCT116	chr. 13	With rearrangements
Htr18_02	HCT116	chr. 18	With rearrangements
Htr21_03	HCT116	chr. 21	With rearrangements
RPE1	-	-	non-cancerous retinal fibroblasts (hTert)
A9	-	-	murine mouse wild type cell line
A9 + chr.8	A9	chr. 8	murine mouse donor
HCT116p0	HCT116	-	passage app. 0; with H2B-GFP
HCT116p20	HCT116	-	passage app. 20; with H2B-GFP; e1, e2 and e3 = three independently passaged cultures
HCT116p40	HCT116	-	passage app. 40; with H2B-GFP; e1, e2 and e3 = three independently passaged cultures
HCT116p50	HCT116	-	passage app. 50; with H2B-GFP; e1, e2 and e3 = three independently passaged cultures
HCT116p60	HCT116	-	passage app. 60; with H2B-GFP; e1, e2 and e3 = three independently passaged cultures
HCT116p80	HCT116	-	passage app. 80; with H2B-GFP; e1, e2 and e3 = three independently passaged cultures
Htr3p0	HCT116	chr. 3	passage app. 0; with H2B-GFP
Htr3p20	HCT116	chr. 3	passage app. 20; with H2B-GFP; e1, e2 and e3 = three independently passaged cultures
Htr3p40	HCT116	chr. 3	passage app. 40; with H2B-GFP; e1, e2 and e3 = three independently passaged cultures
Htr3p50	HCT116	chr. 3	passage app. 50; with H2B-GFP; e1, e2 and e3 = three independently passaged cultures
Htr3p60	HCT116	chr. 3	passage app. 60; with H2B-GFP; e1, e2 and e3 = three independently passaged cultures
Htr3p80	HCT116	chr. 3	passage app. 80; with H2B-GFP; e1, e2 and e3 = three independently passaged cultures
Htr5p0	HCT116	chr. 5	passage app. 0; with H2B-GFP
Htr5p50	HCT116	chr. 5	passage app. 50; with H2B-GFP
Hte5p0	HCT116	chr. 5	passage app. 0; with H2B-GFP
Hte5p20	HCT116	chr. 5	passage app. 20; with H2B-GFP; e1, e2 and e3 = three independently passaged cultures
Hte5p40	HCT116	chr. 5	passage app. 40; with H2B-GFP; e1, e2 and e3 = three independently passaged cultures

Hte5p50	HCT116	chr. 5	passage app. 50; with H2B-GFP; e1, e2 and e3 = three independently passaged cultures
Hte5p50	HCT116	chr. 5	passage app. 50; with H2B-GFP
Hte5p60	HCT116	chr. 5	passage app. 60; with H2B-GFP; e1, e2 and e3 = three independently passaged cultures
Hte5p80	HCT116	chr. 5	passage app. 80; with H2B-GFP; e1, e2 and e3 = three independently passaged cultures
Rtr21p0	RPE1	chr. 21	passage app. 0; with H2B-GFP
Rtr21p50	RPE1	chr. 21	passage app. 50; with H2B-GFP
HPT1	HCT116		post-tetraploid single cell colony derived

Methods

Cell line origin

A9 cells with human additional chromosome were obtained from the Health Science Research Resources Bank (HSRRB), Osaka 590–0535, Japan and used as donor cell line during the MMCT (see below). HCT116, a human colorectal cancer cell line, was purchased from ATCC (CCL-247). Hte5_01 was a gift from Minoru Koi, Baylor University Medical Centre, Dallas, TX, USA. hTERT RPE1 (hereafter RPE1), the "retinal pigment epithelium" cell line is telomerase immortalized (hTERT) and was a gift from Prof. Erich Nigg (MPI Biochemistry, Martinsried, Germany) and Dr. Stephen Taylor (The University of Manchester, UK, Manchester Cancer Research Centre). For the cell lines with H2B-GFP, the pBOS-H2BGFP construct (BD Pharmingen) was used for transfection. MMCT (see below) was used previously to introduce an additional human chromosome to the cell lines. The karyotype was determined prior to the work in this thesis using array-based or sequencing approaches [137] (**Figure 37**). The passaged cells Htr5 p50, Hte5 p50, Rtr21 p50 were generated previously by general cell culture without antibiotic selection for the additional chromosome (Sara Schunter, Martinsried, Germany). The passaged cell lines HCT116 p20-p80, Htr3 p20-p80 and Hte5 p20-p80 were generated by culturing three independent biological replicates for 80 passages. All 20 passages cells were taken for experiments and frozen as a backup. During the cell culture the confluency of cells was reduced to app. 10% twice a week by trypsinization (see below). No antibiotic selection of the additional chromosome was perfomed. Post xenograft cell lines (px) were generated previously by subcutaneous injection of aneuploid HCT116 cell lines in nude mice and extraction and re-culturing of cells after the tumor growth [139]. HPT cell lines

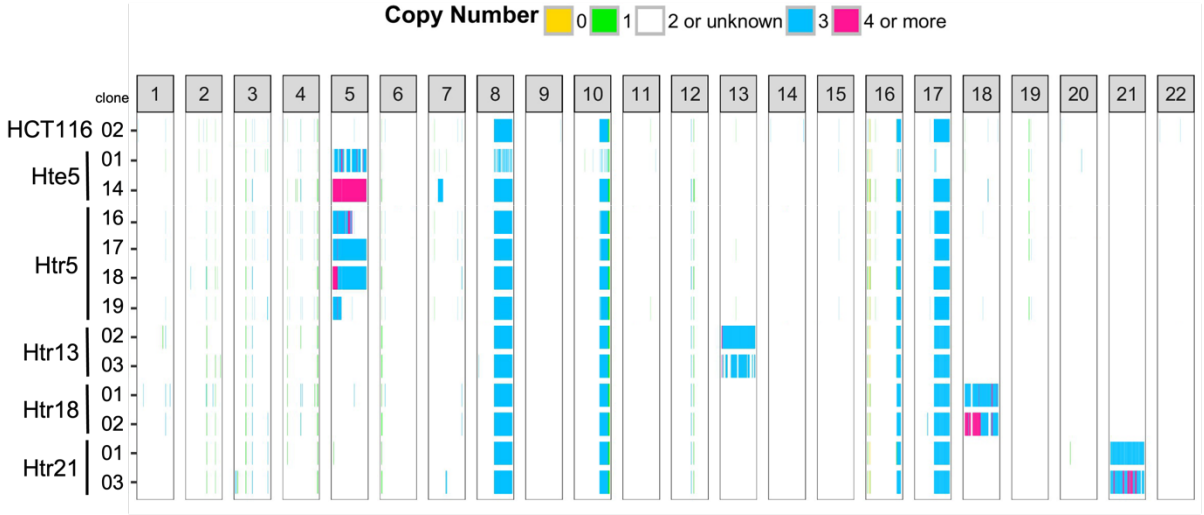

Figure 37: CN analysis. CN changes >100 kb were calculated from SMASH or SNP array data (subset shown here, Kneissig et al, 2019 [137]). Rows represent cell lines and columns the individual autosomes. The position on the chromosome can be read from left to right. The color code corresponds to the copy number. H=HCT116; tr=trisomy; te=tetrasomy. The following number corresponds to the additional chromosome. The clone number in the naming convention distinguishes different generated cell lines using the MMCT (adapted from Kneissig et al, 2019 [137]).

were generated previously by treatment of the cells with 0.75 µM DCD for 18 h and subsequent single

cell colony selection [165]. Young tetraploid cells were freshly generated each time using the same protocol but without single cell selection. DCD was washed out 3x with PBS

Cell culture based methods

Culture conditions

Cell lines were cultured in Dulbecco´s Modified Eagle Medium GlutaMAX (DMEM) (Gibco) with 10% fetal bovine serum (FBS) (Gibco) and 1% Pen-Strep (50 IU/ml penicillin, and 50µg/mL streptomycin, (Gibco) (DMEM +/+) at 5% CO_2 in a humid 37°C temperature chamber. Detachment of the cells was performed with 0.25% Trypsin-EDTA (Gibco). Trypsin inhibition was performed with at least double the volume of trypsin. For experiments cells were either collected in a falcon or plated in 96 well plates for screening. Freezing was performed by collecting the cells in a falcon, washing two times with PBS resuspension of cells in Freezing solution.

Micronuclei-mediated chromosome transfer (MMCT)

A9 donor cells were treated for 48 h with 50 ng/ml colchicine and subsequently cells were detached using trypsin and collected in a falcon. Next, the cells were transferred to bullets (polycarbonate slides with one round side (**Figure 38**) for a time frame of app. 4h that allows them to attach. Every two of them were then transferred back-to-back to centrifuge tubes filled with 10mg/ml dihydroxy cytochalasin B in DMEM that liquidities the cytosol so that the nuclei are "centrifuged out of the cells". Subsequent filtration steps (8um, 5um and 3um) should ensure the purity of the MN. For the fusion, first, PHA-P is used, which leads to the MN to adhere on the recipient cells surface. Second, PEG is used as fusogen to temporarily corrupt the cell membrane for the MN to enter the cell. Subsequent

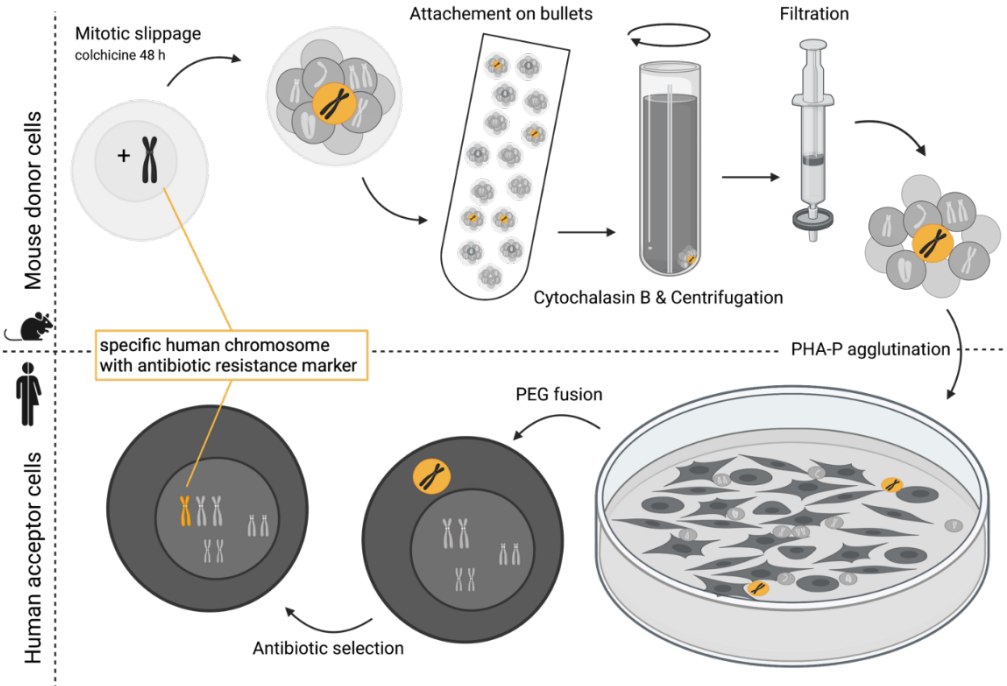

Figure 38: Micronuclei mediated chromosome transfer (MMCT). Top panel: Steps performed in the mouse donor cell line. Bottom panel: Steps performed with the recipient cell line. The black and yellow marks highlight the chromosome in a respective micronucleus that carries the resistance cassette for selection (created with Biorender.com).

culture for one cell cycle is essential to incorporate the MN in the main nucleus mass before the selection with the respective antibiotic leads to leftover colonies harboring the additional transferred chromosome (**Figure 38**). Single colonies were picked, and their karyotype determined.

Proliferation assay

The proliferation of cells was studied using the kit CellTiter-Glo® Luminescent Cell Viability Assay (Promega) following manufacturer's instructions. $1.5x10^3$ cells/well of RPE1 derived cells and $6x10^3$ cells/well of HCT116 derived cells were seeded in triplicates into a 96 well plate. Every 24h the 96 well the 50ul of the CellTiter-Glo® reagent was added to the well. The cells were incubated for 2 min and shaked at RT for 10 min. Luminescence of cells was measured with the GloMax Explorer plate reader (Promega).

Soft agar assay

Cells were collected at a confluency of app. 70% and centrifuged. 1% low melting agarose and 0.7% low melting agarose were prepared for the individual layers. The bottom layer in a 6 well plate was filled with a quick mixture of 0.5 ml DMEM and 0.5 ml 1% low melting agarose. After it was dried, the middle layer was added using a quick mixture of 0.5 ml of hand warm 0.7% low melting agarose and 0.5 ml of cell suspension with 1000 cells/ml. After the solidification a layer of nutrition using 0.5 ml DMEM +/+ was added and the cells were incubated at 37°C in a humid incubator for 14 days a with 5% CO_2. For colony counting, each well was divided into seven section and counting was performed manually using an inverted microscope (Motic AE2000).

Protein detection methods

Protein isolation

$1x10^6$ cells were seeded in 6 cm dishes or $2.2x10^6$ cells were seeded in 10 cm dishes. Replication stress induction as positive control was performed using 1µM doxorubicin, or 200nM aphidicolin for 24 h. Cells were collected in a 15 ml falcon after trypsinization. Cells were centrifuged at 1300 rpm for 3 min at RT (Rotina 420R). Washing was performed with PBS. Subsequently, the pellet was dissolved in 50-200 µl RIPA buffer (supplemented with protease (Roche Diagnostics GmbH) and phosphatase inhibitors (Roche Diagnostics GmbH)). Afterwards, samples were sonicated on ice for 12 min and centrifuged in the microcentrifuge (Eppendorf) for 10 min at 13200 rpm at 4°C to remove cell debris. Pellets were discarded and protein concentrations were measured using 1ul of the lysates for a Bradford protein assay. Adjustment of protein concentration was performed to either 1 µg/µl or 10 µg/µl in 1x Laemmli buffer. Denaturation was performed for 5 - 10 min at 95°C. Samples could be stored at -20°C.

Protein fractionation

The Subcellular Protein Fractionation Kit (Thermo Fisher Scientific) was used following manufacturer´s instructions to purify the protein and stepwise separate the following fractions: cytoplasmic fraction, membrane bound fraction, nuclear soluble fraction, chromatin bound fraction and cytoskeletal fraction. Protein concentrations were assessed using the Pierce BCA protein assay following manufacturer´s instructions followed by absorbance measurement using the Promega GloMax EXPLORER.

SDS-PAGE and immunoblotting

Separation of proteins was performed using SDS PAGE with 10% or 12.5% gels. The PrecisionPlus All Blue protein marker (Bio-Rad, Hercules,USA) was used to estimate protein sizes. 10-15 µg of total protein was loaded on the gel. Gels were run at 85-100V for app. 30 min. Next the transfer was performed: Trans-Blot® TurboTM (BioRad Laboratories, Hercules, USA) and Bjerrum-Schäfer-Nielsen buffer were used for semidry transfer to a water activated nitrocellulose membrane (Amersham Protran Premium 0.45 NC, GE Healthcare Life Sciences, Sunnyvale, USA). A wet transfer was performed at 4°C overnight at 0.16A or for 1 h at 100V. 5 min incubation of the membrane with Ponceau staining solution allowed for verification of the transfer. Blocking was performed in %-10% skim milk in TBS-T (Fluka, Taufkirchen, Germany) for 1h at RT. Primary antibody incubation was performed overnight at 4 °C with respective antibody concentration diluted in Bovine Serum Albumin (BSA) or 5% skim milk. Next day, membranes were washed in TBS-T 3x for 5 min each and incubated with corresponding secondary antibodies (R&D Systems) diluted in 5% skim milk for at least 1h at RT. After washing three times for 5 min with TBS-T protein signals were detected by using the ClarityTM Western ECL substrate solution (BioRad) and the Azure c300 system (Azure Biosystems, Dublin, USA). Signal quantification was performed using ImageJ (v. 1.52i).

Identification of interacting proteins

Katarzyna Seget-Trzensiok performed the co-immunoprecipitation of USP28. Nagarunja Nagaraj performed the Mass Spectrometry at the Core Facility of the MPI Biochemistry, Martinsried, Germany as previously described [298]. Preprocessing was performed by Markus Räschle using MaxQuant V. Subsequently, the data set was cleaned by removal of invalid values, site only, reverse and contaminant peptides and missing values were imputed according to a gaussian distribution in Perseus V1.6.2.3. Using the volcano plot function significantly enriched proteins were identified. For this a t-test with a false discovery rate (FDR) of 0.05 and a S_0 of 0.1 was performed.

Tandem mass tag (TMT) mass spectrometry

$1x10^6$ cells were collected by trypsinization and washed using PBS. Pellets were stored in -80°C after snap-freezing in liquid N_2. The TMT isobaric mass tagging was performed by Angela Wieland using the TMTduplex™ Isobaric Mass Tagging Kit (Thermo Fisher Scientific) according to manufacturer's instructions. A 10-plex system was chosen for HCT116, HCT116p50, Hte5, Hte5p50, Hte5px1, Hte5px3, Htr5, Htr5, Htr5p50, Htr5px2 and Htr5px3 which were individually tagged. Three biological replicates were measured. TMT-labelled peptides were fractionated into 8 pH fractions using the high pH Reversed-Phase Peptide Fractionation Kit following manufacturer's instructions (Thermo Fisher Scientific) after mixture of individually labelled samples. Mass Spectrometry was performed by Angela Wieland and Markus Räschle at the Center for MS Analytics of the Technical University of Kaiserslautern. Preprocessing was performed by Markus Räschle using MaxQuant V and data cleaning, log2 transformation, normalization and batch effect removal was performed in R (package limma V3.52) by Jan Eric Bökenkamp.

Lipofectamine transfection

Transfection with Lipofectamine 2000 was performed following manufacturer's instructions. In brief, cells were cultured to a confluency of app. 70%. Transfection reagent was diluted in Opti-Mem (Gibco). Separately, DNA was diluted in Opti-Mem. After 5 min of incubation at RT, the diluted transfection reagent and the DNA dilution were mixed 1:1 and incubated for 15 min at RT. Then, the lipid-DNA-complex was added to the cells and incubated overnight at 37°C in Opti-MEM before usage for further experiments.

Immunofluorescence staining

Cells were cultured in black 96-well plates with flat glass bottom to a confluency of app. 70%. 3.7% formaldehyde or ice-cold methanol and acetic acid (3:1) for 12 min at RT was used to fix the cells. Permeabilization was performed using 0.5% Triton X-100 in PBS for 5 min. Blocking was performed using either 10% FBS and 0.1% Triton X-100 or 0.1% BSA for 30 min. Primary antibodies were incubated with the fixed and permeabilized cells overnight at 4°C and secondary antibodies were incubated for 1h at RT. The DNA was counterstained using either a PBS solution with DAPI (1 mg/ml) or SYTOX™ Green (0.2 mM (if cells with H2B-GFP) or 2 mM (if cells without H2B-GFP)) and RNase A (0,01 mg/ml). 96 well plates were stored at 4°C and wells were prevented from drying and contamination with 1% NaN3 in PBS. For the isolated MN the fixation was performed three times using ice-cold methanol and acetic acid (3:1). The fixed MN were dropped onto a glass slide. The rest of the protocol is the same.

DNA detection methods

Chromosome spreads

Cells were treated with 50 ng/mL colchicine for 4-6h. Subsequently, cells were collected using trypsin and centrifuged for 5 min at 1000 rpm. The pellet was dropwise resuspended in prewarmed hypotonic solution (0.0075M KCL). Suspension was incubated at 37°C for 20 min. After following centrifugation at 1000 rpm for 5 min a fixation solution of 3:1 methanol: acetic acid was used as fixative and dropwise added to the pellet. This step was repeated 3 times. For chromosome spreads, cells were dropped from app. 1m height on a glass slide and processed in two ways: First, spreads were counterstained with DAPI mounting medium for subsequent microscopy analysis of metaphase chromsomes. Second, for mFISH, the DNA probe mixture 24XCyte Human Multicolor FISH Probe Kit (MetaSystems) was used as described in Kuznetsova et al. 2015 [165] (previously performed).

DNA staining

$1.5x10^4$ cells per well were seeded into 96 well plates in triplicates. Positive controls were treated for 24 h with 0.2µM aphidicolin and 0.73mM caffeine. Fixation was performed with 3.7% formaldehyde in PBS for 12 min at RT. Washing with PBS-T was performed three times for 5 min. DNA was stained using either a PBS solution with DAPI (1 mg/ml) or SYTOX™ Green (0.2 mM (if cells with H2B-GFP) or 2 mM (if cells without H2B-GFP)).

EdU Click-It Reaction and Flow Cytometry

Cells were grown to a confluency of app. 70% and then pulse labelled with 10µM EdU. Next the cells were collected using trypsin. After centrifugation (3min, 1300rpm, Rotina 420R) the cell pellet was fixed using the Fix-Perm buffer (Thermo Fisher Scientific) according to the manufacturer's instructions. Subsequently, fixed and permeabilized samples were washed using Perm wash (Thermo Fisher Scientific). Next, samples were incubated with EdU Click-iT Reaction Mix (1µM Eterneon Red (baseclick GmbH), 6.6% (v/v) 1.5M Tris (pH 8.8), 500µM CuSO4, 100mM Ascorbic Acid in PBS) for 20 min at RT. After washing (centrifugation for 2min at 1600rpm (Eppendorf centrifuge 5415R), 30 min of incubation with antipRPA2 S33 was performed. After each step, washing steps were performed using three times the Perm-Wash buffer. Next, 1h incubation with the secondary antibody was performed and the cell pellet was resuspended in PBS with 1µg/ml DAPI and 10µg/ml RNase (RNase Zap, Invitrogen). Flow cytometry measurements were performed using an Attune™ Nxt acoustic focusing cytometer (Life Technologies). For Etherneon Red (EdU signal) 638 nm laser and for DAPI 440/50 nm laser were used. To gate single cells and analyze the data the software FlowJo V10.2 (Becton Dickinson) was used.

Replication assay

RPE1 cells were pulse-labelled 20 h after fusion during the MMCT with 10mM 5-Ethynyl-2'-deoxyuridine (EdU). Fixation was performed with 3.7% paraformaldehyde for 15 min. Subsequently, cells were permeabilized with 0.1% TritonX-100 in PBS and the EdU Click-iT reaction mix was used following manufacturer's instructions to visualize replicating DNA. DNA was counterstained with SYTOX™ Green (2 mM)

DNA sequencing

DNA was isolated in 3 biological replicates using the DNA easy® Blood and Tissue kit (Qiagen) (>20 ng/ul). Whole-genome sequencing was performed at the NIG Integrative Genomics Core Unit, Göttingen, Germany using single-end libraries of 150 bp read length. Sequence reads were aligned to GRCh37.p13 using the Illumina DRAGEN Bio-IT Platform. CN calling was performed by Jan Eric Bökenkamp using HMMcopy V1.38.

Array CGH

Array CGH data were obtained previously on behalf of Silvia Coenen (2010/2011). The IMGM laboratories in Martinsried, Germany performed the Agilent Human Genome CGH Microarrays (4x44K format) using a two-color based hybridization protocol with a commercially available reference gDNA. The Agilent DNA Microarray Scanner and the Agilent Genomic Workbench 7.0 were used to scan the array and pre-process the data.

DNA combing

Aneuploid and wild type cells were cultured to a confluency of 70%. Tetraploid cells were generated as described and cultured for additional 20 h to reach the respective confluency and a maximum of cells in S phase.

Replication inhibition as positive control was performed using 100nM aphidicolin for 2h. Cells were pulse labelled with the thymidine analogues CIdU (0.1mM) and subsequently IdU (0.1mM) for 30 min each. DNA extraction was performed according to manufacturer's instructions (FiberPrep DNA Extraction Kit, Genomic Vision). In brief, after cell collection via trypsinization, 100 000 - 300 000 cells were packed in agarose plugs to gently isolate the DNA. After agar digestion the Replication Combing Assay (RCA, Genomic Vision) was performed by binding the DNA onto silanized coverslips (CombiCoverslips, Genomic Vision). The FiberComb machine (Genomic Vision) pulls up the coverslips out of the DNA suspension with a specific force, that gives the defined stretching factor. The DNA on the coverslips was incubated for 2h at 65°C. Subsequent antibody staining allowed detection of the thymidine analogues and ssDNA (**Figure 39**A). Coverslips were sent to Genomic Vision for scanning. The scans were visited tracks were analyzed in the Fiberstudio V2.0.1 (Genomic Vision) (**Figure 39**B).

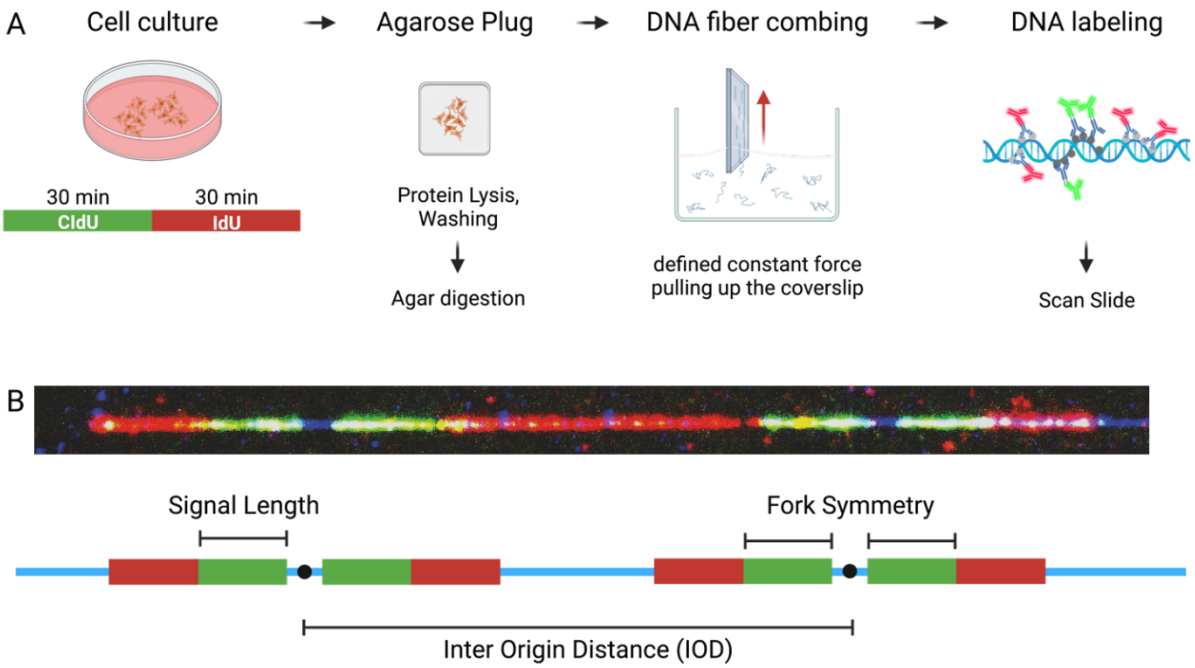

Figure 39: DNA combing. A: Experimental workflow. **B:** Pattern of signals on DNA and its usage for replication dynamics: signal length, fork symmetry and inter origin distance.

The analysis of the image data is based on the tracks produced by incorporation of CldU and IdU. This allows to computationally assign fiber identifiers, signal identifiers, origin or termination identifiers. Further, by computing the number of pixels for a specific signal length the algorithm of Genomic Vision calculates the length of the signal in µm. Using the treatment time and stretching factor, a signal length is converted in the replication rate (RR) (**Equation 1**). A second quantified parameter is the fork stability (FS) calculated from the fork symmetry. For this, opposing signals originating from the same origin of replication by each other to see if they are equally long (**Equation 2**). If that so-called symmetry coefficient (s) exceeds a threshold of < 0.5 or > 2, the respective forks were marked as unstable. This does not tell, though, whether the fork progression is stalled or just slowed. A third parameter is computed by Genomic Vision and reflects the distance between two neighboring origins on a single fiber. This so-called inter origin distance (IOD) gives insights in the number of active origins on a fiber (**Equation 3**, **Figure 39** B). For calculation of replication dynamics only tracks with neighboring signals were used to minimize the technical error.

$$RR = \frac{LF}{t}$$

Equation 1: Replication rate (RR) (kB/min). L = signal length (µm). F = stretching factor used in FiberComb machine (=2). t = time of CldU or IdU incorporation.

$$s = \frac{L_x}{L_y}$$

Equation 2: Symmetry coefficient (s). L = signal length (µm), x and y correspond to opposite signals originating from the same origin.

$$IOD = \left(\frac{L_a + L_n}{2} + \sum_{i=a+1}^{n-1} L_i \right) * F$$

Equation 3: Inter origin distance (IOD) (kB). L = signal length (µm), a is the ID for the signal starting with the first origin on the fiber of interest and a+1 refers to the signal next to L_a in the direction of the second / neighboring origin on the same fiber of interest, n reflects the last identifier ending with second / neighboring origin on the same fiber of interest. F = stretching factor used in combing machine (2).

Other methods

Microscopy

Microscopy was performed using a semi-automated inverted Zeiss microscope (AxioObserver Z1) equipped with a CSU-X1 spinning disk confocal head, a LaserStack with selectable laser lines and an epifluorescence X-Cite 120 Series lamp. Images were acquired using SlideBook 6 (Intelligent Imaging Innovations) and a CoolSNAP HQ2 camera. The 20x air ,40x air or 63x oil objectives were used.

RNA sequencing

RNA was isolated in three biological replicates using the RNeasy® Mini kit (Qiagen) (>60 ng/ul). RNA sequencing was performed at the NIG Integrative Genomics Core Unit, Göttingen, Germany using single-end libraries of 50 bp read length. Mapping, statistics, and quality control were performed by Alexander Wolf, Universitätsmedizin Göttingen, Germany. Extended data analysis including pathway enrichment was performed by Jan Eric Bökenkamp.

Statistical analysis

For statistical analysis and visualization GraphPad Prism 9 was used. The R software V 4.2.1 and Perseus V1.6.2.3. and V1.6.15.0 were used to analyze large-scale data. Mann-Whitney tests were performed when a gaussian distribution was not applicable. The genomic location of the LRR and histograms as side plots were illustrated using ggplot2 V3.4.0.

Supplementary information

Supplementary figures

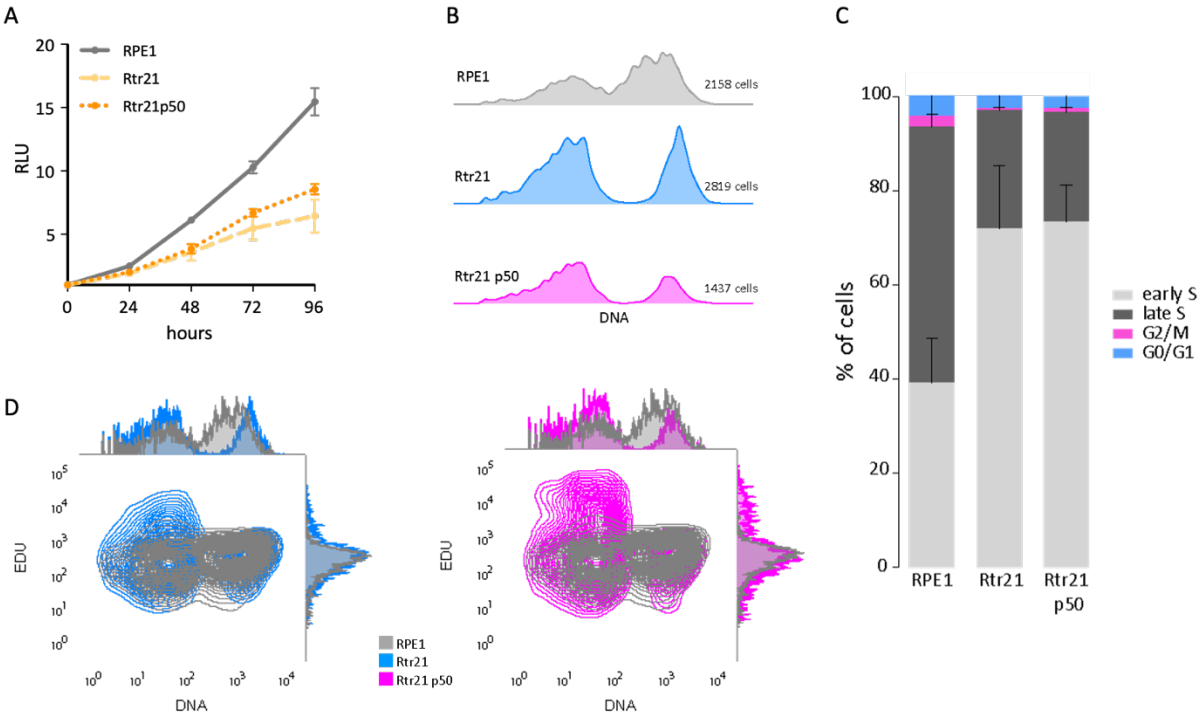

Supplementary figure 1: Proliferation and cell cycle analysis of RPE1 derived aneuploid cells before and after evolution. **A:** Cell titer glo assay based relative luminescence units (RLU) of RPE1 (grey), Rtr21 (yellow) and Rtr21 p50 (orange). Three biological replicates with SEM is shown. **B:** Representative flow cytometry-based DNA profiles of RPE1 (grey), Rtr21 (blue) and Rtr21 p50 (pink) with corresponding number of measured cells. **C:** Percentage of cells in cell cycle phases according to legend, Standard deviation out of three biological replicates is shown. D: EDU signal (y-axis) and DNA (SYTOX™ Green) signal (x-axis) of RPE1 (grey) and Rtr21 (blue, left panel) or RPE1 (grey) and Rtr21 p50 (pink) is shown. Respective histograms are added to the sides of the graphs.

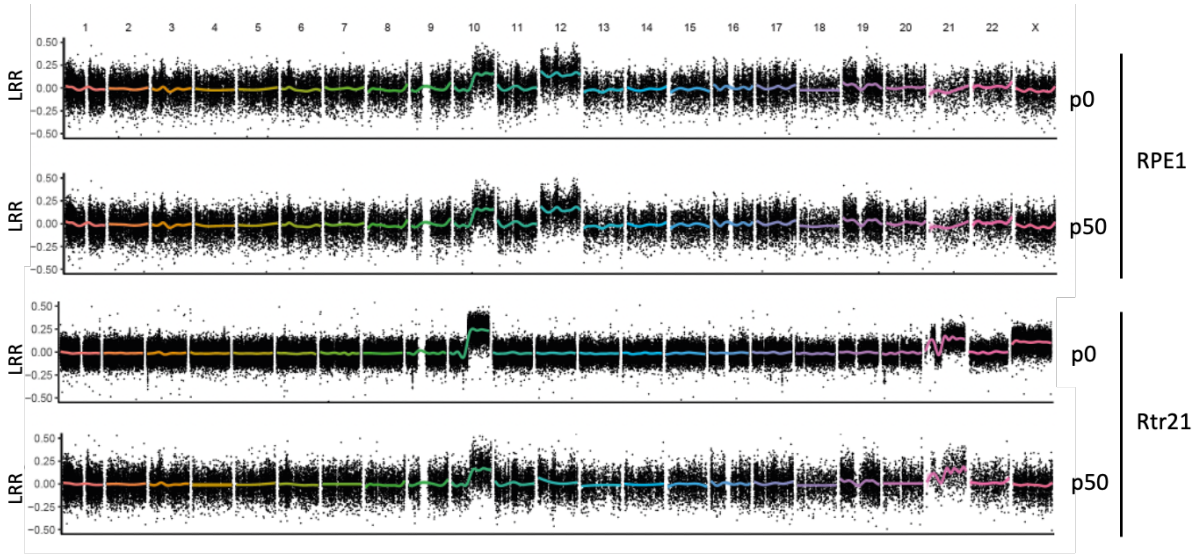

Supplementary figure 2: Array CGH based log r ratio (LRR) as estimate for the copy number. Previously performed array CGH (project of Silvia Stingele) was used to graph the LRR for RPE1, RPE1 p50, Rtr21 and Rtr21 p50 (rows) per chromosomal location (columns). LOESS smoothing line was applied (colored line).

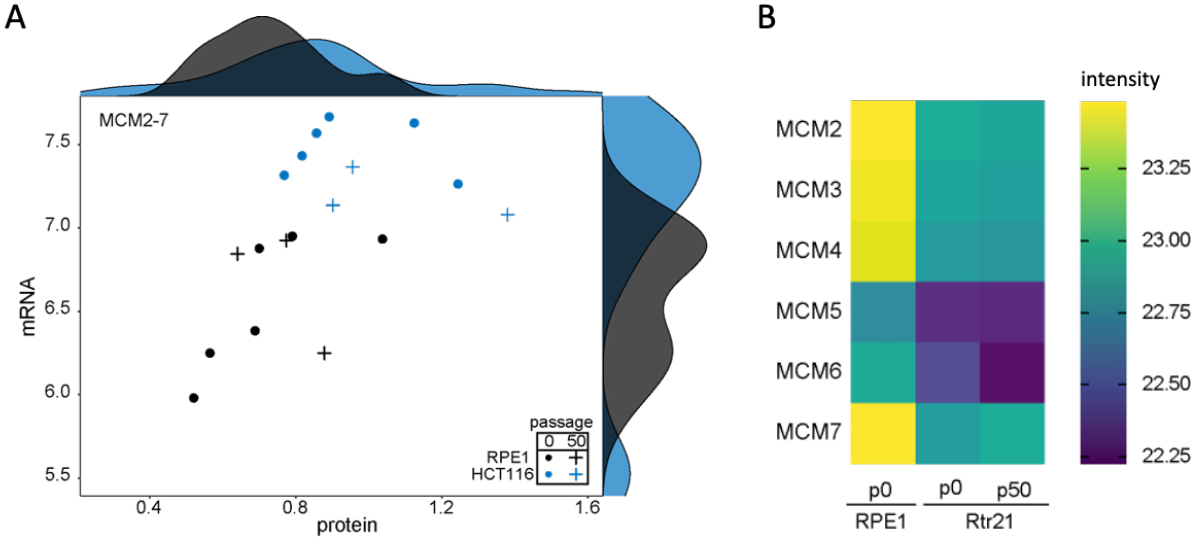

Supplementary figure 3: MCM 2-7 on mRNA and protein level. A: Correlation with histograms of mean MCM 2-7 on transcriptome level (counts per million) and mean protein abundance from immunoblotting for HCT116 and RPE1 derived evolved cell lines. three biological replicates are shown B: MCM 2-7 heatmap obtained by TMT mass spectrometry. Cleaned, loess normalized, and batch effect removed intensities are shown (together with Jan-Eric Bökenkamp).

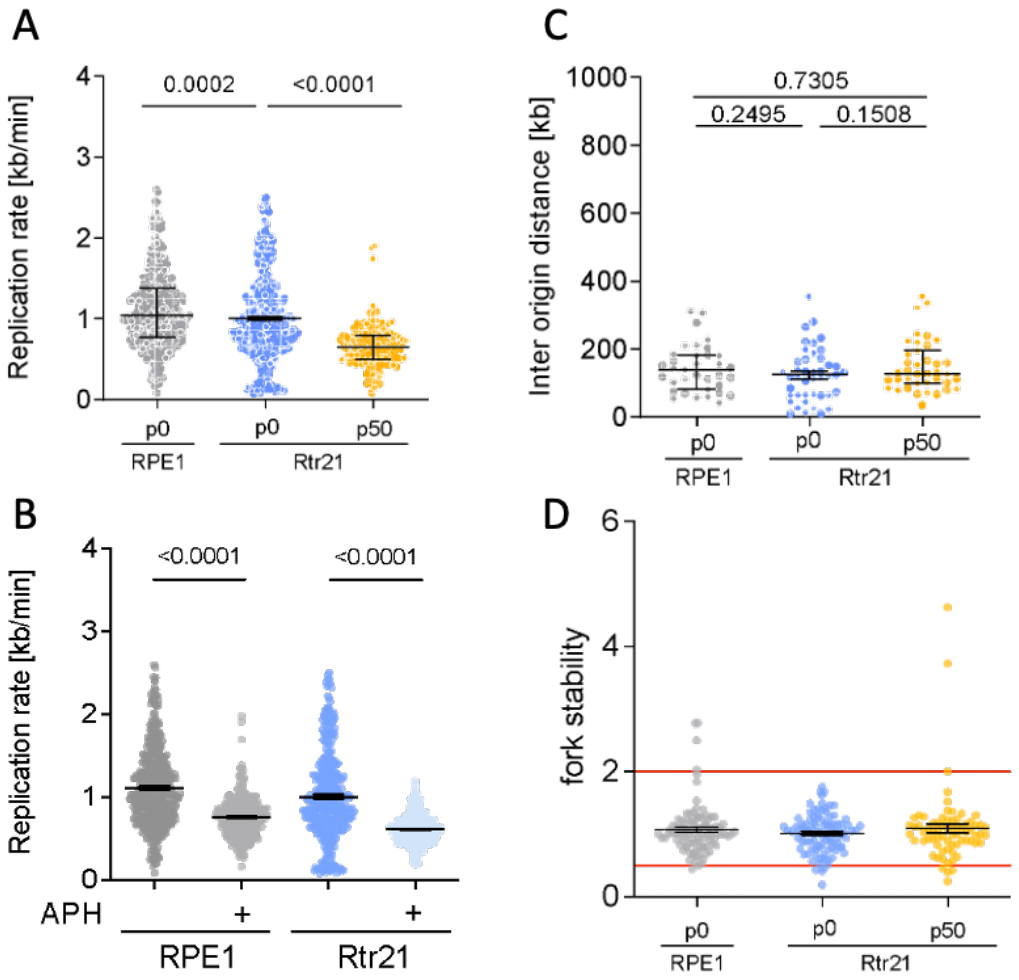

Supplementary figure 4: Replication dynamics RPE1. A: Replication rate in Rtr21 before and after 50 passages. B: Replication rate in RPE1 and Rtr21 with and without 2 h of 100 nm aphidicolin treatment. C: Inter origin distance measurements. Mann-Whitney p values are shown. D: fork stability based on neighboring forks.

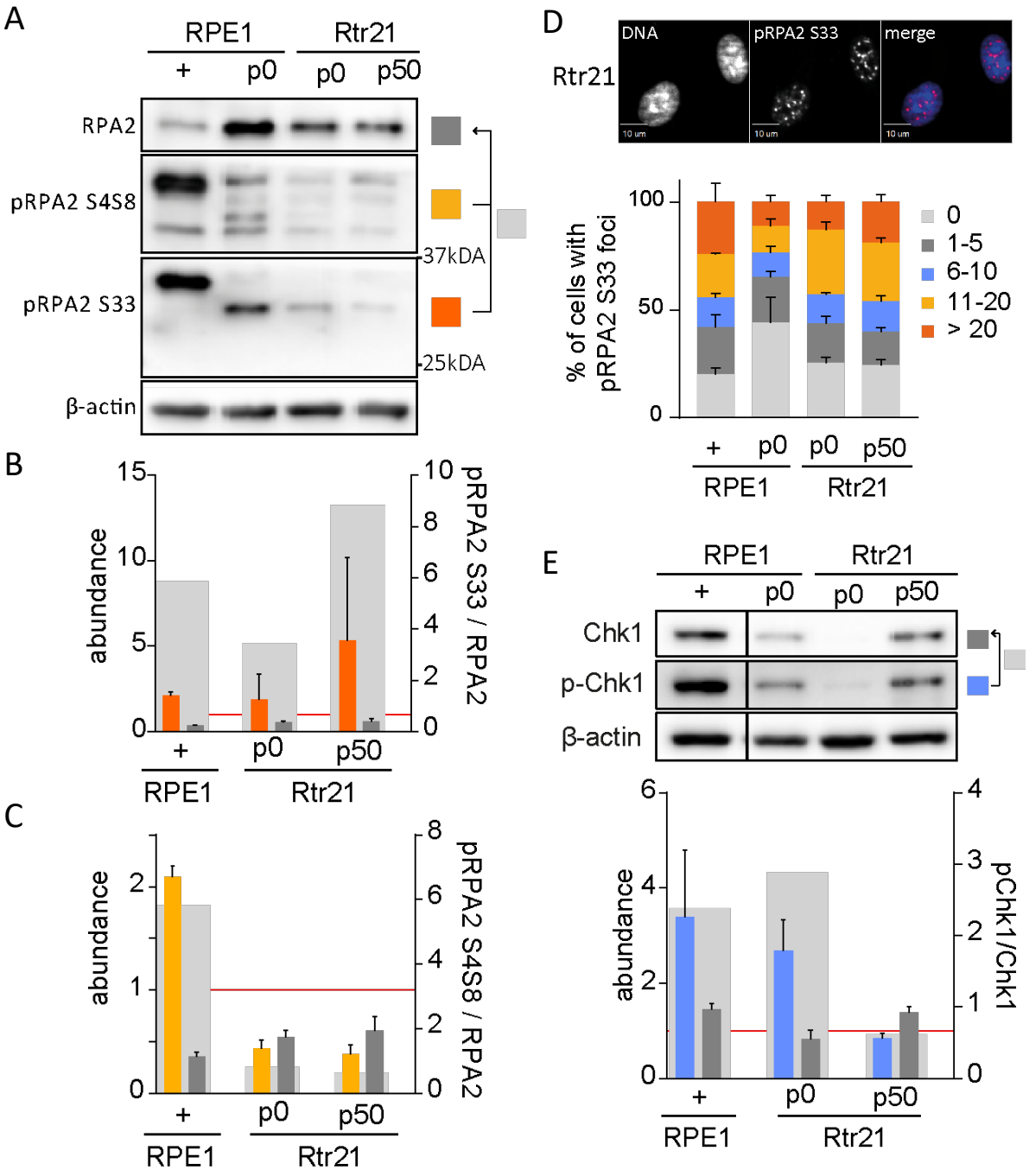

Supplementary figure 5: RPA2 and Chk1 signaling in RPE1 derived aneuploid and evolved cells. A: Exemplary western blot of RPA2, pRPA2 S33 and pRPA2 S4S8. **B:** Quantification of pRPA S33 (orange) and RPA2 (dark grey) (left y-axis) and ratio of pRPA2 S33 / RPA2 (light grey) (right y-axis). RPE1 wild type is represented by the red line. **C:** Quantification of pRPA S4S8 (yellow) and RPA2 (dark grey) (left y-axis) and ratio of pRPA2 S4S8 / RPA2 (light grey) (right y-axis). RPE1 wild type is represented by the red line. Positive control (+) in A-C is 1 µM doxorubicin. Three biological replicates were quantified. **D:** Upper panel: representative capture of Rtr21 with pRPA S33 foci. DNA was stained with DAPI. Scale bar = 10 µm. lower panel: Percentage of cells with pRPA S33 foci according to legend and SEM. **E:** Upper panel: Representative Western Blot of Chk1 and pChk1. Lower panel: Quantification of pChk1 (blue) and Chk1 (dark grey) (left y-axis) and ratio of pChk1/Chk1 (light grey) (right y-axis). RPE1 wild type is represented by the red line. Positive control (+) is 1 µM doxorubicin. Three biological replicates were quantified (together with Carina Heinrich and René Göbel).

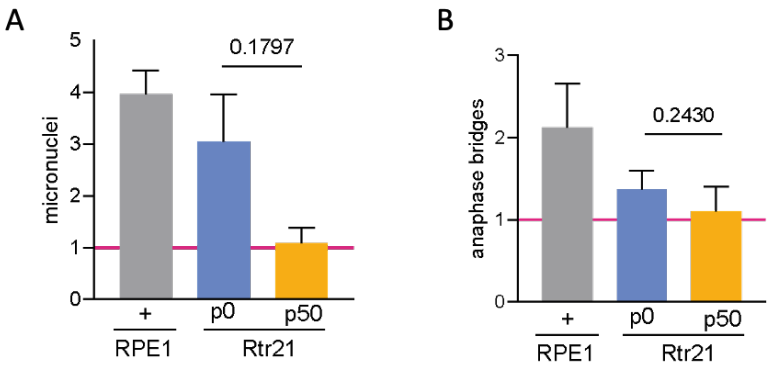

Supplementary figure 6: Mitotic errors. A: Percentage of micronuclei per counted nuclei. B: Percentage of anaphase bridges per counted anaphases. Three biological replicates with students t-test p-values are shown. Red line represents RPE1 wild type. At least 30 anaphases were counted for each replicate. Positive control (+) was treated for 24 h with 200 nM Aphidicolin and 0.73 µM caffeine (together with Carina Heinrich and René Göbel).

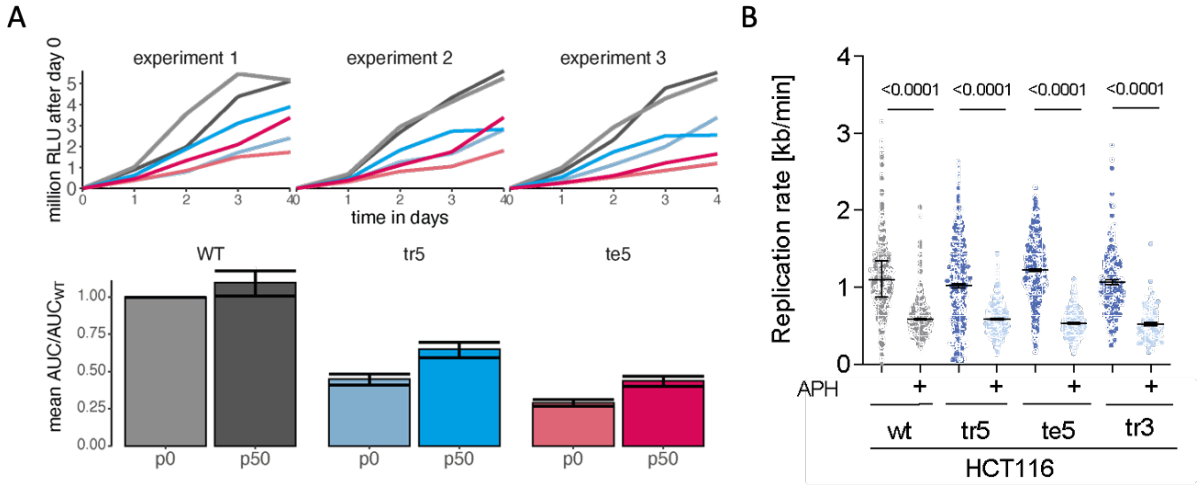

Supplementary figure 7: Proliferation and replication in aneuploid cells. A: Upper panel: Growth curves of three independent experiments performed with CellTiter-Glo®. Lower panel: Area under the curve (AUC) normalized to HCT116 p0. Confidence intervals are shown (together with Sara Schunter and Jan Eric Bökenkamp). **B:** Replication rate measurements by DNA combing of aneuploid cells with and without 2 h of 100 nm aphidicolin (APH) treatment. Mann-Whitney p values and SEM of at least 100 fork measurements per treatment are shown (together with Efat Ozeri).

Supplementary figure 8: LC3 levels in trisomic HCT116. Percentage of >5 LC3 foci in HCT116 and Htr5 derived evolved cell lines. Calculation of percentage was based on a single replicate with >400 cells.

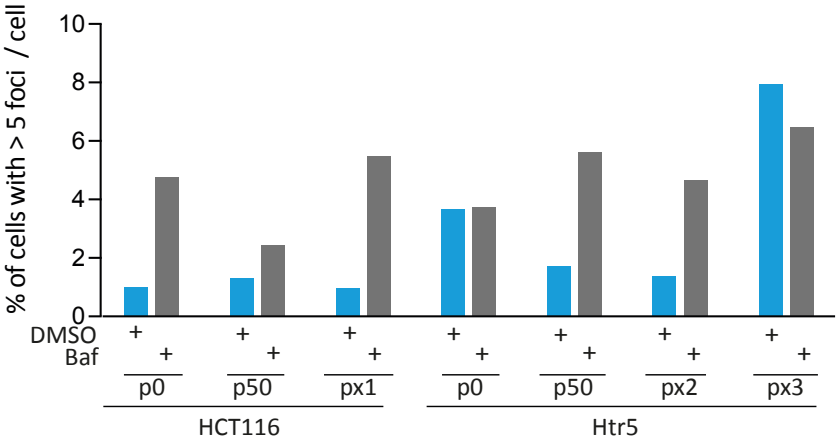

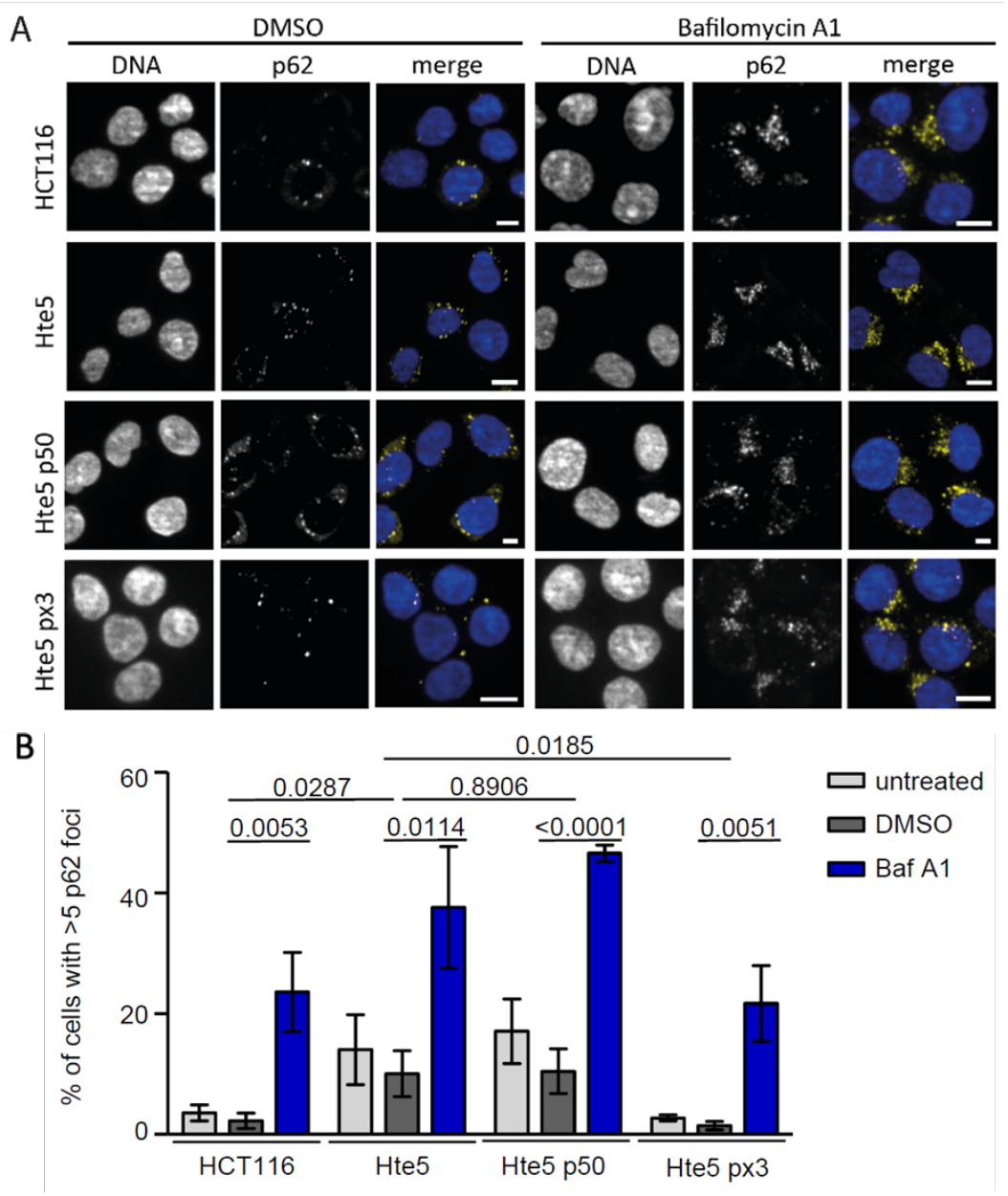

Supplementary figure 9: Immunofluorescence of p62 in tetrasomic HCT116 before and after evolution. A: Exemplary captures of p62 with and without bafilomycin A1 (Baf A1) as positive control. Scale bar: 10 µm. **B:** Percentage of cells with >5 p62 foci. SEM and unpaired students t-test p values are shown. At least 2300 cells were quantified in three biological replicates per cell line (together with Amelie Becker)

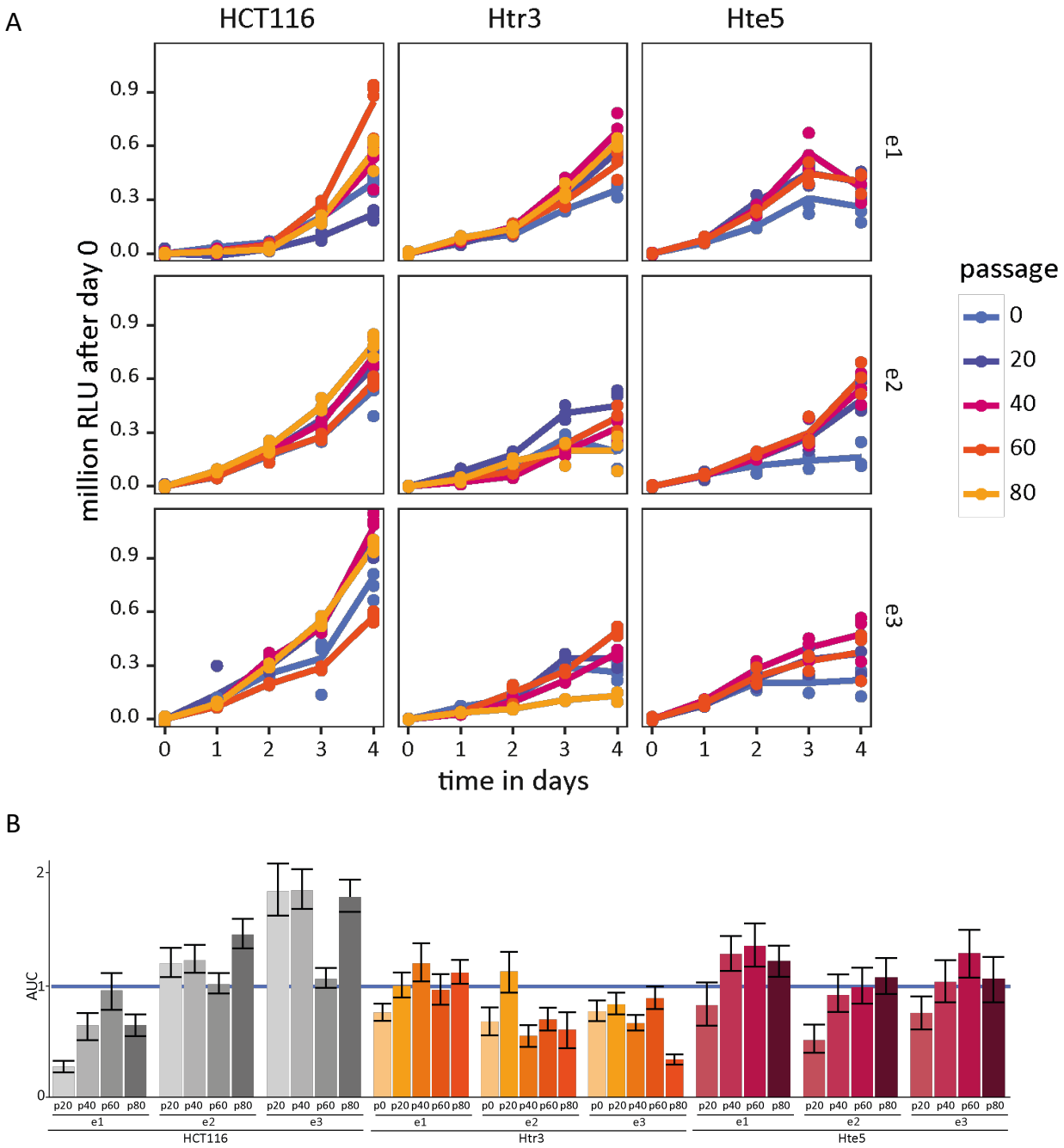

Supplementary figure 10: Proliferation of prolonged HCT116 evolution. A: CellTiter-Glo® growth curves of HCT116 derived evolution cell lines that were passaged up to 80 times (app. 260 generations) in three independent cultures (e1, e2, e3). Every 20 passages cells were collected for experiments. **B:** Quantification of the area under the curve (AUC) and confidence intervals are shown. Normalized to p0 of respective biological replicate, p0 is indicated as blue line (together with Assel Nurbekova, Leah Johnson and Jan Eric Bökenkamp).

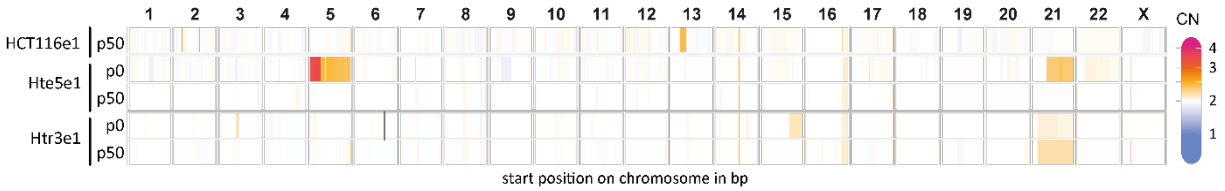

Supplementary figure 11: Karyotype analysis new evolution. Copy numbers (CN, see color scale) of individual chromosomes (columns) in analyzed cell lines (rows) per chromosome (columns) are shown. The copy number was normalized to HCT116 and is gradually color-coded (together with Jan Eric Bökenkamp).

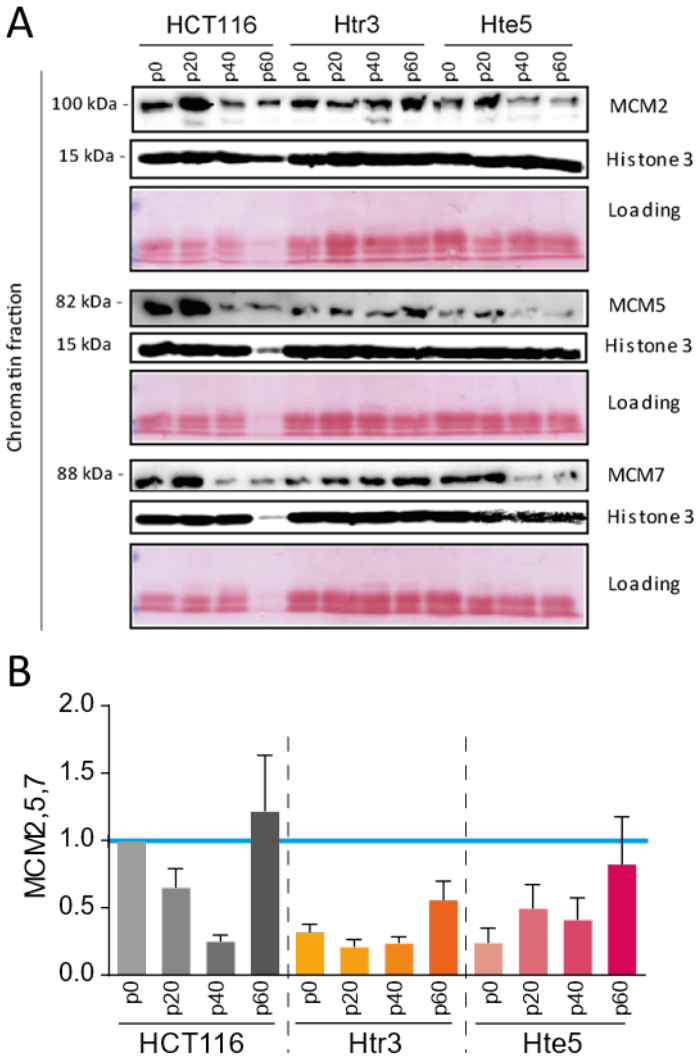

Supplementary figure 12: Western blots of MCM2,5 and 7 for chromatin bound protein fraction of aneuploid cells during evolution. A: representative Western blot. **B:** Quantification of two biological replicates, SEM (together with Assel Nurbekova).

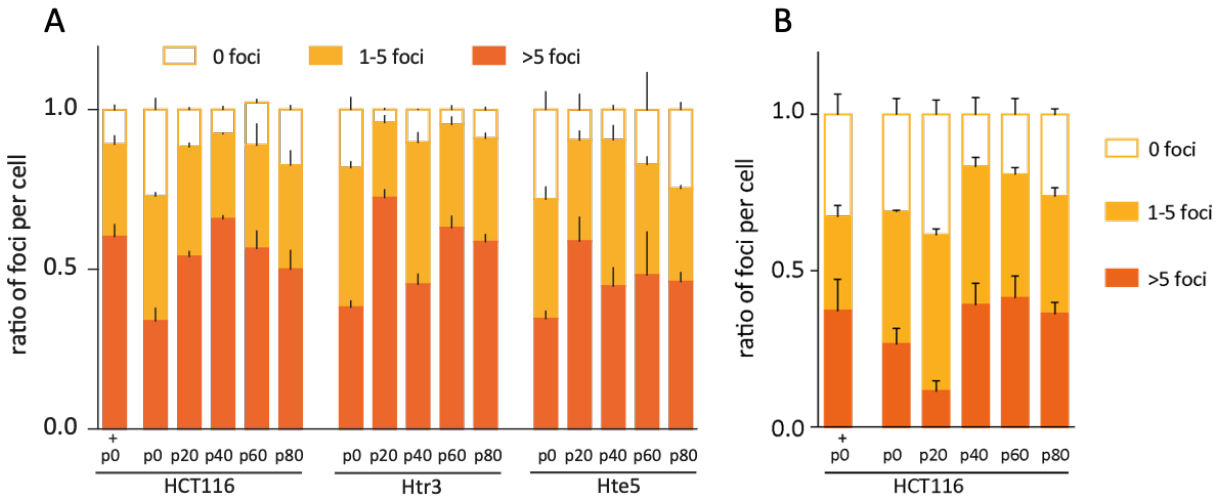

Supplementary figure 13: Replication stress and DNA damage in a prolonged evolution. A: pRPA S33 ratio of number of foci according to legend per cell. **B:** γ-H2A.x ratio of number of foci according to legend per cell. **A and B:** Positive control is aphidicolin and caffeine treated for 24h. Standard deviation of three biological replicates is shown (together with Assel Nurbekova and Leah Johnson).

Supplementary figure 14: Replication stress and DNA damage clusters of 60 passages of Hte5 and Htr3 derived aneuploid cells. Scored was the percentage of cells with foci > 5 of γ-H2A.x and with foci > 10 of pRPA2 S33 (together with Assel Nurbekova and Leah Johnson).

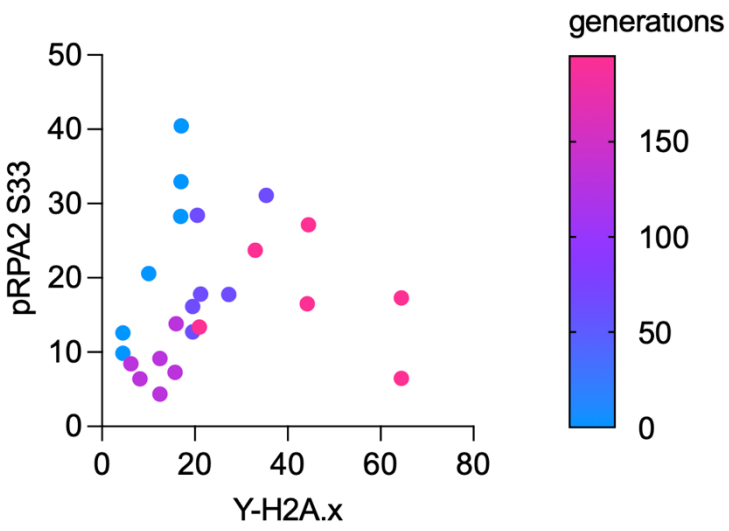

List of figures

List of tables

List of abbreviations

Table 9: List of abbreviations.

53BP1	p53-binding protein 1
AB	Anaphase bridge
alt-EJ	Alternative end-joining
APH	Aphidicolin
app.	approximately
ATM	Ataxia telangiectasia mutated
ATR	Ataxia telangiectasia and Rad3 related
CDC6	Cell division cycle 6
CDK	Cyclin dependent kinases
CDT1	CDC10-dependent transcript
CF	Cytokinesis failure
Chk1	Checkpoint kinase 1
Chk2	Checkpoint kinase 2
chr	Chromosome
CIN	Chromosomal instability
CldU	5-Chloro-2′-deoxyuridine
CMG	CDC45-MCM 2-7-GINS
CN	Copy number
DCD	Dihydroxycytochalasin D
DDK	DBF4-dependent kinase
DMEM	Dulbecco´s modified Eagle´s medium
DNA	deoxyribonucleic acid
DNA-PK	DNA-dependent protein kinase complex
DSB	Double-strand breaks
dsDNA	Double-strand DNA
EBV	Epstein–Barr virus
EdU	5-Ethynyl-2'-deoxyuridine
EnR	Endoreplication
ESC	Embryonic stem cells
FANCD2	Fanconi anemia complementation group D2
FBS	Fetal bovine serum
FoSTeS	Fork stalling and template switching
FS	Fork stability
GIN	Genome instability
HCT116	Human colon cancer cell line

HPT	HCT116 derived post-tetraploid
HR	Homologous recombination
IdU	5-Iodo-2'-Deoxyuridine
IF	Immunofluorescence
IOD	Inter origin distance
MAP1LC3B / LC3	Microtubule-associated proteins 1A/1B light chain 3B
MCM 2-7	Mini-chromosome maintenance 2-7
mFISH	Multicolor fluorescence *in situ* hybridization
MMBIR	Microhomology-mediated break induced repair
MMCT	Micronuclei-mediated chromosome transfer
MN	Micronucleus
MS	Mitotic slippage
MTOC	Microtubule organizing centers
NHEJ	Non-homologous end joining
OG	Oncogene
ORC	Origin recognition complex
ORI	Origin of replication
p50	Passage 50
PCNA	Proliferating-Cell-Nuclear-Antigen
PDX	Patient derived xenograft
PEG	Polyethylenglycol
PHA-P	Phytohemagglutinin
PN	Primary nucleus
Pol	Polymerase
pre-IC	Pre-initiation complex
px	Post xenograft
ROS	Reactive oxygen species
RPA	Replication protein A
RPE1	Retinal pigment epithelial cell line
RR	Replication rate
SAC	Spindle assembly checkpoint
SSB	Single-strand break
ssDNA	Single-strand DNA
TSG	Tumor suppressor gene
ULK	Unc-51 like autophagy activating kinase
USP28	Ubiquitin-Specific-Processing Protease 28
WCA	Whole chromosome aneuploidies
WGD	Whole genome doubling
WGS	Whole genome sequencing
WHO	World Health Organization

Acknowledgment

Many people have contributed through small and large efforts to the fact that I now have my doctoral thesis in front of me. I would like to thank you all from the bottom of my heart.

First, I would like to thank Prof. Dr. Zuzana Storchová, who made the Ph.D. topic possible for me and supervised me within this framework to promote my scientific career.

Furthermore, I would like to thank Prof. Dr. Jörg Fahrer and Prof. Dr. Tanja Maritzen who kindly agreed to take over essential positions in my thesis committee.

I would also like to thank the DFG group FOR2800, which funded my project, discussed research results, and was thus instrumental in its progress.

Finally, my credits go to my "Aneuploidy Evolution" team: Jan Eric Bökenkamp, Stefan Redel, Leah Johnson, Amelie Becker, René Göbel, Assel Nurbekova, and Carina Heinrich. Without your curiosity, effort, and expertise during your bachelor's and master's thesis, the project would not be where it is today. I enjoyed the time with you!

Furthermore, I thank the whole lab for making me feel at home, I will miss you guys. Especially, I thank Angela who pushed me, weekly during the writing phase, and Sara who always had an open ear during the experimental phase.

Besides work, my volunteer work in the Red Cross has ensured that I have remained down to earth and still know what matters in life. Therefore, I would like to thank the valuable members of the DRK Kreisverband Kaiserslautern Stadt e.V. for fun evenings and learning-intensive courses, for the opportunity to help people in need, and for the feeling of doing something good. This gave me a lot of self-confidence and kept me going in a joyful mood.

Next, I thank Leon for all the evenings when you listened to my lab stories with an open ear and for the periods of relaxation that gave me energy again. You see me, value me, and give me the support I need to be able to perform at such a high level.

The last words of gratitude go to my family, who have always supported me in my thirst for knowledge and action since I was a little child. You gave me the feeling that I could achieve anything I wanted, and this feeling persists. Thank you for your never-ending love, trust, and feeling of comfort.

Curriculum Vitae Kristina Keuper

Scientific Experience & Academic Education

Since 02/2019	**Ph.D. studies** Technical University of Kaiserslautern, Department of Molecular Genetics
11/2018 – 02/2019	Workflow-Developer/-Designer Walther Werke in Eisenberg (Topic: Process Analysis)
10/2016 – 08/2018	**Master of Science** Microbial- and Plant- Biotechnology at the Technical University of Kaiserslautern Focus: Big Data Analysis Master thesis: "Chromosomal rearrangement discovery in aneuploid cells " (Supervisor: Prof. Dr. Zuzana Storchová)
10/2013 – 08/2016	**Bachelor of Science** Life Sciences at the Technical University of Kaiserslautern
03/2013	General University Entrance Qualification: Gymnasium Saarburg

Stipends, Prices & Conferences

12/2017	Erasmus stipend for the studies abroad at the University Medical Center Utrecht, Netherlands
06/2021	Award of the *Stifterverband* for the Instagram channel *@guardians_of_the_genome* (Among the top 10 in scientific communication)
05/2022	Talk selected from abstract at the EMBO Conference in Vienna, Austria ("Chromosome segregation and aneuploidy") Topic: „Adaptive changes during evolution alleviate the consequences of aneuploidy"

Participation in Workshops, Further Training

10/2022	Workshop: Supervision and Leadership
05/2022	Workshop: Good Scientific Practice
01/2022	Workshop: Grant Proposal Writing
11/2021	Workshop: Communication Skills Training
09/2021	Workshop: Leadership Skills for Young Leaders
09/2021	Workshop: Project Management in the Final Phase
06/2021	Science Campus Fraunhofer Institute, Topics: Agile Project Management, Lasting Health, Design of Energy Transition
05/2021	Workshop: Successful Self-Presentation in Talks

Publication bibliography

1 Ferlay J, Ervik M, Lam F, Colombet M, Mery L, Piñeros M. Global Cancer Observatory: International Agency for Research on Cancer. *Cancer Today. Lyon*. 2020.

2 Littré E. *Oeuvres complètes d'Hippocrates:* Baillière; 1861.

3 Boveri T. Über den Anteil des Spermatozoon an der Teilung des Eies. *Sitzungsber. Ges. Morph. Physiol. München*. 1887;(3):151-164.

4 Boveri T. Zellenstudien II: Die Befruchtung und Teilung des Eies von Ascaris megalocephala. *Jena Z. Naturwiss*. 1888;(22):685–882.

5 Boveri T. Über mehrpolige Mitosen als Mittel zur Analyse des Zellkerns. *Verh Phys Med Gesellschaft Würzburg*. 1902;(35):67-90.

6 Boveri T. Die Blastomerenkerne von Ascaris megalocephala und die Theorie der Chromosomenindividualität. *Archiv für Zellforschung*. 1909;(3):181–268.

7 Boveri T. Zur Frage der Entstehung maligner Tumoren. Fischer. *Jena Z. Naturwiss*. 1914.

8 Hanahan D, Weinberg RA. The Hallmarks of Cancer. *Cell*. 2000;100(1):57-70. doi:10.1016/S0092-8674(00)81683-9.

9 Hanahan D, Weinberg RA. Hallmarks of Cancer: The Next Generation. *Cell*. 2011;144(5):646-674. doi:10.1016/j.cell.2011.02.013.

10 Hanahan D. Hallmarks of Cancer: New Dimensions. *Cancer Discov*. 2022;12(1):31-46. doi:10.1158/2159-8290.CD-21-1059.

11 Hashimoto T, Shibasaki F. Hypoxia-inducible factor as an angiogenic master switch. *Front Pediatr*. 2015;3:33. doi:10.3389/fped.2015.00033.

12 Yang Y, Sun M, Wang L, Jiao B. HIFs, angiogenesis, and cancer. *J Cell Biochem*. 2013;114(5):967-974. doi:10.1002/jcb.24438.

13 Fouad YA, Aanei C. Revisiting the hallmarks of cancer. *Am J Cancer Res*. 2017;7(5):1016-1036.

14 Warburg O, Posener K, Negelein E. Über den Stoffwechsel der Carcinomzelle. *Berlin - Biochem. Z.* 1924.

15 Warburg O. Über die chemische Konstitution des Atmungsferments. *Naturwissenschaften*. 1928;16(20):345-350. doi:10.1007/BF01505412.

16 Warburg O. The oxygen-transferring ferment of respiration. *Nobel Lectures*. 1931.

17 Warburg O. On the origin of cancer cells. *Science*. 1956;123(3191):309-314. doi:10.1126/science.123.3191.309.

18 Shay JW. Role of Telomeres and Telomerase in Aging and Cancer. *Cancer Discov*. 2016;6(6):584-593. doi:10.1158/2159-8290.CD-16-0062.

19 Dunn GP, Bruce AT, Ikeda H, Old LJ, Schreiber RD. Cancer immunoediting: from immunosurveillance to tumor escape. *Nat Immunol*. 2002;3(11):991-998. doi:10.1038/ni1102-991.

20 Malladi S, Macalinao DG, Jin X, et al. Metastatic Latency and Immune Evasion through Autocrine Inhibition of WNT. *Cell*. 2016;165(1):45-60. doi:10.1016/j.cell.2016.02.025.

21 Faller A. *Der Körper des Menschen: Einführung in Bau und Funktion ; [4 Poster mit Übersichten ; Skelett, Gefäße, Nerven, Muskeln.* 16., überarb. Aufl. Stuttgart, New York: Thieme; 2012.

22 Srinivas US, Tan BWQ, Vellayappan BA, Jeyasekharan AD. ROS and the DNA damage response in cancer. *Redox Biol*. 2019;25:101084. doi:10.1016/j.redox.2018.101084.

23 Olinski R, Zastawny T, Budzbon J, Skokowski J, Zegarski W, Dizdaroglu M. DNA base modifications in chromatin of human cancerous tissues. *FEBS Letters*. 1992;309(2):193-198. doi:10.1016/0014-5793(92)81093-2.

24 Bakhoum SF, Silkworth WT, Nardi IK, Nicholson JM, Compton DA, Cimini D. The mitotic origin of chromosomal instability. *Curr Biol*. 2014;24(4):R148-9. doi:10.1016/j.cub.2014.01.019.

25 Giam M, Rancati G. Aneuploidy and chromosomal instability in cancer: a jackpot to chaos. *Cell Div*. 2015;10:3. doi:10.1186/s13008-015-0009-7.
26 Schukken KM, Foijer F. CIN and Aneuploidy: Different Concepts, Different Consequences. *Bioessays*. 2018;40(1). doi:10.1002/bies.201700147.
27 Zhu J, Tsai H-J, Gordon MR, Li R. Cellular Stress Associated with Aneuploidy. *Dev Cell*. 2018;44(4):420-431. doi:10.1016/j.devcel.2018.02.002.
28 Schukken KM, Sheltzer JM. Extensive protein dosage compensation in aneuploid human cancers. *Genome Res*. 2022;32(7):1254-1270. doi:10.1101/gr.276378.121.
29 Stingele S, Stoehr G, Peplowska K, Cox J, Mann M, Storchova Z. Global analysis of genome, transcriptome and proteome reveals the response to aneuploidy in human cells. *Mol Syst Biol*. 2012;8:608. doi:10.1038/msb.2012.40.
30 Orr B, Compton DA. A double-edged sword: how oncogenes and tumor suppressor genes can contribute to chromosomal instability. *Front Oncol*. 2013;3:164. doi:10.3389/fonc.2013.00164.
31 Bielski CM, Zehir A, Penson AV, et al. Genome doubling shapes the evolution and prognosis of advanced cancers. *Nat Genet*. 2018;50(8):1189-1195. doi:10.1038/s41588-018-0165-1.
32 Quinton RJ, DiDomizio A, Vittoria MA, et al. Whole-genome doubling confers unique genetic vulnerabilities on tumour cells. *Nature*. 2021;590(7846):492-497. doi:10.1038/s41586-020-03133-3.
33 Zack TI, Schumacher SE, Carter SL, et al. Pan-cancer patterns of somatic copy number alteration. *Nat Genet*. 2013;45(10):1134-1140. doi:10.1038/ng.2760.
34 Fujiwara T, Bandi M, Nitta M, Ivanova EV, Bronson RT, Pellman D. Cytokinesis failure generating tetraploids promotes tumorigenesis in p53-null cells. *Nature*. 2005;437(7061):1043-1047. doi:10.1038/nature04217.
35 Lens SMA, Medema RH. Cytokinesis defects and cancer. *Nat Rev Cancer*. 2019;19(1):32-45. doi:10.1038/s41568-018-0084-6.
36 Gentric G, Celton-Morizur S, Desdouets C. Polyploidy and liver proliferation. *Clin Res Hepatol Gastroenterol*. 2012;36(1):29-34. doi:10.1016/j.clinre.2011.05.011.
37 Weaver BAA, Cleveland DW. Does aneuploidy cause cancer? *Curr Opin Cell Biol*. 2006;18(6):658-667. doi:10.1016/j.ceb.2006.10.002.
38 Stephens PJ, Greenman CD, Fu B, et al. Massive genomic rearrangement acquired in a single catastrophic event during cancer development. *Cell*. 2011;144(1):27-40. doi:10.1016/j.cell.2010.11.055.
39 Keuper K, Wieland A, Räschle M, Storchova Z. Processes shaping cancer genomes - From mitotic defects to chromosomal rearrangements. *DNA Repair (Amst)*. 2021;107:103207. doi:10.1016/j.dnarep.2021.103207.
40 HOWARD A, PELC S. Nuclear incorporation of P as demonstrated by autoradiographs. *Experimental Cell Research*. 1951;2(2):178-187. doi:10.1016/0014-4827(51)90083-3.
41 Campbell NA. *Campbell Biologie*. München: Pearson Deutschland; 2015.
42 Matthews HK, Bertoli C, Bruin RAM de. Cell cycle control in cancer. *Nat Rev Mol Cell Biol*. 2022;23(1):74-88. doi:10.1038/s41580-021-00404-3.
43 Morgan DO. Cyclin-dependent kinases: engines, clocks, and microprocessors. *Annu Rev Cell Dev Biol*. 1997;13:261-291. doi:10.1146/annurev.cellbio.13.1.261.
44 Gartel AL, Tyner AL. Transcriptional regulation of the p21((WAF1/CIP1)) gene. *Experimental Cell Research*. 1999;246(2):280-289. doi:10.1006/excr.1998.4319.
45 el-Deiry WS, Tokino T, Velculescu VE, et al. WAF1, a potential mediator of p53 tumor suppression. *Cell*. 1993;75(4):817-825. doi:10.1016/0092-8674(93)90500-p.

46 Yang J, Yu Y, Hamrick HE, Duerksen-Hughes PJ. ATM, ATR and DNA-PK: initiators of the cellular genotoxic stress responses. *Carcinogenesis*. 2003;24(10):1571-1580. doi:10.1093/carcin/bgg137.
47 Nigg EA, Stearns T. The centrosome cycle: Centriole biogenesis, duplication and inherent asymmetries. *Nat Cell Biol*. 2011;13(10):1154-1160. doi:10.1038/ncb2345.
48 Puklowski A, Homsi Y, Keller D, et al. The SCF-FBXW5 E3-ubiquitin ligase is regulated by PLK4 and targets HsSAS-6 to control centrosome duplication. *Nat Cell Biol*. 2011;13(8):1004-1009. doi:10.1038/ncb2282.
49 Morgan D. *The cell cycle: Principles of control*. Corby, Oxford, Sunderland, MA: Oxford University Press; Sinauer; 2007.
50 Malumbres M, Barbacid M. Cell cycle, CDKs and cancer: a changing paradigm. *Nat Rev Cancer*. 2009;9(3):153-166. doi:10.1038/nrc2602.
51 Landis MW, Pawlyk BS, Li T, Sicinski P, Hinds PW. Cyclin D1-dependent kinase activity in murine development and mammary tumorigenesis. *Cancer Cell*. 2006;9(1):13-22. doi:10.1016/j.ccr.2005.12.019.
52 Musgrove EA, Caldon CE, Barraclough J, Stone A, Sutherland RL. Cyclin D as a therapeutic target in cancer. *Nat Rev Cancer*. 2011;11(8):558-572. doi:10.1038/nrc3090.
53 Gennaro VJ, Stanek TJ, Peck AR, et al. Control of CCND1 ubiquitylation by the catalytic SAGA subunit USP22 is essential for cell cycle progression through G1 in cancer cells. *Proc Natl Acad Sci U S A*. 2018;115(40):E9298-E9307. doi:10.1073/pnas.1807704115.
54 Gao A, Sun T, Ma G, et al. LEM4 confers tamoxifen resistance to breast cancer cells by activating cyclin D-CDK4/6-Rb and ERα pathway. *Nat Commun*. 2018;9(1):4180. doi:10.1038/s41467-018-06309-8.
55 Onn I, Heidinger-Pauli JM, Guacci V, Unal E, Koshland DE. Sister chromatid cohesion: a simple concept with a complex reality. *Annu Rev Cell Dev Biol*. 2008;24:105-129. doi:10.1146/annurev.cellbio.24.110707.175350.
56 Jin F, Wang Y. The signaling network that silences the spindle assembly checkpoint upon the establishment of chromosome bipolar attachment. *Proc Natl Acad Sci U S A*. 2013;110(52):21036-21041. doi:10.1073/pnas.1307595111.
57 Mukherjee S, Sandri BJ, Tank D, et al. A Gradient in Metaphase Tension Leads to a Scaled Cellular Response in Mitosis. *Dev Cell*. 2019;49(1):63-76.e10. doi:10.1016/j.devcel.2019.01.018.
58 Stern BM, Murray AW. Lack of tension at kinetochores activates the spindle checkpoint in budding yeast. *Curr Biol*. 2001;11(18):1462-1467. doi:10.1016/S0960-9822(01)00451-1.
59 McVey SL, Cosby JK, Nannas NJ. Aurora B Tension Sensing Mechanisms in the Kinetochore Ensure Accurate Chromosome Segregation. *Int J Mol Sci*. 2021;22(16). doi:10.3390/ijms22168818.
60 Kapoor TM, Mayer TU, Coughlin ML, Mitchison TJ. Probing spindle assembly mechanisms with monastrol, a small molecule inhibitor of the mitotic kinesin, Eg5. *J Cell Biol*. 2000;150(5):975-988. doi:10.1083/jcb.150.5.975.
61 Musacchio A, Salmon ED. The spindle-assembly checkpoint in space and time. *Nat Rev Mol Cell Biol*. 2007;8(5):379-393. doi:10.1038/nrm2163.
62 Lampson MA, Renduchitala K, Khodjakov A, Kapoor TM. Correcting improper chromosome-spindle attachments during cell division. *Nat Cell Biol*. 2004;6(3):232-237. doi:10.1038/ncb1102.
63 Loncarek J, Kisurina-Evgenieva O, Vinogradova T, et al. The centromere geometry essential for keeping mitosis error free is controlled by spindle forces. *Nature*. 2007;450(7170):745-749. doi:10.1038/nature06344.

64 Guerrero AA, Martínez-A C, van Wely KH. Merotelic attachments and non-homologous end joining are the basis of chromosomal instability. *Cell Div*. 2010;5:13. doi:10.1186/1747-1028-5-13.
65 Krämer A, Ho AD. Centrosome aberrations and cancer. *Onkologie*. 2001;24(6):538-544. doi:10.1159/000055141.
66 Chunduri NK, Storchová Z. The diverse consequences of aneuploidy. *Nat Cell Biol*. 2019;21(1):54-62. doi:10.1038/s41556-018-0243-8.
67 Fragkos M, Ganier O, Coulombe P, Méchali M. DNA replication origin activation in space and time. *Nat Rev Mol Cell Biol*. 2015;16(6):360-374. doi:10.1038/nrm4002.
68 Blow JJ, Ge XQ, Jackson DA. How dormant origins promote complete genome replication. *Trends Biochem Sci*. 2011;36(8):405-414. doi:10.1016/j.tibs.2011.05.002.
69 Mazouzi A, Velimezi G, Loizou JI. DNA replication stress: causes, resolution and disease. *Experimental Cell Research*. 2014;329(1):85-93. doi:10.1016/j.yexcr.2014.09.030.
70 Zeman MK, Cimprich KA. Causes and consequences of replication stress. *Nat Cell Biol*. 2014;16(1):2-9. doi:10.1038/ncb2897.
71 Gómez-González B, Aguilera A. Transcription-mediated replication hindrance: a major driver of genome instability. *Genes Dev*. 2019;33(15-16):1008-1026. doi:10.1101/gad.324517.119.
72 Bartkova J, Horejsí Z, Koed K, et al. DNA damage response as a candidate anti-cancer barrier in early human tumorigenesis. *Nature*. 2005;434(7035):864-870. doi:10.1038/nature03482.
73 Gorgoulis VG, Vassiliou L-VF, Karakaidos P, et al. Activation of the DNA damage checkpoint and genomic instability in human precancerous lesions. *Nature*. 2005;434(7035):907-913. doi:10.1038/nature03485.
74 Macheret M, Halazonetis TD. DNA replication stress as a hallmark of cancer. *Annu Rev Pathol*. 2015;10:425-448. doi:10.1146/annurev-pathol-012414-040424.
75 Maya-Mendoza A, Ostrakova J, Kosar M, et al. Myc and Ras oncogenes engage different energy metabolism programs and evoke distinct patterns of oxidative and DNA replication stress. *Mol Oncol*. 2015;9(3):601-616. doi:10.1016/j.molonc.2014.11.001.
76 Macheret M, Halazonetis TD. Intragenic origins due to short G1 phases underlie oncogene-induced DNA replication stress. *Nature*. 2018;555(7694):112-116. doi:10.1038/nature25507.
77 Bester AC, Roniger M, Oren YS, et al. Nucleotide deficiency promotes genomic instability in early stages of cancer development. *Cell*. 2011;145(3):435-446. doi:10.1016/j.cell.2011.03.044.
78 Toledo LI, Altmeyer M, Rask M-B, et al. ATR prohibits replication catastrophe by preventing global exhaustion of RPA. *Cell*. 2013;155(5):1088-1103. doi:10.1016/j.cell.2013.10.043.
79 Zhong Y, Nellimoottil T, Peace JM, et al. The level of origin firing inversely affects the rate of replication fork progression. *J Cell Biol*. 2013;201(3):373-383. doi:10.1083/jcb.201208060.
80 Wold MS. Replication protein A: a heterotrimeric, single-stranded DNA-binding protein required for eukaryotic DNA metabolism. *Annu Rev Biochem*. 1997;66:61-92. doi:10.1146/annurev.biochem.66.1.61.
81 Vassin VM, Anantha RW, Sokolova E, Kanner S, Borowiec JA. Human RPA phosphorylation by ATR stimulates DNA synthesis and prevents ssDNA accumulation during DNA-replication stress. *J Cell Sci*. 2009;122(22):4070-4080. doi:10.1242/jcs.053702.
82 McNeely S, Beckmann R, Bence Lin AK. CHEK again: revisiting the development of CHK1 inhibitors for cancer therapy. *Pharmacol Ther*. 2014;142(1):1-10. doi:10.1016/j.pharmthera.2013.10.005.
83 Lee D-H, Pan Y, Kanner S, Sung P, Borowiec JA, Chowdhury D. A PP4 phosphatase complex dephosphorylates RPA2 to facilitate DNA repair via homologous recombination. *Nat Struct Mol Biol*. 2010;17(3):365-372. doi:10.1038/nsmb.1769.

84 Liaw H, Lee D, Myung K. DNA-PK-Dependent RPA2 Hyperphosphorylation Facilitates DNA Repair and Suppresses Sister Chromatid Exchange. *PLOS ONE*. 2011;6(6). doi:10.1371/journal.pone.0021424.
85 Saldivar JC, Hamperl S, Bocek MJ, et al. An intrinsic S/G2 checkpoint enforced by ATR. *Science*. 2018;361(6404):806-810. doi:10.1126/science.aap9346.
86 Lemmens B, Hegarat N, Akopyan K, et al. DNA Replication Determines Timing of Mitosis by Restricting CDK1 and PLK1 Activation. *Mol Cell*. 2018;71(1):117-128.e3. doi:10.1016/j.molcel.2018.05.026.
87 Buisson R, Boisvert JL, Benes CH, Zou L. Distinct but Concerted Roles of ATR, DNA-PK, and Chk1 in Countering Replication Stress during S Phase. *Mol Cell*. 2015;59(6):1011-1024. doi:10.1016/j.molcel.2015.07.029.
88 Jazayeri A, Falck J, Lukas C, et al. ATM- and cell cycle-dependent regulation of ATR in response to DNA double-strand breaks. *Nat Cell Biol*. 2006;8(1):37-45. doi:10.1038/ncb1337.
89 Maréchal A, Zou L. DNA damage sensing by the ATM and ATR kinases. *Cold Spring Harb Perspect Biol*. 2013;5(9). doi:10.1101/cshperspect.a012716.
90 Saldivar JC, Cortez D, Cimprich KA. The essential kinase ATR: ensuring faithful duplication of a challenging genome. *Nat Rev Mol Cell Biol*. 2017;18(10):622-636. doi:10.1038/nrm.2017.67;
91 Yoo HY, Kumagai A, Shevchenko A, Shevchenko A, Dunphy WG. Ataxia-telangiectasia mutated (ATM)-dependent activation of ATR occurs through phosphorylation of TopBP1 by ATM. *J Biol Chem*. 2007;282(24):17501-17506. doi:10.1074/jbc.M701770200.
92 Ping B, He X, Xia W, et al. Cytoplasmic expression of p21CIP1/WAF1 is correlated with IKKβ overexpression in human breast cancers. *Int J Oncol*. 2006. doi:10.3892/ijo.29.5.1103.
93 Capparelli C, Chiavarina B, Whitaker-Menezes D, et al. CDK inhibitors (p16/p19/p21) induce senescence and autophagy in cancer-associated fibroblasts, “fueling” tumor growth via paracrine interactions, without an increase in neo-angiogenesis. *Cell Cycle*. 2012;11(19):3599-3610. doi:10.4161/cc.21884.
94 Eykelenboom JK, Harte EC, Canavan L, et al. ATR activates the S-M checkpoint during unperturbed growth to ensure sufficient replication prior to mitotic onset. *Cell Rep*. 2013;5(4):1095-1107. doi:10.1016/j.celrep.2013.10.027.
95 Naim V, Rosselli F. The FANC pathway and BLM collaborate during mitosis to prevent micro-nucleation and chromosome abnormalities. *Nat Cell Biol*. 2009;11(6):761-768. doi:10.1038/ncb1883.
96 Naim V, Rosselli F. The FANC pathway and mitosis: a replication legacy. *Cell Cycle*. 2009;8(18):2907-2911. doi:10.4161/cc.8.18.9538.
97 Fragkos M, Naim V. Rescue from replication stress during mitosis. *Cell Cycle*. 2017;16(7):613-633. doi:10.1080/15384101.2017.1288322.
98 Chan KL, Palmai-Pallag T, Ying S, Hickson ID. Replication stress induces sister-chromatid bridging at fragile site loci in mitosis. *Nat Cell Biol*. 2009;11(6):753-760. doi:10.1038/ncb1882.
99 Terradas M, Martín M, Genescà A. Impaired nuclear functions in micronuclei results in genome instability and chromothripsis. *Arch Toxicol*. 2016;90(11):2657-2667. doi:10.1007/s00204-016-1818-4.
100 Broustas CG, Lieberman HB. DNA damage response genes and the development of cancer metastasis. *Radiat Res*. 2014;181(2):111-130. doi:10.1667/RR13515.1.
101 Zhang P, Wang J, Gao W, Yuan B-Z, Rogers J, Reed E. CHK2 kinase expression is down-regulated due to promoter methylation in non-small cell lung cancer. *Mol Cancer*. 2004;3:14. doi:10.1186/1476-4598-3-14.
102 Jeggo PA, Pearl LH, Carr AM. DNA repair, genome stability and cancer: a historical perspective. *Nat Rev Cancer*. 2016;16(1):35-42. doi:10.1038/nrc.2015.4.

103 Wilhelm T, Olziersky A-M, Harry D, et al. Mild replication stress causes chromosome mis-segregation via premature centriole disengagement. *Nat Commun*. 2019;10(1):3585. doi:10.1038/s41467-019-11584-0.
104 Böhly N, Kistner M, Bastians H. Mild replication stress causes aneuploidy by deregulating microtubule dynamics in mitosis. *Cell Cycle*. 2019;18(20):2770-2783. doi:10.1080/15384101.2019.1658477.
105 Burrell RA, McClelland SE, Endesfelder D, et al. Replication stress links structural and numerical cancer chromosomal instability. *Nature*. 2013;494(7438):492-496. doi:10.1038/nature11935.
106 Yang Z, Klionsky DJ. Mammalian autophagy: core molecular machinery and signaling regulation. *Curr Opin Cell Biol*. 2010;22(2):124-131. doi:10.1016/j.ceb.2009.11.014.
107 Mizushima N, Komatsu M. Autophagy: renovation of cells and tissues. *Cell*. 2011;147(4):728-741. doi:10.1016/j.cell.2011.10.026.
108 Hewitt G, Korolchuk VI. Repair, Reuse, Recycle: The Expanding Role of Autophagy in Genome Maintenance. *Trends Cell Biol*. 2017;27(5):340-351. doi:10.1016/j.tcb.2016.11.011.
109 Kimura S, Fujita N, Noda T, Yoshimori T. Monitoring autophagy in mammalian cultured cells through the dynamics of LC3. *Methods Enzymol*. 2009;452:1-12. doi:10.1016/S0076-6879(08)03601-X.
110 Komatsu M, Ichimura Y. Physiological significance of selective degradation of p62 by autophagy. *FEBS Letters*. 2010;584(7):1374-1378. doi:10.1016/j.febslet.2010.02.017.
111 Coryell PR, Goraya SK, Griffin KA, Redick MA, Sisk SR, Purvis JE. Autophagy regulates the localization and degradation of p16INK4a. *Aging Cell*. 2020;19(7):e13171. doi:10.1111/acel.13171.
112 Fenech M, Kirsch-Volders M, Natarajan AT, et al. Molecular mechanisms of micronucleus, nucleoplasmic bridge and nuclear bud formation in mammalian and human cells. *Mutagenesis*. 2011;26(1):125-132. doi:10.1093/mutage/geq052.
113 Zhang C-Z, Spektor A, Cornils H, et al. Chromothripsis from DNA damage in micronuclei. *Nature*. 2015;522(7555):179-184. doi:10.1038/nature14493.
114 Voronina N, Wong JKL, Hübschmann D, et al. The landscape of chromothripsis across adult cancer types. *Nat Commun*. 2020;11(1):2320. doi:10.1038/s41467-020-16134-7.
115 Cortés-Ciriano I, Lee JJ-K, Xi R, et al. Comprehensive analysis of chromothripsis in 2,658 human cancers using whole-genome sequencing. *Nat Genet*. 2020;52(3):331-341. doi:10.1038/s41588-019-0576-7.
116 Batanian JR, Eswara MS. De novo apparently balanced complex chromosome rearrangement (CCR) involving chromosomes 4, 18, and 21 in a girl with mental retardation: report and review. *Am J Med Genet*. 1998;78(1):44-51.
117 Lee N-C, Chen M, Ma G-C, et al. Complex rearrangements between chromosomes 6, 10, and 11 with multiple deletions at breakpoints. *Am J Med Genet A*. 2010;152A(9):2327-2334. doi:10.1002/ajmg.a.33581.
118 McDermott DH, Gao J-L, Liu Q, et al. Chromothriptic cure of WHIM syndrome. *Cell*. 2015;160(4):686-699. doi:10.1016/j.cell.2015.01.014.
119 Baca SC, Prandi D, Lawrence MS, et al. Punctuated evolution of prostate cancer genomes. *Cell*. 2013;153(3):666-677. doi:10.1016/j.cell.2013.03.021.
120 Shen MM. Chromoplexy: a new category of complex rearrangements in the cancer genome. *Cancer Cell*. 2013;23(5):567-569. doi:10.1016/j.ccr.2013.04.025.
121 Berger MF, Lawrence MS, Demichelis F, et al. The genomic complexity of primary human prostate cancer. *Nature*. 2011;470(7333):214-220. doi:10.1038/nature09744.

122 Liu P, Erez A, Nagamani SCS, et al. Chromosome catastrophes involve replication mechanisms generating complex genomic rearrangements. *Cell*. 2011;146(6):889-903. doi:10.1016/j.cell.2011.07.042.
123 Holland AJ, Cleveland DW. Chromoanagenesis and cancer: mechanisms and consequences of localized, complex chromosomal rearrangements. *Nat Med*. 2012;18(11):1630-1638. doi:10.1038/nm.2988.
124 Nones K, Waddell N, Wayte N, et al. Genomic catastrophes frequently arise in esophageal adenocarcinoma and drive tumorigenesis. *Nat Commun*. 2014;5:5224. doi:10.1038/ncomms6224.
125 Taniwaki M. Recent advancements in molecular cytogenetics for hematological malignancies: identification of novel PVT1 fusion genes. *Rinsho Ketsueki*. 2015;56(10):2056-2065. doi:10.11406/rinketsu.56.2056.
126 Shoshani O, Brunner SF, Yaeger R, et al. Chromothripsis drives the evolution of gene amplification in cancer. *Nature*. 2021;591(7848):137-141. doi:10.1038/s41586-020-03064-z.
127 Korbel JO, Campbell PJ. Criteria for inference of chromothripsis in cancer genomes. *Cell*. 2013;152(6):1226-1236. doi:10.1016/j.cell.2013.02.023.
128 Forment JV, Kaidi A, Jackson SP. Chromothripsis and cancer: causes and consequences of chromosome shattering. *Nat Rev Cancer*. 2012;12(10):663-670. doi:10.1038/nrc3352.
129 Crasta K, Ganem NJ, Dagher R, et al. DNA breaks and chromosome pulverization from errors in mitosis. *Nature*. 2012;482(7383):53-58. doi:10.1038/nature10802.
130 Terzoudi GI, Karakosta M, Pantelias A, Hatzi VI, Karachristou I, Pantelias G. Stress induced by premature chromatin condensation triggers chromosome shattering and chromothripsis at DNA sites still replicating in micronuclei or multinucleate cells when primary nuclei enter mitosis. *Mutat Res Genet Toxicol Environ Mutagen*. 2015;793:185-198. doi:10.1016/j.mrgentox.2015.07.014.
131 Liu S, Kwon M, Mannino M, et al. Nuclear envelope assembly defects link mitotic errors to chromothripsis. *Nature*. 2018;561(7724):551-555. doi:10.1038/s41586-018-0534-z.
132 Hatch EM, Fischer AH, Deerinck TJ, Hetzer MW. Catastrophic nuclear envelope collapse in cancer cell micronuclei. *Cell*. 2013;154(1):47-60. doi:10.1016/j.cell.2013.06.007.
133 Guo X, Dai X, Wu X, et al. Understanding the birth of rupture-prone and irreparable micronuclei. *Chromosoma*. 2020;129(3-4):181-200. doi:10.1007/s00412-020-00741-w.
134 Mohr L, Toufektchan E, Morgen P von, Chu K, Kapoor A, Maciejowski J. ER-directed TREX1 limits cGAS activation at micronuclei. *Mol Cell*. 2021;81(4):724-738.e9. doi:10.1016/j.molcel.2020.12.037.
135 Ly P, Brunner SF, Shoshani O, et al. Chromosome segregation errors generate a diverse spectrum of simple and complex genomic rearrangements. *Nat Genet*. 2019;51(4):705-715. doi:10.1038/s41588-019-0360-8.
136 Chiang C, Jacobsen JC, Ernst C, et al. Complex reorganization and predominant non-homologous repair following chromosomal breakage in karyotypically balanced germline rearrangements and transgenic integration. *Nat Genet*. 2012;44(4):390-7, S1. doi:10.1038/ng.2202.
137 Kneissig M, Keuper K, Pagter MS de, et al. Micronuclei-based model system reveals functional consequences of chromothripsis in human cells. *Elife*. 2019;8. doi:10.7554/eLife.50292.
138 Passerini V, Ozeri-Galai E, Pagter MS de, et al. The presence of extra chromosomes leads to genomic instability. *Nat Commun*. 2016;7:10754. doi:10.1038/ncomms10754.
139 Sheltzer JM, Ko JH, Replogle JM, et al. Single-chromosome Gains Commonly Function as Tumor Suppressors. *Cancer Cell*. 2017;31(2):240-255. doi:10.1016/j.ccell.2016.12.004.

140 Michel LS, Liberal V, Chatterjee A, et al. MAD2 haplo-insufficiency causes premature anaphase and chromosome instability in mammalian cells. *Nature*. 2001;409(6818):355-359. doi:10.1038/35053094.
141 Ohashi A, Ohori M, Iwai K, et al. Aneuploidy generates proteotoxic stress and DNA damage concurrently with p53-mediated post-mitotic apoptosis in SAC-impaired cells. *Nat Commun*. 2015;6:7668. doi:10.1038/ncomms8668.
142 Sotillo R, Hernando E, Díaz-Rodríguez E, et al. Mad2 overexpression promotes aneuploidy and tumorigenesis in mice. *Cancer Cell*. 2007;11(1):9-23. doi:10.1016/j.ccr.2006.10.019.
143 Weaver BAA, Silk AD, Montagna C, Verdier-Pinard P, Cleveland DW. Aneuploidy acts both oncogenically and as a tumor suppressor. *Cancer Cell*. 2007;11(1):25-36. doi:10.1016/j.ccr.2006.12.003.
144 Foijer F, Xie SZ, Simon JE, et al. Chromosome instability induced by Mps1 and p53 mutation generates aggressive lymphomas exhibiting aneuploidy-induced stress. *Proc Natl Acad Sci U S A*. 2014;111(37):13427-13432. doi:10.1073/pnas.1400892111.
145 Upender MB, Habermann JK, McShane LM, et al. Chromosome transfer induced aneuploidy results in complex dysregulation of the cellular transcriptome in immortalized and cancer cells. *Cancer Res*. 2004;64(19):6941-6949. doi:10.1158/0008-5472.CAN-04-0474.
146 Santaguida S, Richardson A, Iyer DR, et al. Chromosome Mis-segregation Generates Cell-Cycle-Arrested Cells with Complex Karyotypes that Are Eliminated by the Immune System. *Dev Cell*. 2017;41(6):638-651.e5. doi:10.1016/j.devcel.2017.05.022.
147 Jiang J, Jing Y, Cost GJ, et al. Translating dosage compensation to trisomy 21. *Nature*. 2013;500(7462):296-300. doi:10.1038/nature12394.
148 Zuo E, Huo X, Yao X, et al. CRISPR/Cas9-mediated targeted chromosome elimination. *Genome Biol*. 2017;18(1):224. doi:10.1186/s13059-017-1354-4.
149 Adikusuma F, Williams N, Grutzner F, Hughes J, Thomas P. Targeted Deletion of an Entire Chromosome Using CRISPR/Cas9. *Mol Ther*. 2017;25(8):1736-1738. doi:10.1016/j.ymthe.2017.05.021.
150 Bosco N, Goldberg A, Johnson AF, et al. *KaryoCreate: a new CRISPR-based technology to generate chromosome-specific aneuploidy by targeting human centromeres*; 2022.
151 Giaginis C, Georgiadou M, Dimakopoulou K, et al. Clinical significance of MCM-2 and MCM-5 expression in colon cancer: association with clinicopathological parameters and tumor proliferative capacity. *Dig Dis Sci*. 2009;54(2):282-291. doi:10.1007/s10620-008-0305-z.
152 Stewart PA, Khamis ZI, Zhau HE, et al. Upregulation of minichromosome maintenance complex component 3 during epithelial-to-mesenchymal transition in human prostate cancer. *Oncotarget*. 2017;8(24):39209-39217. doi:10.18632/oncotarget.16835.
153 Wojnar A, Pula B, Piotrowska A, et al. Correlation of intensity of MT-I/II expression with Ki-67 and MCM-2 proteins in invasive ductal breast carcinoma. *Anticancer Res*. 2011;31(9):3027-3033.
154 Zhong H, Chen B, Neves H, et al. Expression of minichromosome maintenance genes in renal cell carcinoma. *Cancer Manag Res*. 2017;9:637-647. doi:10.2147/CMAR.S146528.
155 Dürrbaum M, Kuznetsova AY, Passerini V, Stingele S, Stoehr G, Storchová Z. Unique features of the transcriptional response to model aneuploidy in human cells. *BMC Genomics*. 2014;15:139. doi:10.1186/1471-2164-15-139.
156 Priestley P, Baber J, Lolkema MP, et al. Pan-cancer whole-genome analyses of metastatic solid tumours. *Nature*. 2019;575(7781):210-216. doi:10.1038/s41586-019-1689-y.
157 Johnson DG, Schwarz JK, Cress WD, Nevins JR. Expression of transcription factor E2F1 induces quiescent cells to enter S phase. *Nature*. 1993;365(6444):349-352. doi:10.1038/365349a0.

158 Lukas J, Petersen BO, Holm K, Bartek J, Helin K. Deregulated expression of E2F family members induces S-phase entry and overcomes p16INK4A-mediated growth suppression. *Mol Cell Biol*. 1996;16(3):1047-1057. doi:10.1128/MCB.16.3.1047.

159 Wu L, Timmers C, Maiti B, et al. The E2F1-3 transcription factors are essential for cellular proliferation. *Nature*. 2001;414(6862):457-462. doi:10.1038/35106593.

160 Dewhurst SM, McGranahan N, Burrell RA, et al. Tolerance of whole-genome doubling propagates chromosomal instability and accelerates cancer genome evolution. *Cancer Discov*. 2014;4(2):175-185. doi:10.1158/2159-8290.CD-13-0285.

161 Shukla A, Nguyen THM, Moka SB, et al. Chromosome arm aneuploidies shape tumour evolution and drug response. *Nat Commun*. 2020;11(1):449. doi:10.1038/s41467-020-14286-0.

162 Watkins TBK, Lim EL, Petkovic M, et al. Pervasive chromosomal instability and karyotype order in tumour evolution. *Nature*. 2020;587(7832):126-132. doi:10.1038/s41586-020-2698-6.

163 Cohen-Sharir Y, McFarland JM, Abdusamad M, et al. Aneuploidy renders cancer cells vulnerable to mitotic checkpoint inhibition. *Nature*. 2021;590(7846):486-491. doi:10.1038/s41586-020-03114-6.

164 Taylor AM, Shih J, Ha G, et al. Genomic and Functional Approaches to Understanding Cancer Aneuploidy. *Cancer Cell*. 2018;33(4):676-689.e3. doi:10.1016/j.ccell.2018.03.007.

165 Kuznetsova AY, Seget K, Moeller GK, et al. Chromosomal instability, tolerance of mitotic errors and multidrug resistance are promoted by tetraploidization in human cells. *Cell Cycle*. 2015;14(17):2810-2820. doi:10.1080/15384101.2015.1068482.

166 Haupt Y, Maya R, Kazaz A, Oren M. Mdm2 promotes the rapid degradation of p53. *Nature*. 1997;387(6630):296-299. doi:10.1038/387296a0.

167 Kubbutat MH, Jones SN, Vousden KH. Regulation of p53 stability by Mdm2. *Nature*. 1997;387(6630):299-303. doi:10.1038/387299a0.

168 Michael D, Oren M. The p53–Mdm2 module and the ubiquitin system. *Seminars in Cancer Biology*. 2003;13(1):49-58. doi:10.1016/s1044-579x(02)00099-8.

169 Aylon Y, Michael D, Shmueli A, Yabuta N, Nojima H, Oren M. A positive feedback loop between the p53 and Lats2 tumor suppressors prevents tetraploidization. *Genes Dev*. 2006;20(19):2687-2700. doi:10.1101/gad.1447006.

170 Ganem NJ, Cornils H, Chiu S-Y, et al. Cytokinesis failure triggers hippo tumor suppressor pathway activation. *Cell*. 2014;158(4):833-848. doi:10.1016/j.cell.2014.06.029.

171 Lanni JS, Jacks T. Characterization of the p53-dependent postmitotic checkpoint following spindle disruption. *Mol Cell Biol*. 1998;18(2):1055-1064. doi:10.1128/MCB.18.2.1055.

172 Andreassen PR, Lohez OD, Lacroix FB, Margolis RL. Tetraploid state induces p53-dependent arrest of nontransformed mammalian cells in G1. *Mol Biol Cell*. 2001;12(5):1315-1328. doi:10.1091/mbc.12.5.1315.

173 Ganem NJ, Godinho SA, Pellman D. A mechanism linking extra centrosomes to chromosomal instability. *Nature*. 2009;460(7252):278-282. doi:10.1038/nature08136.

174 Kuffer C, Kuznetsova AY, Storchová Z. Abnormal mitosis triggers p53-dependent cell cycle arrest in human tetraploid cells. *Chromosoma*. 2013;122(4):305-318. doi:10.1007/s00412-013-0414-0.

175 Fava LL, Schuler F, Sladky V, et al. The PIDDosome activates p53 in response to supernumerary centrosomes. *Genes Dev*. 2017;31(1):34-45. doi:10.1101/gad.289728.116.

176 Fox DT, Gall JG, Spradling AC. Error-prone polyploid mitosis during normal Drosophila development. *Genes Dev*. 2010;24(20):2294-2302. doi:10.1101/gad.1952710.

177 Belyaeva ES, Zhimulev IF, Volkova EI, Alekseyenko AA, Moshkin YM, Koryakov DE. Su(UR)ES: a gene suppressing DNA underreplication in intercalary and pericentric heterochromatin of Drosophila melanogaster polytene chromosomes. *Proc Natl Acad Sci U S A*. 1998;95(13):7532-7537. doi:10.1073/pnas.95.13.7532.

178 Edgar BA, Zielke N, Gutierrez C. Endocycles: a recurrent evolutionary innovation for post-mitotic cell growth. *Nat Rev Mol Cell Biol*. 2014;15(3):197-210. doi:10.1038/nrm3756.
179 Hannibal RL, Chuong EB, Rivera-Mulia JC, Gilbert DM, Valouev A, Baker JC. Copy number variation is a fundamental aspect of the placental genome. *PLoS Genet*. 2014;10(5):e1004290. doi:10.1371/journal.pgen.1004290.
180 Belyakin SN, Christophides GK, Alekseyenko AA, et al. Genomic analysis of Drosophila chromosome underreplication reveals a link between replication control and transcriptional territories. *Proc Natl Acad Sci U S A*. 2005;102(23):8269-8274. doi:10.1073/pnas.0502702102.
181 Nordman J, Li S, Eng T, Macalpine D, Orr-Weaver TL. Developmental control of the DNA replication and transcription programs. *Genome Res*. 2011;21(2):175-181. doi:10.1101/gr.114611.110.
182 Sher N, Bell GW, Li S, et al. Developmental control of gene copy number by repression of replication initiation and fork progression. *Genome Res*. 2012;22(1):64-75. doi:10.1101/gr.126003.111.
183 Yarosh W, Spradling AC. Incomplete replication generates somatic DNA alterations within Drosophila polytene salivary gland cells. *Genes Dev*. 2014;28(16):1840-1855. doi:10.1101/gad.245811.114.
184 Spradling AC, Mahowald AP. Amplification of genes for chorion proteins during oogenesis in Drosophila melanogaster. *Proc Natl Acad Sci U S A*. 1980;77(2):1096-1100. doi:10.1073/pnas.77.2.1096.
185 Wu N, Liang C, DiBartolomeis SM, Smith HS, Gerbi SA. Developmental progression of DNA puffs in Sciara coprophila: amplification and transcription. *Dev Biol*. 1993;160(1):73-84. doi:10.1006/dbio.1993.1287.
186 Calvi BR, Lilly MA, Spradling AC. Cell cycle control of chorion gene amplification. *Genes Dev*. 1998;12(5):734-744. doi:10.1101/gad.12.5.734.
187 Claycomb JM, Orr-Weaver TL. Developmental gene amplification: insights into DNA replication and gene expression. *Trends Genet*. 2005;21(3):149-162. doi:10.1016/j.tig.2005.01.009.
188 Rausch T, Jones DTW, Zapatka M, et al. Genome sequencing of pediatric medulloblastoma links catastrophic DNA rearrangements with TP53 mutations. *Cell*. 2012;148(1-2):59-71. doi:10.1016/j.cell.2011.12.013.
189 Rücker FG, Dolnik A, Blätte TJ, et al. Chromothripsis is linked to TP53 alteration, cell cycle impairment, and dismal outcome in acute myeloid leukemia with complex karyotype. *Haematologica*. 2018;103(1):e17-e20. doi:10.3324/haematol.2017.180497.
190 Molenaar JJ, Koster J, Zwijnenburg DA, et al. Sequencing of neuroblastoma identifies chromothripsis and defects in neuritogenesis genes. *Nature*. 2012;483(7391):589-593. doi:10.1038/nature10910.
191 Fontana MC, Marconi G, Feenstra JDM, et al. Chromothripsis in acute myeloid leukemia: biological features and impact on survival. *Leukemia*. 2018;32(7):1609-1620. doi:10.1038/s41375-018-0035-y.
192 Cox J, Mann M. 1D and 2D annotation enrichment: a statistical method integrating quantitative proteomics with complementary high-throughput data. *BMC Bioinformatics*. 2012;13 Suppl 16:S12. doi:10.1186/1471-2105-13-S16-S12.
193 Finardi A, Massari LF, Visintin R. Anaphase Bridges: Not All Natural Fibers Are Healthy. *Genes (Basel)*. 2020;11(8). doi:10.3390/genes11080902.
194 Bernhard SV, Seget-Trzensiok K, Kuffer C, et al. Loss of USP28 and SPINT2 expression promotes cancer cell survival after whole genome doubling. *Cell Oncol (Dordr)*. 2022;45(1):103-119. doi:10.1007/s13402-021-00654-5.

195 Merdes A, Ramyar K, Vechio JD, Cleveland DW. A Complex of NuMA and Cytoplasmic Dynein Is Essential for Mitotic Spindle Assembly. *Cell*. 1996;87(3):447-458. doi:10.1016/s0092-8674(00)81365-3.
196 Zhang D, Zaugg K, Mak TW, Elledge SJ. A role for the deubiquitinating enzyme USP28 in control of the DNA-damage response. *Cell*. 2006;126(3):529-542. doi:10.1016/j.cell.2006.06.039.
197 Gemble S, Wardenaar R, Keuper K, et al. Genetic instability from a single S phase after whole-genome duplication. *Nature*. 2022;604(7904):146-151. doi:10.1038/s41586-022-04578-4.
198 Prasad K, Bloomfield M, Levi H, et al. Whole-Genome Duplication Shapes the Aneuploidy Landscape of Human Cancers. *Cancer Res*. 2022;82(9):1736-1752. doi:10.1158/0008-5472.CAN-21-2065.
199 Tan Z, Chan YJA, Chua YJK, et al. Environmental stresses induce karyotypic instability in colorectal cancer cells. *Mol Biol Cell*. 2019;30(1):42-55. doi:10.1091/mbc.E18-10-0626.
200 Bloomfield M, Chen J, Cimini D. Spindle Architectural Features Must Be Considered Along With Cell Size to Explain the Timing of Mitotic Checkpoint Silencing. *Front Physiol*. 2020;11:596263. doi:10.3389/fphys.2020.596263.
201 Pantelias A, Karachristou I, Georgakilas AG, Terzoudi GI. Interphase Cytogenetic Analysis of Micronucleated and Multinucleated Cells Supports the Premature Chromosome Condensation Hypothesis as the Mechanistic Origin of Chromothripsis. *Cancers (Basel)*. 2019;11(8). doi:10.3390/cancers11081123.
202 Camps J, Wangsa D, Falke M, et al. Loss of lamin B1 results in prolongation of S phase and decondensation of chromosome territories. *FASEB J*. 2014;28(8):3423-3434. doi:10.1096/fj.14-250456.
203 Utani K, Okamoto A, Shimizu N. Generation of micronuclei during interphase by coupling between cytoplasmic membrane blebbing and nuclear budding. *PLOS ONE*. 2011;6(11):e27233. doi:10.1371/journal.pone.0027233.
204 Shimizu N, Itoh N, Utiyama H, Wahl GM. Selective entrapment of extrachromosomally amplified DNA by nuclear budding and micronucleation during S phase. *J Cell Biol*. 1998;140(6):1307-1320. doi:10.1083/jcb.140.6.1307.
205 He B, Gnawali N, Hinman AW, Mattingly AJ, Osimani A, Cimini D. Chromosomes missegregated into micronuclei contribute to chromosomal instability by missegregating at the next division. *Oncotarget*. 2019;10(28):2660-2674. doi:10.18632/oncotarget.26853.
206 Maciejowski J, Chatzipli A, Dananberg A, et al. APOBEC3-dependent kataegis and TREX1-driven chromothripsis during telomere crisis. *Nat Genet*. 2020;52(9):884-890. doi:10.1038/s41588-020-0667-5.
207 Dreesen O, Chojnowski A, Ong PF, et al. Lamin B1 fluctuations have differential effects on cellular proliferation and senescence. *J Cell Biol*. 2013;200(5):605-617. doi:10.1083/jcb.201206121.
208 Freund A, Laberge R-M, Demaria M, Campisi J. Lamin B1 loss is a senescence-associated biomarker. *Mol Biol Cell*. 2012;23(11):2066-2075. doi:10.1091/mbc.E11-10-0884.
209 Butin-Israeli V, Adam SA, Jain N, et al. Role of lamin b1 in chromatin instability. *Mol Cell Biol*. 2015;35(5):884-898. doi:10.1128/MCB.01145-14.
210 Vergnes L, Péterfy M, Bergo MO, Young SG, Reue K. Lamin B1 is required for mouse development and nuclear integrity. *Proc Natl Acad Sci U S A*. 2004;101(28):10428-10433. doi:10.1073/pnas.0401424101.
211 Li L, Du Y, Kong X, et al. Lamin B1 is a novel therapeutic target of betulinic acid in pancreatic cancer. *Clin Cancer Res*. 2013;19(17):4651-4661. doi:10.1158/1078-0432.CCR-12-3630.

212 Shimizu N, Misaka N, Utani K. Nonselective DNA damage induced by a replication inhibitor results in the selective elimination of extrachromosomal double minutes from human cancer cells. *Genes Chromosomes Cancer*. 2007;46(10):865-874. doi:10.1002/gcc.20473.
213 Shimizu N, Ochi T, Itonaga K. Replication timing of amplified genetic regions relates to intranuclear localization but not to genetic activity or G/R band. *Experimental Cell Research*. 2001;268(2):201-210. doi:10.1006/excr.2001.5286.
214 Itoh N, Shimizu N. DNA replication-dependent intranuclear relocation of double minute chromatin. *J Cell Sci*. 1998;111 (Pt 22):3275-3285. doi:10.1242/jcs.111.22.3275.
215 Rodríguez L, Cerbón-Ambriz J, Muñoz ML. Effects of colchicine and colchiceine in a biochemical model of liver injury and fibrosis. *Arch Med Res*. 1998;29(2):109-116.
216 Ergul M, Bakar-Ates F. Investigation of molecular mechanisms underlying the antiproliferative effects of colchicine against PC3 prostate cancer cells. *Toxicol In Vitro*. 2021;73:105138. doi:10.1016/j.tiv.2021.105138.
217 Foisy S, Bibor-Hardy V. Synthesis of nuclear lamins in BHK-21 cells synchronized with aphidicolin. *Biochemical and Biophysical Research Communications*. 1988;156(1):205-210. doi:10.1016/S0006-291X(88)80825-8.
218 Scherlach K, Boettger D, Remme N, Hertweck C. The chemistry and biology of cytochalasans. *Nat Prod Rep*. 2010;27(6):869-886. doi:10.1039/b903913a.
219 Theodoropoulos PA, Gravanis A, Tsapara A, et al. Cytochalasin B may shorten actin filaments by a mechanism independent of barbed end capping. *Biochem Pharmacol*. 1994;47(10):1875-1881. doi:10.1016/0006-2952(94)90318-2.
220 Jung CY, Rampal AL. Cytochalasin B binding sites and glucose transport carrier in human erythrocyte ghosts. *J Biol Chem*. 1977;252(15):5456-5463.
221 Ridler MA, Smith GF. The response of human cultured lymphocytes to cytochalasin B. *J Cell Sci*. 1968;3(4):595-602. doi:10.1242/jcs.3.4.595.
222 Schroeder TE. The contractile ring. II. Determining its brief existence, volumetric changes, and vital role in cleaving Arbacia eggs. *J Cell Biol*. 1972;53(2):419-434. doi:10.1083/jcb.53.2.419.
223 Spooner BS, Wessells NK. Effects of cytochalasin B upon microfilaments involved in morphogenesis of salivary epithelium. *Proc Natl Acad Sci U S A*. 1970;66(2):360-361. doi:10.1073/pnas.66.2.360.
224 Liu G, Stevens JB, Horne SD, et al. Genome chaos: survival strategy during crisis. *Cell Cycle*. 2014;13(4):528-537. doi:10.4161/cc.27378.
225 Rosswog C, Bartenhagen C, Welte A, et al. Chromothripsis followed by circular recombination drives oncogene amplification in human cancer. *Nat Genet*. 2021;53(12):1673-1685. doi:10.1038/s41588-021-00951-7.
226 Mardin BR, Drainas AP, Waszak SM, et al. A cell-based model system links chromothripsis with hyperploidy. *Mol Syst Biol*. 2015;11(9):828. doi:10.15252/msb.20156505.
227 Spann TP, Goldman AE, Wang C, Huang S, Goldman RD. Alteration of nuclear lamin organization inhibits RNA polymerase II-dependent transcription. *J Cell Biol*. 2002;156(4):603-608. doi:10.1083/jcb.200112047.
228 Tang CW, Maya-Mendoza A, Martin C, et al. The integrity of a lamin-B1-dependent nucleoskeleton is a fundamental determinant of RNA synthesis in human cells. *J Cell Sci*. 2008;121(Pt 7):1014-1024. doi:10.1242/jcs.020982.
229 Spann TP, Moir RD, Goldman AE, Stick R, Goldman RD. Disruption of nuclear lamin organization alters the distribution of replication factors and inhibits DNA synthesis. *J Cell Biol*. 1997;136(6):1201-1212. doi:10.1083/jcb.136.6.1201.

230 Kim H, Nguyen N-P, Turner K, et al. Extrachromosomal DNA is associated with oncogene amplification and poor outcome across multiple cancers. *Nat Genet*. 2020;52(9):891-897. doi:10.1038/s41588-020-0678-2.
231 Chen G, Bradford WD, Seidel CW, Li R. Hsp90 stress potentiates rapid cellular adaptation through induction of aneuploidy. *Nature*. 2012;482(7384):246-250. doi:10.1038/nature10795.
232 Yona AH, Manor YS, Herbst RH, et al. Chromosomal duplication is a transient evolutionary solution to stress. *Proc Natl Acad Sci U S A*. 2012;109(51):21010-21015. doi:10.1073/pnas.1211150109.
233 Ravichandran MC, Fink S, Clarke MN, Hofer FC, Campbell CS. Genetic interactions between specific chromosome copy number alterations dictate complex aneuploidy patterns. *Genes Dev*. 2018;32(23-24):1485-1498. doi:10.1101/gad.319400.118.
234 Kaya A, Mariotti M, Tyshkovskiy A, et al. Molecular signatures of aneuploidy-driven adaptive evolution. *Nat Commun*. 2020;11(1):588. doi:10.1038/s41467-019-13669-2.
235 Rutledge SD, Douglas TA, Nicholson JM, et al. Selective advantage of trisomic human cells cultured in non-standard conditions. *Sci Rep*. 2016;6:22828. doi:10.1038/srep22828.
236 Ben-David U, Amon A. Context is everything: aneuploidy in cancer. *Nat Rev Genet*. 2020;21(1):44-62. doi:10.1038/s41576-019-0171-x.
237 Freedman V. Cellular tumorigenicity in nude mice: Correlation with cell growth in semi-solid medium. *Cell*. 1974;3(4):355-359. doi:10.1016/0092-8674(74)90050-6.
238 Cantor JR, Abu-Remaileh M, Kanarek N, et al. Physiologic Medium Rewires Cellular Metabolism and Reveals Uric Acid as an Endogenous Inhibitor of UMP Synthase. *Cell*. 2017;169(2):258-272.e17. doi:10.1016/j.cell.2017.03.023.
239 Gui DY, Sullivan LB, Luengo A, et al. Environment Dictates Dependence on Mitochondrial Complex I for NAD+ and Aspartate Production and Determines Cancer Cell Sensitivity to Metformin. *Cell Metab*. 2016;24(5):716-727. doi:10.1016/j.cmet.2016.09.006.
240 Palm W, Park Y, Wright K, Pavlova NN, Tuveson DA, Thompson CB. The Utilization of Extracellular Proteins as Nutrients Is Suppressed by mTORC1. *Cell*. 2015;162(2):259-270. doi:10.1016/j.cell.2015.06.017.
241 Muir A, Danai LV, Gui DY, Waingarten CY, Lewis CA, Vander Heiden MG. Environmental cystine drives glutamine anaplerosis and sensitizes cancer cells to glutaminase inhibition. *Elife*. 2017;6. doi:10.7554/eLife.27713.
242 Biancur DE, Paulo JA, Małachowska B, et al. Compensatory metabolic networks in pancreatic cancers upon perturbation of glutamine metabolism. *Nat Commun*. 2017;8:15965. doi:10.1038/ncomms15965.
243 Davidson SM, Papagiannakopoulos T, Olenchock BA, et al. Environment Impacts the Metabolic Dependencies of Ras-Driven Non-Small Cell Lung Cancer. *Cell Metab*. 2016;23(3):517-528. doi:10.1016/j.cmet.2016.01.007.
244 Possemato R, Marks KM, Shaul YD, et al. Functional genomics reveal that the serine synthesis pathway is essential in breast cancer. *Nature*. 2011;476(7360):346-350. doi:10.1038/nature10350.
245 Yau EH, Kummetha IR, Lichinchi G, Tang R, Zhang Y, Rana TM. Genome-Wide CRISPR Screen for Essential Cell Growth Mediators in Mutant KRAS Colorectal Cancers. *Cancer Res*. 2017;77(22):6330-6339. doi:10.1158/0008-5472.CAN-17-2043.
246 Alvarez SW, Sviderskiy VO, Terzi EM, et al. NFS1 undergoes positive selection in lung tumours and protects cells from ferroptosis. *Nature*. 2017;551(7682):639-643. doi:10.1038/nature24637.
247 Ben-David U, Siranosian B, Ha G, et al. Genetic and transcriptional evolution alters cancer cell line drug response. *Nature*. 2018;560(7718):325-330. doi:10.1038/s41586-018-0409-3.

248 Ben-David U, Ha G, Tseng Y-Y, et al. Patient-derived xenografts undergo mouse-specific tumor evolution. *Nat Genet*. 2017;49(11):1567-1575. doi:10.1038/ng.3967.
249 Ben-David U, Arad G, Weissbein U, et al. Aneuploidy induces profound changes in gene expression, proliferation and tumorigenicity of human pluripotent stem cells. *Nat Commun*. 2014;5:4825. doi:10.1038/ncomms5825.
250 Sakaue-Sawano A, Kurokawa H, Morimura T, et al. Visualizing spatiotemporal dynamics of multicellular cell-cycle progression. *Cell*. 2008;132(3):487-498. doi:10.1016/j.cell.2007.12.033.
251 Iyer DR, Rhind N. Replication fork slowing and stalling are distinct, checkpoint-independent consequences of replicating damaged DNA. *PLoS Genet*. 2017;13(8). doi:10.1371/journal.pgen.1006958.
252 Macheret M, Halazonetis TD. Monitoring early S-phase origin firing and replication fork movement by sequencing nascent DNA from synchronized cells. *Nat Protoc*. 2019;14(1):51-67. doi:10.1038/s41596-018-0081-y.
253 Labit H, Goldar A, Guilbaud G, Douarche C, Hyrien O, Marheineke K. A simple and optimized method of producing silanized surfaces for FISH and replication mapping on combed DNA fibers. *Biotechniques*. 2008;45(6):649-52, 654, 656-8. doi:10.2144/000113002.
254 Lorin S, Hamaï A, Mehrpour M, Codogno P. Autophagy regulation and its role in cancer. *Seminars in Cancer Biology*. 2013;23(5):361-379. doi:10.1016/j.semcancer.2013.06.007.
255 Karantza-Wadsworth V, Patel S, Kravchuk O, et al. Autophagy mitigates metabolic stress and genome damage in mammary tumorigenesis. *Genes Dev*. 2007;21(13):1621-1635. doi:10.1101/gad.1565707.
256 Katayama M, Kawaguchi T, Berger MS, Pieper RO. DNA damaging agent-induced autophagy produces a cytoprotective adenosine triphosphate surge in malignant glioma cells. *Cell Death Differ*. 2007;14(3):548-558. doi:10.1038/sj.cdd.4402030.
257 Rosenfeldt MT, O'Prey J, Morton JP, et al. p53 status determines the role of autophagy in pancreatic tumour development. *Nature*. 2013;504(7479):296-300. doi:10.1038/nature12865.
258 Elgendy M, Sheridan C, Brumatti G, Martin SJ. Oncogenic Ras-induced expression of Noxa and Beclin-1 promotes autophagic cell death and limits clonogenic survival. *Mol Cell*. 2011;42(1):23-35. doi:10.1016/j.molcel.2011.02.009.
259 Young ARJ, Narita M, Ferreira M, et al. Autophagy mediates the mitotic senescence transition. *Genes Dev*. 2009;23(7):798-803. doi:10.1101/gad.519709.
260 Vanzo R, Bartkova J, Merchut-Maya JM, et al. Autophagy role(s) in response to oncogenes and DNA replication stress. *Cell Death Differ*. 2020;27(3):1134-1153. doi:10.1038/s41418-019-0403-9.
261 Guo JY, Chen H-Y, Mathew R, et al. Activated Ras requires autophagy to maintain oxidative metabolism and tumorigenesis. *Genes Dev*. 2011;25(5):460-470. doi:10.1101/gad.2016311.
262 Torres EM, Sokolsky T, Tucker CM, et al. Effects of aneuploidy on cellular physiology and cell division in haploid yeast. *Science*. 2007;317(5840):916-924. doi:10.1126/science.1142210.
263 Donnelly RP, Loftus RM, Keating SE, et al. mTORC1-dependent metabolic reprogramming is a prerequisite for NK cell effector function. *J Immunol*. 2014;193(9):4477-4484. doi:10.4049/jimmunol.1401558.
264 Santaguida S, Vasile E, White E, Amon A. Aneuploidy-induced cellular stresses limit autophagic degradation. *Genes Dev*. 2015;29(19):2010-2021. doi:10.1101/gad.269118.115.
265 Krivega M, Stiefel CM, Karbassi S, et al. Genotoxic stress in constitutive trisomies induces autophagy and the innate immune response via the cGAS-STING pathway. *Commun Biol*. 2021;4(1):831. doi:10.1038/s42003-021-02278-9.
266 Liu EY, Xu N, O'Prey J, et al. Loss of autophagy causes a synthetic lethal deficiency in DNA repair. *Proc Natl Acad Sci U S A*. 2015;112(3):773-778. doi:10.1073/pnas.1409563112.

267 Wang Y, Zhang N, Zhang L, et al. Autophagy Regulates Chromatin Ubiquitination in DNA Damage Response through Elimination of SQSTM1/p62. *Mol Cell*. 2016;63(1):34-48. doi:10.1016/j.molcel.2016.05.027.
268 Gabriel M, Balle D, Bigault S, et al. Time-lapse contact microscopy of cell cultures based on non-coherent illumination. *Sci Rep*. 2015;5:14532. doi:10.1038/srep14532.
269 Selmecki AM, Maruvka YE, Richmond PA, et al. Polyploidy can drive rapid adaptation in yeast. *Nature*. 2015;519(7543):349-352. doi:10.1038/nature14187.
270 GREGORY TR, MABLE BK. Polyploidy in Animals. In: *The Evolution of the Genome*: Elsevier; 2005:427-517.
271 Wendel JF, Flagel LE, Adams KL. Jeans, Genes, and Genomes: Cotton as a Model for Studying Polyploidy. In: Soltis PS, Soltis DE, eds. *Polyploidy and Genome Evolution*. Berlin, Heidelberg: Springer Berlin Heidelberg; 2012:181-207.
272 Zhen Y, Knobel PA, Stracker TH, Reverter D. Regulation of USP28 deubiquitinating activity by SUMO conjugation. *J Biol Chem*. 2014;289(50):34838-34850. doi:10.1074/jbc.M114.601849.
273 Knobel PA, Belotserkovskaya R, Galanty Y, Schmidt CK, Jackson SP, Stracker TH. USP28 is recruited to sites of DNA damage by the tandem BRCT domains of 53BP1 but plays a minor role in double-strand break metabolism. *Mol Cell Biol*. 2014;34(11):2062-2074. doi:10.1128/MCB.00197-14.
274 Diefenbacher ME, Popov N, Blake SM, et al. The deubiquitinase USP28 controls intestinal homeostasis and promotes colorectal cancer. *J Clin Invest*. 2014;124(8):3407-3418. doi:10.1172/JCI73733.
275 Okumura M, Natsume T, Kanemaki MT, Kiyomitsu T. Dynein-Dynactin-NuMA clusters generate cortical spindle-pulling forces as a multi-arm ensemble. *Elife*. 2018;7. doi:10.7554/eLife.36559.
276 Quintyne NJ, Reing JE, Hoffelder DR, Gollin SM, Saunders WS. Spindle multipolarity is prevented by centrosomal clustering. *Science*. 2005;307(5706):127-129. doi:10.1126/science.1104905.
277 Salvador Moreno N, Liu J, Haas KM, et al. The nuclear structural protein NuMA is a negative regulator of 53BP1 in DNA double-strand break repair. *Nucleic Acids Res*. 2019;47(6):2703-2715. doi:10.1093/nar/gkz138.
278 Maréchal A, Zou L. RPA-coated single-stranded DNA as a platform for post-translational modifications in the DNA damage response. *Cell Res*. 2015;25(1):9-23. doi:10.1038/cr.2014.147.
279 S Pedersen R, Karemore G, Gudjonsson T, et al. Profiling DNA damage response following mitotic perturbations. *Nat Commun*. 2016;7:13887. doi:10.1038/ncomms13887.
280 Nano M, Gemble S, Simon A, et al. Cell-Cycle Asynchrony Generates DNA Damage at Mitotic Entry in Polyploid Cells. *Curr Biol*. 2019;29(22):3937-3945.e7. doi:10.1016/j.cub.2019.09.041.
281 Anglana M, Apiou F, Bensimon A, Debatisse M. Dynamics of DNA Replication in Mammalian Somatic Cells. *Cell*. 2003;114(3):385-394. doi:10.1016/s0092-8674(03)00569-5.
282 Ge XQ, Blow JJ. Chk1 inhibits replication factory activation but allows dormant origin firing in existing factories. *J Cell Biol*. 2010;191(7):1285-1297. doi:10.1083/jcb.201007074.
283 Woodward AM, Göhler T, Luciani MG, et al. Excess Mcm2-7 license dormant origins of replication that can be used under conditions of replicative stress. *J Cell Biol*. 2006;173(5):673-683. doi:10.1083/jcb.200602108.
284 Yeo JE, Lee EH, Hendrickson EA, Sobeck A. CtIP mediates replication fork recovery in a FANCD2-regulated manner. *Hum Mol Genet*. 2014;23(14):3695-3705. doi:10.1093/hmg/ddu078.
285 Petermann E, Helleday T. Pathways of mammalian replication fork restart. *Nat Rev Mol Cell Biol*. 2010;11(10):683-687. doi:10.1038/nrm2974.
286 Sedlackova H, Rask M-B, Gupta R, Choudhary C, Somyajit K, Lukas J. Equilibrium between nascent and parental MCM proteins protects replicating genomes. *Nature*. 2020;587(7833):297-302. doi:10.1038/s41586-020-2842-3.

287 Maya-Mendoza A, Moudry P, Merchut-Maya JM, Lee M, Strauss R, Bartek J. High speed of fork progression induces DNA replication stress and genomic instability. *Nature*. 2018;559(7713):279-284. doi:10.1038/s41586-018-0261-5.

288 Wangsa D, Quintanilla I, Torabi K, et al. Near-tetraploid cancer cells show chromosome instability triggered by replication stress and exhibit enhanced invasiveness. *FASEB J*. 2018;32(7):3502-3517. doi:10.1096/fj.201700247RR.

289 Viganó C, Schubert C von, Ahrné E, et al. Quantitative proteomic and phosphoproteomic comparison of human colon cancer DLD-1 cells differing in ploidy and chromosome stability. *Mol Biol Cell*. 2018;29(9):1031-1047. doi:10.1091/mbc.E17-10-0577.

290 Remacle F, Graeber TG, Levine RD. Thermodynamic energetics underlying genomic instability and whole-genome doubling in cancer. *Proc Natl Acad Sci U S A*. 2020;117(31):18880-18890. doi:10.1073/pnas.1920870117.

291 Karin M, Eddy RL, Henry WM, Haley LL, Byers MG, Shows TB. Human metallothionein genes are clustered on chromosome 16. *Proc Natl Acad Sci U S A*. 1984;81(17):5494-5498. doi:10.1073/pnas.81.17.5494.

292 Corsello SM, Nagari RT, Spangler RD, et al. Discovering the anti-cancer potential of non-oncology drugs by systematic viability profiling. *Nat Cancer*. 2020;1(2):235-248. doi:10.1038/s43018-019-0018-6.

293 Diehl FF, Miettinen TP, Elbashir R, et al. Nucleotide imbalance decouples cell growth from cell proliferation. *Nat Cell Biol*. 2022;24(8):1252-1264. doi:10.1038/s41556-022-00965-1.

294 Forey R, Poveda A, Sharma S, et al. Mec1 Is Activated at the Onset of Normal S Phase by Low-dNTP Pools Impeding DNA Replication. *Mol Cell*. 2020;78(3):396-410.e4. doi:10.1016/j.molcel.2020.02.021.

295 Crevel G, Hashimoto R, Vass S, et al. Differential requirements for MCM proteins in DNA replication in Drosophila S2 cells. *PLOS ONE*. 2007;2(9):e833. doi:10.1371/journal.pone.0000833.

296 Ge XQ, Jackson DA, Blow JJ. Dormant origins licensed by excess Mcm2-7 are required for human cells to survive replicative stress. *Genes Dev*. 2007;21(24):3331-3341. doi:10.1101/gad.457807.

297 Ibarra A, Schwob E, Méndez J. Excess MCM proteins protect human cells from replicative stress by licensing backup origins of replication. *Proc Natl Acad Sci U S A*. 2008;105(26):8956-8961. doi:10.1073/pnas.0803978105.

298 Tyanova S, Temu T, Cox J. The MaxQuant computational platform for mass spectrometry-based shotgun proteomics. *Nat Protoc*. 2016;11(12):2301-2319. doi:10.1038/nprot.2016.136.